

UC Riverside

UC Riverside Electronic Theses and Dissertations

Title

Cyclic Peptide-Based Probes for Matrix Metalloproteinase 2 (MMP2) and Extracellular Signal-Regulated Kinase (ERK)

Permalink

<https://escholarship.org/uc/item/7c513298>

Author

Sarkar, Priyanka

Publication Date

2021

Copyright Information

This work is made available under the terms of a Creative Commons Attribution License, available at <https://creativecommons.org/licenses/by/4.0/>

Peer reviewed|Thesis/dissertation

UNIVERSITY OF CALIFORNIA
RIVERSIDE

Cyclic Peptide-Based Probes for Matrix Metalloproteinase 2 (MMP2) and Extracellular
Signal-Regulated Kinase (ERK)

A Dissertation submitted in partial satisfaction
of the requirements for the degree of

Doctor of Philosophy

in

Chemistry

by

Priyanka Sarkar

June 2021

Dissertation Committee:

Dr. Min Xue, Chairperson

Dr. Yinsheng Wang

Dr. Quan Jason Cheng

Copyright by
Priyanka Sarkar
2021

The Dissertation of Priyanka Sarkar is approved:

Committee Chairperson

University of California, Riverside

Acknowledgements

I am really grateful to many people who made sure that I am always loved and cared for every day of my life. I feel very thankful to have amazing parents and uncles who, even when I was a kid, always inspired me to do a Ph.D. someday. I have always looked up to my dad; to me, he is still a superman. He consistently encourages my love for science and learning more. My mom always motivates me to never give up on a problem. Where would I be today without my siblings, Ananya and Sammo! Because of their unconditional love, I know that I will always have someone even when I am down. I cannot thank my husband, Jawad, enough, who has always been there for me, especially for the last five years. To make my Ph.D. dream come true, he probably sacrificed the most.

My labmates had stayed with me through thick and thin; the team spirit always uplifted me through all my struggles. I am also very grateful to our postdocs; their patience and cooperation made all my research work possible.

Most importantly, I feel blessed to have Dr. Min Xue as my advisor; it would have been impossible to do my Ph.D. without his guidance. I have learned and still learning so many things from him; my heartfelt gratitude goes to him. Thank you so much, Min, for giving us an inspiring, fearless learning environment; it meant the world to me.

The text in this dissertation is a reprint of the following publication:

Chapter 2: Sarkar, P.; Li, Z.; Ren, W.; Wang, S.; Shao, S.; Sun, J.; Ren, X.; Perkins, N. G.; Guo, Z.; Chang, C. E. A.; Song, J.; Xue, M. Inhibiting matrix metalloproteinase-2 activation by perturbing protein-protein interactions using a cyclic peptide. *J Med Chem* **2020**, 63, 6979–6990.

Dedication

To my loving family

ABSTRACT OF THE DISSERTATION

Cyclic Peptide-Based Probes for Matrix Metalloproteinase 2 (MMP2) and Extracellular Signal-Regulated Kinase (ERK)

by

Priyanka Sarkar

Doctor of Philosophy, Graduate Program in Chemistry

University of California, Riverside, June 2021

Dr. Min Xue, Chairperson

Aberrant protein activities are frequently observed in various diseases, especially cancer, where these proteins can promote oncogenesis and tumor progression. Many of those abnormal activities involve protein-protein interactions (PPI), which are often critical to protein activation and signal transduction. Developing chemical probes that can specifically interrogate and modulate PPI is attractive, as those probes promise therapeutic benefits and a better understanding of the underlying disease mechanisms. This dissertation presents our work of developing cyclic peptide-based probes that target two proteins: matrix metalloproteinase 2 (MMP2) and extracellular signal-regulated kinase (ERK), both of which are heavily implicated in cancer. In the first project, we report a cyclic peptide that can specifically inhibit MMP2 proenzyme activation, which decreased cancer cell invasion and migration abilities. In the second project, we demonstrate the potential of using the MMP2-targeting cyclic peptide as an imaging

agent. In the final project, we showcase the development of cyclic peptide probes that bind to specific epitopes on the ERK protein and report its phosphorylation status.

Table of contents

Chapter 1: Introduction	
1.1 Types of PPI modulators.....	1
1.2 Mode of PPI modulation.....	2
1.3 Strategies to find PPI modulators.....	2
1.4 Peptides targeting PPIs.....	4
1.5 Cyclic Peptide as Reporters.....	5
1.6 References.....	6
Chapter 2: Inhibiting Matrix Metalloproteinase-2 Activation by Perturbing Protein-Protein Interactions Using a Cyclic Peptide	
2.1 Introduction.....	8
2.2 Experimental.....	12
2.3 Results and Discussion.....	28
2.4 Conclusion.....	88
2.5 References.....	89
Chapter 3: Towards MRI imaging probes for MMP2	
3.1 Introduction.....	95
3.2 Experimental.....	98
3.3 Results and Discussion.....	102
3.4 Conclusion.....	106
3.5 References.....	107
Chapter 4: Cyclic peptide-based fluorescence reporters for ERK isoforms	
4.1 Introduction.....	109
4.2 Experimental.....	110
4.3 Results and Discussion	114
4.4 Conclusion.....	120
4.5 References.....	120
Concluding remarks.....	122

List of Figures

Figure 2.1. Sequence alignment and homology search result for the MMP-2 catalytic domain (R88-P250) using protein BLAST® against other MMPs. The catalytic domain sequence is shown in the left (light blue background). The MMPs with the sequence homology found from the search are shown in the right two columns.....9

Figure 2.2. Sequence alignment and homology search result for the epitope (D570-A583) using protein BLAST® against the complete human proteome. The MMP2 epitope is shown in the first line (navy background). The top nine hits from the search with the highest sequence homology are shown in rows 2-10. Empty boxes represent completely mismatched residues.....9

Figure 2.3. Mechanism of inhibiting MMP2 activation by blocking the TIMP2-proMMP2 interaction. (a) Simplified illustration of the MMP2 activation process. The binding between TIMP2 and proMMP2 is critical to MMP2 activation mediated by another enzyme, MT1-MMP. (b) Blocking the PPI between TIMP2 and proMMP2 can prevent MMP2 activation. (c) Crystal structure of proMMP2 as adapted from PDB: 1GXD. The TIMP2-binding region on proMMP2 (D570-A583, highlighted in red) appears to be a structureless coil.

Figure 2.4. Validation of the hit sequences generated from library screening. (a) Generic structure of the cyclic peptide library. (b) Identified hits from the screening. (c) Förster resonance energy transfer (FRET) signals generated from the binding between 100 nM fluorescein-labeled epitope (Fluo-epitope) and varying concentrations of rhodamine B-modified ligand (Rhod-peptide). (d) Structure of cy(WPHPY) with and without the rhodamine B tag. (e) Competitive FRET results obtained using 100 nM Fluo-epitope, 100 nM Rhod-cy(WPHPY), and varying concentrations of cy(WPHPY) as the donor, acceptor, and competitor, respectively. The interaction between unlabeled cy(WPHPY) and Fluo-epitope displaced Rhod-cy(WPHPY), causing decreased FRET signals. (f) Fluorescence polarization (FP) assay results demonstrating the binding affinity between Rhod-cy(WPHPY) (100 nM) and the full-length recombinant proMMP2. (g) Competitive FP results demonstrating the binding between the unlabeled cy(WPHPY) and recombinant proMMP2 (100 nM). Here, the unlabeled cy(WPHPY) displaced Rhod-cy(WPHPY) (100 nM) and led to decreased FP values.....29,30

Figure 2.5. (Top) The generic structure of the one-bead-two-compound 80% Cyclic and 20% linear peptide library. X1-X5: comprehensive 18 natural L-amino acids, excluding Cys and Met. The library was built using 90 µm-sized TantaGel® S-NH₂ resins. Lower) After two steps of Edman degradation, the cyclic sequence contains a PTH moiety, while the linear one does not. A mass difference of 368 can be observed on the corresponding MS spectrum.....31

Figure 2.6. Structure and MALDI-TOF mass spectrum of the biotinylated epitope used in the library screening (Az4: L-azidolysine).....	32
Figure 2.7. Schematic illustration of the automated preclear procedure and epitope targeting library screening strategy. The library was precleared using a fluorescence-activated BioSorter® and a panel of fluorophores and fluorescently labeled proteins. The precleared library was then screened against the biotinylated epitope. A binding between the epitope and the hit sequences promoted an in situ click reaction, which anchored biotin tags on the resin. The hits were then identified through the biotin tag by using the avidin-alkaline phosphatase (AP) and its colorimetric substrate BCIP (5-bromo-4-chloro-3'-indolyphosphate p-toluidine salt) /NBT (nitroblue tetrazolium chloride). The stained hits were picked out and processed for sequencing.....	33
Figure 2.8. HPLC chromatogram (560 nm absorption) and MALDI-TOF mass spectrum for Rhod-cy(WPHPY).....	34
Figure 2.9. HPLC chromatogram (560 nm absorption) and MALDI-TOF mass spectrum for Rhod-cy(EWWFR).....	35
Figure 2.10. HPLC chromatogram (560 nm absorption) and MALDI-TOF mass spectrum for Rhod-cy(THNWP).	36
Figure 2.11. HPLC chromatogram (560 nm absorption) and MALDI-TOF mass spectrum for Rhod-cy(IDYSP). The bump at the end of the chromatogram is because of the sudden change in the flow rate.	37
Figure 2.12. HPLC chromatogram (560 nm absorption) and MALDI-TOF mass spectrum for Rhod-cy(VEYSP). The bump at the end of the chromatogram is because of the sudden change in the flow rate.	38
Figure 2.13. HPLC chromatogram (560 nm absorption) and MALDI-TOF mass spectrum for Rhod-cy(RNWIR). The bump at the end of the chromatogram is because of the sudden change in the flow rate.	39
Figure 2.14. HPLC chromatogram (560 nm absorption) and MALDI-TOF mass spectrum for Rhod-cy(IHWRW). The bump at the end of the chromatogram is because of the sudden change in the flow rate.....	40
Figure 2.15. HPLC chromatogram (560 nm absorption) and MALDI-TOF mass spectrum and for Rhod-cy(RNWLR).....	41
Figure 2.16. HPLC chromatogram (560 nm absorption) and MALDI-TOF mass spectrum for Rhod-cy(WRLKG). The bump at the end of the chromatogram is because of the sudden change in the flow rate.....	42

Figure 2.17. HPLC chromatogram (560 nm absorption) and MALDI-TOF mass spectrum for Rhod-cy(WRIKG)	43
Figure 2.18. HPLC chromatogram (560 nm absorption) and MALDI-TOF mass spectrum for Rhod-cy(QTNWF)	44
Figure 2.19. HPLC chromatogram (560 nm absorption) and MALDI-TOF mass spectrum for Rhod-cy(WFQDS).....	45
Figure 2.20. HPLC chromatogram (560 nm absorption) and MALDI-TOF mass spectrum and for Rhod-cy(LDYSP)	46
Figure 2.21. HPLC chromatogram (560 nm absorption) and MALDI-TOF mass spectrum for Rhod-cy(LHWRW)	46
Figure 2.22. HPLC chromatogram (560 nm absorption) and MALDI-TOF mass spectrum for Rhod-cy(RAPWW)	47
Figure 2.23. MALDI-TOF mass spectrum for the fluorescein-labeled epitope.....	48
Figure 2.24. a-o. Varying concentrations of rhodamine B-conjugated hit peptides were mixed with 100 nM of the fluorescein-labeled epitope, and the FRET intensities were measured. The curves were fitted using a Hill function to obtain the Kd values.....	49
Figure 2.25. FRET signal obtained from the binding between 100 nM of rhodamine B-labeled ligand (Rhod-cy(WPHPY)) and varying concentrations of the fluorescein-labeled epitope (Fluo-Epitope). The binding affinity obtained was similar to the original one (Fig 2.24, o)	50-52
Figure 2.26. Residual fluorescence as a result of the binding between 100 nM of BHQ2-modified epitope and Rhod-cy(WPHPY). The dark quencher BHQ2 quenched the rhodamine fluorescence through a FRET mechanism.....	53
Figure 2.27. FRET signal obtained from the binding between 100 nM of Rhod-Epitope and varying concentrations of fluorescein-labeled ligand (Fluo-cy(WPHPY)). Changing the tag on the ligand resulted in a total loss of binding.....	54
Figure 2.28. Analytical HPLC chromatogram (280 nm absorption) and MALDI-TOF mass spectrum and for the unmodified cyclic peptide ligand cy(WPHPY).....	57
Figure 2.29. The representative conformation of an MD run for cy(WPHPY) is shown in van der Waals (middle) and stick (right) representations. This conformation constitutes 57.7% conformations of a 20-ns long MD trajectory. The RMSD of the MD calculation is 1.066 angstrom. The average total energy for 20 ns is -15250.89 kcal/mol, the average	

kinetic energy is 3571.86 kcal/mol, and the average potential energy is -18822.76 kcal/mol. E-total = E-kinetic + E-potential is used. This energy is for the whole system (cy(WPHPY) + water + one Cl-).60

Figure 2.30. Analysis of the structure–activity relationship. (a) Optimal conformations of cy(WPHPY) as calculated using molecular dynamics (MD) approaches. The blue wire is the most representative conformation generated from the conformation search. The orange wires illustrate the conformations that were evenly extracted every 2 ns from the MD simulation trajectory. (b) Alanine scanning variations of cy(WPHPY). (c) Competitive FP results obtained using alanine-substituted cy(WPHPY) variations. The competitive FP results of cy(WPHPY) were included as a reference (red line, peptide 1). (d) Partially scrambled epitope sequences in comparison with the original epitope. (e) FRET signals generated from the binding between 100 nM Fluo-epitope variations and varying concentrations of Rhod-cy(WPHPY). The result from the original Fluo-epitope was included as a reference. C5 was not able to bind to Rhod-cy(WPHPY), while M5 and N5 retained the binding affinity. (f) Competitive FRET assay results demonstrating the lack of binding affinity between the unlabeled cy(WPHPY) and the partially scrambled epitopes (M5 and N5). Unlabeled cy(WPHPY) could not displace Rhod-cy(WPHPY) from the epitope; therefore, the FRET intensities did not change. The result from the original Fluo- epitope was included as a reference.61-62

Figure 2.31. Circular dichroism (CD) spectrum of 20 μ M of the fluorescein-labeled epitope (D570-A583) in PBS. No apparent secondary structure was observed, and the epitope appeared to be a random coil.64

Figure 2.32. Circular dichroism (CD) spectrum of 20 μ M of the fluorescein-labeled randomized epitope (C5) in PBS. No apparent secondary structure was observed.65

Figure 2.33. Circular dichroism (CD) spectrum of 20 μ M of the fluorescein-labeled randomized epitope (M5) in PBS. No apparent secondary structure was observed.66

Figure 2.34. Circular dichroism (CD) spectrum of 20 μ M of the fluorescein-labeled randomized epitope (N5) in PBS. No apparent secondary structure was observed.67

Figure 2.35. Since changing C5 showed a total loss of binding, this time we kept the first five amino acids at the C terminal unchanged and randomized the last nine amino acids. We ran a FRET assay using this epitope (N9) and rhodamine tagged ligand which also showed loss of binding.68

Figure 2.36. MALDI-TOF mass spectrum of the unmodified epitope.69

Figure 2.37. a. Emission spectra of the mutated ligand cy(WAHPY) (10 μ M), the epitope (10 μ M), and a mixture containing both. The spectra were obtained using an excitation wavelength of 288 nm. b. Similar emission spectra obtained using cy(WPHPY) (10 Mm),

the epitope (10 μ M), and their mixture. c,d. Bar graph representations of a and b showing the fluorescence intensities at 350 nm. Only the cy(WPHPY)-epitope interaction led to an increased Trp fluorescence intensity.....70

Figure 2.38. cy(WPHPY) inhibited the TIMP2–proMMP2 interaction and prevented proMMP2 activation. (a) Principle and results of the ELISA-based competitive binding assay. Surface-immobilized recombinant TIMP2 can pull down MMP2 from the solution, while cy(WPHPY) binds to MMP2 and blocks this interaction. Phosphate-buffered saline (PBS) was used in place of cy(WPHPY) in the control sample. (b–f) Schematic illustration and results of the *in vitro* bioactivity assay evaluating the function of cy(WPHPY). (b) Media from WM115 cell culture were collected and incubated with varying concentrations of cy(WPHPY). The corresponding MMP2 activities were analyzed using an MMP2-specific fluorogenic substrate. The assay buffer was used in place of cy(WPHPY) in the control sample. (c) WM115 culture media were incubated with TIMP2 and cy(WPHPY), and the corresponding MMP2 activities were evaluated. For the control samples, the assay buffer was used in place of cy(WPHPY) and TIMP2. (d–f) WM115 cells were cultured with varying concentrations of cy(WPHPY), and the corresponding media were collected for subsequent analyses. Serum-free media without cy(WPHPY) were used for the control samples. (d) Gelatin zymography and western blotting results demonstrate that cy(WPHPY) inhibited the MMP2 activity in the WM115 cell culture. (e, f) Enzymatic activity assays show that cy(WPHPY) was highly specific to MMP2 activities and did not affect MMP9. (g, h) Confocal microscopy images of WM115 cells showing membrane-bound MMP2 immunofluorescence. The scale bars are 10 μ m. Media without cy(WPHPY) were used in the control sample. (i) Comparison of the single-cell MMP2 immunofluorescence signals extracted from the confocal images. A total of 30 single cells were analyzed for each image. The boxes denote the middle two quartiles, and the horizontal blue bars represent median values. The whiskers show the standard deviation values.....72-73

Figure 2.39. The structure of the MMP2-specific fluorogenic peptide substrate. Green lines highlight the MMP cleaving sites.....75

Figure 2.40. Positive and Negative controls used in the MMP2 specific substrate assay using MCA-P-L-A~Nva-Dap(DNP)-A-R-NH₂. The positive control consists of the serum-free media collected from WM115 cells. This media was then concentrated with a centrifugal membrane filter (10 kDa cut-off, Amicon). Once concentrated, the total protein content was quantified using a BCA assay kit (Thermo). In a 96 well microplate, 10 μ l (1 μ g/ μ l protein content) of the media was mixed with 90 μ l of TNC assay buffer (50 mM Tris base, 0.15 M NaCl, 10 mM CaCl₂, pH 7.5). The plate was left for 5 min at 37 °C for equilibration, and then 100 μ L of MMP2 specific substrate (3 μ M) was added. The plate was then incubated at 37 °C for 20 min. The fluorescence was measured using a SYNERGY H1 microplate reader. One of the negative controls has the ligand (1 μ M) in the serum-free media in which later the 3 μ M substrate was added, and the other one is

the MMP2 specific substrate by itself in the serum-free media. The fluorescence was measured with a SYNERGY H1 microplate reader.....76

Figure 2.41. The intensities of the gelatin zymogram bands were measured using ImageJ software and plotted. The IC50 value was estimated to be around 20 nM.....78

Figure 2.42. The structure of the MMP9-specific fluorogenic peptide substrate. Green lines highlight the MMP cleaving sites.....79

Figure 2.43. Positive and Negative controls used in the MMP9 specific substrate assay using DNP-P-Cha-G~C(Me)-H-A-K(N-Me-Abz)-NH₂. The positive control consists of the serum-free media collected from WM115 cells. This media was then concentrated with a centrifugal membrane filter (10 kDa cut-off, Amicon). Once concentrated, the total protein content was quantified using a BCA assay kit (Thermo). In a 96 well microplate, 10 µl (1 µg/µl protein content) of the protein solution was mixed with 90 µl of TNC assay buffer (50 mM Tris base, 0.15 M NaCl, 10 mM CaCl₂, pH 7.5). The plate was left for 5 min at 37 °C for equilibration, and then 100 µL of MMP9 specific substrate (3 µM) was added. The plate was then incubated at 37 °C for 20 min. The fluorescence was measured using a SYNERGY H1 microplate reader. One of the negative controls has the ligand (1µM) in the serum-free media in which later the 3 uM substrate was added, and the other one is the MMP9 specific substrate by itself in the serum-free media. The fluorescence was measured with a SYNERGY H1 microplate reader.....80

Figure 2.44. The linear sequence WPHPY was synthesized to see if it shows any inhibition efficiency. WM115 cells were cultured in full media to 80% confluency and then changed to serum-free media containing varying concentrations of the linear sequence. The culture media was then taken out, and the active MMP2 specific fluorogenic substrate was added to it. No significant change in the intensity was observed.....81

Figure 2.45. cy(WPHPY) inhibited cell migration. (a) Schematic illustration of the scratch wound-healing experiment. (b) Results of the scratch wound healing experiment demonstrate that cy(WPHPY) treatments led to fewer cells migrating to the scratch wound. (c) Schematic illustration of the trans-well cell invasion assay. Active MMP2 was required for the cells to digest the Matrigel and invade through the porous membrane. Before the final imaging stage, cells were fixed and stained with crystal violet. (d) Results of the trans-well assay demonstrate that cy(WPHPY) significantly inhibited cell invasion. Images were taken after 24 hours of incubation.....83-84

Figure 2.46. Sequence alignment and homology search result for the TIMP2 binding epitope on the 4th hemopexin blade of proMMP-2 using protein BLAST®. The epitope sequence is placed in the first line (navy background). The other MMPs with the sequence homology found from the search are shown in rows 2-7. Empty boxes represent completely mismatched residues.....86

Figure 3.1: An illustration of atherosclerotic plaque formation process.....97

Figure 3.2. Binding affinity of Gd conjugated peptides. (a) (b) Different concentrations of Gd conjugated peptides were incubated with 200 nM rhodamine tagged peptide and 200 nM fluorescein-labeled epitope. For both linkers, there is no evident concentration-dependent FRET intensity change. (c) For the competitive FP, various concentrations of the Gd-2° amine-cy(WPHPY) were incubated with 100 nM of recombinant MMP2 protein and Rhod-cy(WPHPY), and no noticeable change is observed. (d) The same process is repeated for Gd-PEG5-cy(WPHPY), and no difference is observed.....103

Figure 3.3. (a) The binding affinity of Gd-DOTA-PEG5-cy(WPHPY) against recombinant MMP2. With a change in the peptide concentration, there is a substantial concentration-dependent increase in the tryptophan fluorescence. (b) To clarify that the fluorescence intensity change is not because of an increase in the concentration of peptide, a spectral scan was done on the Gd conjugated peptide incubated with the recombinant protein and for the peptide and protein by itself. Figure b represents the emission spectra of Trp fluorescence at different concentrations. The upper part shows an increase in fluorescence intensity when the peptide was incubated with recombinant MMP2. The lower part shows the fluorescence intensity only for the protein and the peptides by themselves.....104

Figure 3.4. The invasion assay result for the Gd conjugated peptide. When cells were treated with different concentrations of the peptide, no apparent change in their invasion property was observed.....105

Figure 4.1. Finding preliminary leads from the hit sequences. (a) List of all 17 sequences. All these sequences were individually synthesized and tagged with rhodamine dye. (b) An illustration of a generic bicyclic peptide structure. (c) The epitope sequences, which were used in screening the library. The epitopes were synthesized and tagged with fluorescein. Later, each of the rhodamine-tagged peptides was tested against the fluorescein-tagged epitopes, and the binding was evaluated using FRET signal intensity. (c) List of identified hits obtained from the FRET data.....116

Figure 4.2. Validation of the hit sequences. (a) Crystal structure of ERK2, adapted from PDB, 3W55 file where the ERK2 epitope, G182-R194 is featured in red and appears to be a random coil. The right part of the panel shows FP data where 100 nM Rhod-B22 was treated with different concentrations of recombinant ERK2 protein. (b) Crystal structure of ERK1, adapted from 2ZOQ, PDB where epitope, G199-R211, is featured in red and appears to be structureless. The right side shows the FP result for Rhod-B22 (100 nM) when it is incubated with different concentrations of recombinant ERK1. (C) Crystal structure of ERK2 as in 3.2a (3W55, PDB), but it features a different epitope, Y312-E326, highlighted in red, which also appears to be a random coil, and the right panel shows FP data for Rhod-C14 (d) Crystal structure of ERK2 as in 3.2b (2ZOQ, PDB). The

epitope, Y327-E341, is highlighted in red which appears to be a combination of alpha-helix and random coil, and the right panel shows the FP result for Rhod-C14.....117

Figure 4.3. (a) FRET based unphosphorylated ERK1 detection method. For the FRET signal to generate, both the peptides need to be binding on the same ERK1 protein. (b) Structures of Cy5-B22 (probe 1) and Rhod-C14 (probe 2).....118

Figure 4.4. (a) Illustration of different treatment conditions. Serum starved U87 cells were stimulated with 50 ng/ml EGF which should increase the presence of more active ERK proteins, followed by treatment with 10 nM MEK inhibitor, trametinib. (b) Changes in FRET signal in the lysates that were collected right after treatment with EGF and inhibitor. (c) The results of in vitro kinase activity where with an increase in active MEK, we could see a decrease in the FRET signal.....119

List of Tables

Table 2.1. The most stable conformations of cy(WPHPY) obtained from free energy calculations. Top 10 most stable conformations from a total of 546 conformations are shown in stick representation with orange and blue color representing two linkages. Conformational search and free energy calculations were performed with VM2 using the implicit solvation model.....58

Table 2.2. Five manually selected conformations with the most significant changes in the dihedral angle in the peptide backbone or sidechain were taken as the initial conformations to start MD simulation in an explicit water model. Free energy is in kcal/mol.....59

Chapter 1 : Introduction

Protein-protein interactions are emerging as an attractive targeting group because of their selectivity and relation to the progression of different diseases. There are about 645,00 disease-related PPIs, and among which only 2% had been targeted for drug development.^{1,2} Many of the protein complexes involved in the PPIs are considered ‘undruggable’, including transcription factors, signaling proteins, and still not fully understood.^{3,4}

Protein-protein binding sites are known as interfaces. All the residues in the protein-protein interfaces do not contribute equally to the binding energy. The critical residues are known as hotspots which contribute most to the binding energy.⁵ These hotspot residues are identified with the help of alanine scanning mutagenesis and X-ray crystallography. With the progression of technology and structural biology, the recognition of ‘hotspots’ in the interaction process has become a popular strategy to find out PPI modulators.⁶

1.1 Types of PPI modulators

The PPI modulators can be broadly classified into three groups- small molecules, peptides, and antibodies. Small molecules have some advantages over others. For example, they are more likely to penetrate the cell membrane and are more suitable for oral administration. On the other hand, peptides can offer better target specificity and binding affinity but can suffer from lack of stability, incompatibility for oral administration, and shorter half-life.⁷ Antibodies that are used as PPI modulators are usually highly specific and show better efficiency but still can cause immunogenicity.

1.2 Mode of PPI modulation

Rather than interacting with the protein-protein interface, the PPI inhibitors can also interact with orthosteric and allosteric sites. In the case of allosteric inhibition, the inhibitors interact with the PPI interface, whereas for the orthosteric inhibition, the modulators interact with any other region other than the PPI interface.⁸ If the hotspots are identified for the PPIs, the modulators can be constructed for direct interaction with it. For cases, when the residues of the hotspots come closer to form some sort of a pocket, the orthosteric ligands could be developed against this pocket to fit and impact the associated interaction. On the other hand, allosteric modulators will be more suitable for the PPIs with hotspots that do not lead to a suitable binding site. PPI stabilization is another promising strategy since it is energetically favorable to bind to an already existing complex compared to inhibiting the formation of the complex.^{9,10} In the case of stabilization, either the modulator binds on the allosteric site and changes the conformation of the target protein so that the binding affinity towards the other protein increases, or if the modulator binds to the PPI interface, it offers more point of interaction for both the target and the associating protein and thereby enhance the binding process.

1.3 Strategies to find PPI modulators

Fragment-based drug discovery (FBDD) is one of the major strategies in finding small molecule modulators. At first, small chemical fragments are identified that can bind to the target with mM binding affinities.¹¹ These chemical fragments are then modified to have stronger binding affinity either through expansion or by linking to other fragments to produce the 'lead'. Several analytical techniques like SPR, NMR, mass spectrometry,

and X-ray crystallography can be used for finding and validating the fragment hits. FBDD offers a better strategy for finding PPI modulators since the PPI interfaces are usually composed of discrete hotspots. But the hit optimization often requires structural information obtained from X-ray crystallography and NMR, which makes the FBDD strategy unsuitable for targeting unknown structures.^{12,13}

High-throughput screening (HTS) has been used in drug discovery for a very long time. In terms of finding PPI modulators, HTS has also been used to find compounds that can interact with the hotspots.¹⁴ Nevertheless, typical small molecule-based libraries used in HTS are not a good option for finding PPI modulators. The uniqueness of the PPI interface requires more diversified compounds in the library, which would create better chances of finding a modulator for the target.

Most of the time, the PPIs do not have any natural small-molecule ligands to interact with, which always poses a problem in designing their modulators. There are two different ways of finding modulators with structure-based design. One of them depends on the structure of the hotspots where small molecule modulators can be developed with the help of de novo designing and bioisosteres.¹⁵ The other one is based on peptidomimetics, where modeling and phage display is used to construct the secondary peptide structures that are involved in PPIs. Presently multiple modulators have been successfully generated focusing on the alpha-helix structure.¹⁶

1.4 Peptides targeting PPIs

Researchers have been working on finding peptide-based PPI modulators for a while. Peptides can be considered as one of the best candidates in targeting PPIs since the peptides can actually mimic the surface of the protein and thus potentially can bind in a competitive manner.¹⁷ There are other advantageous features of the peptide that make them suitable for targeting PPIs. Peptides can be easily synthesized with solid-phase peptide synthesis protocols and also can be easily adapted to high-throughput screening strategies. One of the major problems with the peptides is their susceptibility to protease enzymes. To overcome this, a lot of different approaches were taken.

The idea behind most of the approaches was to deviate from the natural structures of peptide scaffolds. This strategy brought some remarkable success in developing PPI modulators.^{18,19} One of the strategies is the introduction of unnatural amino acids, which resulted in improving the binding affinity toward the target as well as protection against proteolysis. Many groups have been working on developing peptide-based inhibitors for PPIs, but the main concern for a lot of them is the lack of membrane penetrability and metabolic instability. To solve these problems, researchers have developed macrocycles, peptidomimetics, cyclic peptides and so on.

Cyclic peptides are composed of polypeptides where the cycle is formed by an amide bond or other stable chemical bonds between two ends of the peptide. There are several naturally found cyclic peptides that are used as therapeutics. For example, cyclosporin A has immunosuppressive properties, and gramicidin acts as an antibiotic, etc. Cyclic peptides have several advantages targeting PPIs over small molecules and antibodies.

Even though targeting PPI with small molecules is a traditional strategy, it does not work that well in the case of many PPI interfaces which do not have the binding pockets because of their flat, large structures and shallow features. On the other hand, antibodies are cell impermeable, expensive, and can be immunogenic.²⁰ In contrast, linear peptides are easy to make, cheap, and usually show better selectivity but often lack stability and membrane penetrability. Cyclic peptides bring a solution to a lot of these problems. Their conformational constraints help with metabolic stability, increases target selectivity and cell permeability. Right now, there are numerous cyclic peptidomimetics that are already being used as drugs. Multiple cyclic peptide candidates targeting PPI have also been going through preclinical and clinical trials.

1.5 Cyclic Peptide as Reporters

Cyclic peptides are often tagged with fluorescent dyes to investigate different biological processes, including in vitro cell-based assays and live-cell imaging. Many cyclic fluorescently-labeled peptides were developed to target cell surface receptors, enzymes as well as other biomarkers, which enabled the visualization of tumor tissues.²² Development in optical methods and advancement in microscopy have made the reporter peptides a valuable tool for understanding and visualizing different signaling pathways and consequences of perturbing the cells with various types of stress.

1.6 References

1. Robertson NS.; Spring DR. Using peptidomimetics and constrained peptides as valuable tools for inhibiting protein–protein interactions. *Molecules* **2018**, 23:959. doi: 10.3390/molecules23040959.
2. Díaz-Eufracio BI.; JesúsNaveja J.; Medina-Franco JL. Protein-protein interaction modulators for epigenetic therapies. In: Donev R, editor. *Advances in protein chemistry and structural biology*. 1. UK: Swansea University; **2018**. pp. 65–84.
3. Yan, C.; Higgins, P.J. Drugging the undruggable: Transcription therapy for cancer. *Biochim. Biophys. Acta Rev Cancer* **2013**, 1835, 76–85.
4. Mabonga L.; Kappo AP. Protein-protein interaction modulators: advances, successes and remaining challenges. *Biophys Rev* **2019**, 11(4):559-581. doi:10.1007/s12551-019-00570x
5. Shangary, S.; Wang, S. Small-molecule inhibitors of the MDM2-p53 protein-protein interaction to reactivate p53 function: a novel approach for cancer therapy. *Annu Rev Pharmacol Toxicol* **2009**, 49, 223–241.
6. Geppert, T.; Hoy, B.; Wessler, S.; & Schneider, G. Context-based identification of protein-protein interfaces and “hotspot” residues. *Chem. Biol.* **2011**, 18, 344–353.
7. Lu, S.; Shen, Q.; Zhang, J. Allosteric methods and their applications: facilitating the discovery of allosteric drugs and the investigation of allosteric mechanisms. *Acc. Chem. Res.* **2019**, 52, 492–500.
8. Fischer, G.; Rossmann, M.; Hyvonen, M. Alternative modulation of protein-protein interactions by small molecules. *Curr. Opin. Biotechnol.* **2015**, 35, 78–85.
9. Thiel, P.; Kaiser, M.; Ottmann, C. Small-molecule stabilization of protein-protein interactions: an underestimated concept in drug discovery? *Angew. Chem. Int. Ed. Engl.* **2012**, 51, 2012–2018.
10. Erlanson DA.; Fesik SW.; Hubbard RE, et al. Twenty years on: the impact of fragments on drug discovery. *Nat. Rev. Drug Discov.* **2016**, 15:605–619. doi: 10.1038/nrd.2016.109.
11. Silvestre, H. L.; Blundell, T. L.; Abell, C.; Ciulli, A. Integrated biophysical approach to fragment screening and validation for fragment-based lead discovery. *Proc. Natl. Acad. Sci. USA* **2013**, 110, 12984–12989.

12. Magee, T. V. Progress in discovery of small-molecule modulators of protein-protein interactions via fragment screening. *Bioorg. Med. Chem. Lett.* **2015**, 25, 2461–2468.
13. Wells, J. A.; McClendon, C. L. Reaching for high-hanging fruit in drug discovery at protein-protein interfaces. *Nature* **2007**, 450, 1001–1009.
14. Sheng, C.; Dong, G.; Miao, Z.; Zhang, W.; Wang, W. State-of-the-art strategies for targeting protein-protein interactions by small-molecule inhibitors. *Chem Soc Rev* **2015**, 44, 8238–8259.
15. Mason, J. M. Design and development of peptides and peptide mimetics as antagonists for therapeutic intervention. *Future Med. Chem.* **2010**, 2, 1813–1822.
16. Haiying, L.; Qiaodan, Z.; Jun, H.; Zhongliang J.; Cheng P.; Rongsheng T.; Jianyou S. Recent advances in the development of protein–protein interactions modulators: mechanisms and clinical trials. *Signal Transduction and Targeted Therapy* **2020**, 5 (1) <https://doi.org/10.1038/s41392-020-00315-3>
17. Ran, X.; Gestwicki, JE. Inhibitors of protein-protein interactions (PPIs): an analysis of scaffold choices and buried surface area. *Curr. Opin. Chem. Biol.* **2018**;44:75-86. doi:10.1016/j.cbpa.2018.06.004
18. Jambunathan, K.; Galande, A.K. Design of a serum stability tag for bioactive peptides. *Protein Pept Lett* **2014**, 21:32–38. doi: 10.2174/09298665113209990069.
19. Di, L. Strategic approaches to optimizing peptide ADME properties. *AAPS J* **2015**, 17:134–143. doi: 10.1208/s12248-014-9687-3
20. Frey, V.; Viaud, J.; Subra, G.; Cauquil, N.; Guichou, J.F.; Casara, P.; Grassy, G.; Chavanieu A. Structure-activity relationships of Bak derived peptides: Affinity and specificity modulations by amino acid replacement. *Eur. J. Med. Chem.* **2008**, 43:966–972. doi: 10.1016/j.ejmech.2007.06.008.
21. Rubin, S.; Qvit N. Cyclic Peptides for Protein-Protein Interaction Targets: Applications to Human Disease. *Crit. Rev. Eukaryot. Gene Expr.* **2016**, 26(3):199-221. doi: 0.1615/CritRevEukaryotGeneExpr.2016016525. PMID: 27650985.
22. Zhang, F.; Niu, G.; Lin, X.; Jacobson, O.; Ma, Y.; Eden H.S.; He, Y.; Lu G.; Chen, X. *Amino Acids* **2012**, 42, 2343

Chapter 2 : Inhibiting Matrix Metalloproteinase-2 Activation by Perturbing Protein–Protein Interactions Using a Cyclic Peptide

2.1 Introduction

Matrix metalloproteinase-2 (MMP2) is a Zn-dependent endopeptidase with diverse biological functions, one of which is to facilitate cell migration by degrading the extracellular matrix and cell adhering molecules.^{1,2} Elevated MMP2 expression levels prevail in pathological processes such as tumor metastasis and atherosclerosis plaque rupture, where MMP2 activities often correlate with disease severity.^{2–4} Results from biomedical studies further support the hypothesis that elevated MMP2 activities promote the progression of those diseases. Consequently, MMP2 inhibitors have attracted significant interest but remain elusive despite decades of drug development efforts.^{5,6}

Because MMP2 is an enzyme with a substrate-binding pocket, the most natural and popular strategy for MMP2 inhibition was to irreversibly halt the catalytic process using substrate analogues.^{7,8} More than 30 small-molecule inhibitors that came out of pharmaceutical pipelines shared this mechanism of action. They all showed promising efficacy in preclinical studies,^{9–11} but none of them demonstrated the desired outcomes in clinical trials. Subsequent analysis has linked those disappointing clinical results to the drugs' offtarget effects on other MMPs, which share significant structural homology with MMP2 but perform distinct physiological functions (Figure 2.1).^{12–16} These results highlight the necessity of improving target specificity during drug development, which has become the current consensus in the field of MMP inhibition.^{16,17} Nevertheless, the aforementioned structural homology makes this task difficult.

MMP-2 catalytic domain	Homology	Protein name
R K P K W D K N Q I T Y R I I G Y T P D L D P E T V D D A F A R A F Q V W S D V T P L R F S R I H D G E A D I M I N F G R W E H G D G Y P F D G K D G L L A H A F A P G T G V G G D S H F D D D E L W S L G K G V G Y S L F L V A A H E F G H A M G L E H S Q D P G A L M A P I Y T Y T K N F R L S Q D D I K G I Q E L Y G A S P	64%	MMP-9 (3-157)
	64%	MMP-13 (6-164)
	59%	MMP-3 (2-162)
	58%	MMP-12 (3-159)
	58%	MMP-20 (2-159)
	56%	MMP-8 (6-163)
	58%	MMP-10 (8-165)
	55%	MMP-1 (7-164)

Figure 2.1. Sequence alignment and homology search result for the MMP-2 catalytic domain (R88-P250) using protein BLAST® against other MMPs. The catalytic domain sequence is shown in the left (light blue background). The MMPs with the sequence homology found from the search are shown in the right two columns.

D P G F P K L I A D A W N A	Homology	Protein Name
P G Y P K L I R D W W	57%	Unnamed protein (121-131)
D P G P F P K L I E W	50%	Cadherin-like protein (73-83)
D P G Y P K L I	50%	Macrophage metalloelastase (135-142)
D P G Y P K M I A	50%	MMP 1 (171-179)
D P G Y P K L I	50%	MΦ metalloelastase preproprotein (306-313)
D P G Y P K M I A	50%	MΦ metalloelastase active form (309-317)
D P G Y P K M I A	50%	MMP 1 preproprotein variant (329-337)
D P G Y P K M I A	50%	Interstitial collagenase 2 (342-350)
D P P Y P R S I A Q W	38%	Vitronectin (458-469)

Figure 2.2. Sequence alignment and homology search result for the epitope (D570-A583) using protein BLAST® against the complete human proteome. The MMP2 epitope is shown in the first line (navy background). The top nine hits from the search with the highest sequence homology are shown in rows 2-10. Empty boxes represent completely mismatched residues.

In light of the challenges associated with inhibiting MMP2 catalytic activity, targeting the MMP2 zymogen activation process has emerged as a promising strategy.¹⁷⁻²⁰ As shown in Figure 2.3a, secreted proMMP2 must be cleaved by a membrane-tethered MMP to generate active MMP2.²¹

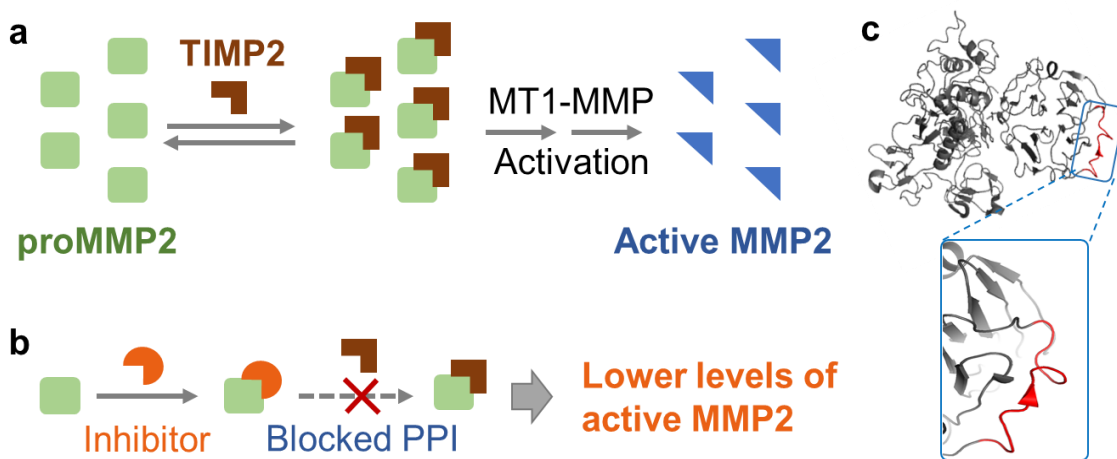


Figure 2.3. Mechanism of inhibiting MMP2 activation by blocking the TIMP2-proMMP2 interaction. (a) Simplified illustration of the MMP2 activation process. The binding between TIMP2 and proMMP2 is critical to MMP2 activation mediated by another enzyme, MT1-MMP. (b) Blocking the PPI between TIMP2 and proMMP2 can prevent MMP2 activation. (c) Crystal structure of proMMP2 as adapted from PDB: 1GXD. The TIMP2-binding region on proMMP2 (D570-A583, highlighted in red) appears to be a structureless coil.

In most cases, this activation process requires the formation of a ternary protein complex that consists of proMMP2, tissue inhibitor of metalloproteinases-2 (TIMP2), and membrane-bound MMP14 (also known as MT1-MMP).²²⁻²⁴ Structural studies led to the hypothesis that inhibiting this protein complex could prevent the cleavage of proMMP2 and consequently decrease the amount of active MMP2 (Figure 2.3b).²⁵

Indeed, previous studies have shown that anti-MT1-MMP antibodies could lower the production of active MMP2. In mice models, these antibodies demonstrated promising therapeutic effects.¹⁹ However, MT1-MMP's biological functions are not limited to MMP2 activation. Therefore, global MT1-MMP inhibition methods, such as the use of anti- MT1-MMP antibodies, still suffer from low specificity.²⁰ The only exception is the murine 9E8 monoclonal antibody, which selectively inhibits MT1-MMP's ability to activate MMP2.²⁰ Nevertheless, developing therapeutics from this murine antibody requires challenging humanization processes. Indeed, 7 years after its discovery, no further progress has been reported. Currently, there is a pressing need for molecularly well-defined compounds (such as small molecules and short peptides) that target this protein complex and specifically inhibit MMP2 activation.

To this end, we propose to target the protein–protein interaction (PPI) between TIMP2 and proMMP2 instead. Because this PPI is unique to MMP2 activation, inhibitors acting on this PPI will be highly specific. Moreover, this PPI interface involves a critical epitope (D570-A583 on proMMP2) that shares little sequence homology with other MMPs and the rest of the human proteome (Figure 2.2).²⁵ Therefore, a ligand that binds to this epitope promises less off-target effects. The technological difficulty here is that this epitope is structureless (Figure 2.3c) and it displays no binding pockets. Such a loop segment is a challenging target for traditional drug discovery strategies focusing on small molecules. As a result, almost 2 decades after the discovery of this PPI, a compound that can inhibit this PPI remains elusive.

Inspired by recent developments in cyclic peptide-based PPI inhibitors,^{26–34} we envisioned that we could address the unmet need using cyclic peptides. Herein, we report on a highly rigid cyclic peptide that specifically binds to the D570-A583 epitope of proMMP2 with a low nM affinity. We validated its ability to interfere with the TIMP2–proMMP2 interaction and tested its efficacy of modulating MMP2 activities using a human melanoma cell line.

2.2 Experimental

Materials

TentaGel S-NH₂ resin (loading capacity 0.28 mmol/g) was purchased from Rapp Polymere GmbH and Rink amide MBHA resin (loading capacity 0.678 mmol/g) from Aapptec (Louisville, KY). All of the Fmoc-protected amino acids were purchased from Anaspec (Fremont, CA) except Fmoc-L-propargylglycine (Pra) and FmocLys(N₃)-OH (Az₄), which were purchased from Chempep (Wellington, FL) and Chem-Impex (Wood Dale, IL), respectively. The coupling reagent 2-(1H-benzotriazol-1-yl)-1,1,3,3-tetramethyluronium hexafluorophosphate (HBTU, 99.6%) was obtained from Chem-Impex (Wood Dale, IL). Diisopropylethylamine (DIEA, 99.5%) was purchased from ACROS (Germany). Phenyl isothiocyanate (PhNCS) and triisopropylsilane (TIPS) were obtained from TCI (Portland, OR). Piperidine was purchased from Alfa Aesar (Ward Hill, MA). Cyanogen bromide (CNBr) and 5(6)-carboxyfluorescein were obtained from ACROS (Pittsburg, PA). Rhodamine B (Rhod), cuprous iodide (CuI), and α -cyano-4-hydroxycinnamic acid (CHCA) were obtained from Sigma-Aldrich (St. Louis, MO). 5-Bromo-4-chloro-3-indolyl-phosphate and nitro blue tetrazolium (BCIP/NBT) were

acquired from Promega (Madison, WI). Tris base, sodium phosphate dibasic anhydrous (Na_2HPO_4 , 99.6%), sodium phosphate monobasic monohydrate (NaH_2PO_4 , 99.4%), sodium chloride (NaCl), ascorbic acid, Tween 20, sodium dodecyl sulfate (SDS), bovine serum albumin (BSA), acetonitrile (CH_3CN), diethyl ether (Et_2O), chloroform (CHCl_3), ethyl acetate (EA), N,N' -dimethylformamide (DMF), and dichloromethane (DCM) were purchased from Thermo Fisher Scientific (Waltham, MA). Recombinant TIMP2 (125639) was purchased from Abcam (Cambridge, MA).

Preparative Reversed-Phase (RP) High-Performance Liquid Chromatography (HPLC)

Preparative HPLC was performed on a Thermo Ultimate 3000BX HPLC instrument, using a Phenomenex C18 reversed-phase preparative column (Kinetex 5 μm EVO, 250 \times 21.2 mm²). Nonlinear gradients of 0–100% acetonitrile (with 0.1% TFA) in water (with 0.1% TFA) were employed, and the gradient parameters were adjusted for each product to achieve desired separation efficiencies. A multiwavelength UV–vis detector was used to monitor the absorbance at 215, 280, 480, and 560 nm.

Analytical HPLC. The purity of the peptide was analyzed on a Thermo Ultimate 3000SD HPLC instrument, using a Phenomenex C18 reversed-phase analytical column (Kinetex 2.6 μm EVO, 250 \times 4.6 mm²). A gradient of 0–100% acetonitrile (with 0.1% TFA) in water (with 0.1% TFA) was employed with a flow rate of 1 mL/min. A UV–vis detector was used to monitor the absorbance at 280 or 560 nm. The purity of all cyclic peptides used for binding assays and biological activity assays was >95%.

Mass Spectrometry

The MS and MS/MS spectra were obtained using a SCIEX 5800 matrix-assisted laser desorption ionization time-of-flight (MALDI-TOF) mass spectrometer.

Solid-Phase Peptide Synthesis

The peptides were synthesized following the standard Fmoc SPPS coupling process. Unless otherwise noted, Rink Amide MBHA resin was used for the synthesis. To couple amino acids to the resin, the Fmoc group on the resin was first removed by 20% piperidine/DMF solution (10 min, three times). Fmoc-AA-OH (3 equiv), DIEA (5 equiv), and HBTU (2.8 equiv) were mixed in DMF for 10 min, and the solution was then introduced to the deprotected resin. The mixture was gently agitated at room temperature for 1 h, followed by draining and washing (DMF, methanol, and DCM, three times each). To label the peptides with fluorophores, poly(ethylene glycol) (PEG), or biotin, the corresponding dye-COOH, Fmoc-PEG-OH, and biotin were coupled at the Nterminal using the SPPS procedure described above.

For constructing cyclic peptides, Fmoc-propargylglycine-OH (Pra) and Fmoc-azidolysine-OH (Az4) were inserted at the N and C terminals, respectively. A Cu-catalyzed click reaction was used for cyclization. Specifically, resins were incubated in 20% piperidine/ DMF with CuI (2.5 equiv) and L-ascorbic acid (5 equiv) at room temperature overnight. After cyclization, the beads were washed with sodium diethyldithiocarbamate (5% w/v) and DIEA (5% v/v) in DMF to remove the copper catalyst. To cleave peptides off from the resin, a cleavage solution composed of TFA/TIPS/ddH₂O (95:2.5:2.5) was used. The crude peptides were purified by

preparative RP-HPLC, and the product purity and identity were confirmed by analytical RP-HPLC and mass spectrometry.

One-Bead–Two-Compound (OBTC) Library Construction

The one-bead–two-compound peptide library was constructed using the split-and-pool strategy on TentaGel S-NH₂ resins. Methionine was first coupled to the resin, followed by glycine. Then, Az4 was coupled at 80% loading capacity. Eighteen natural amino acids (Ala, Arg, Asn, Asp, Gln, Glu, Gly, His, Ile, Leu, Lys, Phe, Pro, Ser, Thr, Trp, Tyr, and Val, all L-stereoisomers) were used as building blocks for the subsequent five randomized positions, and a Pra residue was attached at the N-terminal. The library was cyclized, as described above. Afterward, an additional Pra was attached to the N-terminal. The protecting groups were removed as described above. The deprotected resins were then washed with DMF, methanol, and DCM and kept under Argon for further use.

OBTC Library Screening. The precleared library (see the Supporting Information) was incubated with 10 μ M biotinylated epitope (biotin-PEG5-D-P-G-F-P-K-L-I-A-D-A-W-N-A-Az4) in 0.1% BSA/TBST at room temperature for 6 h. The library was then washed with 0.1% BSA/TBST, TBST, and TBS solution and incubated with 7.5 M guanidine-HCl (pH 2.0) at room temperature for 2 h. Afterward, the beads were washed with water and incubated overnight in 1% BSA/TBST at 4 °C. The library was then incubated with streptavidin-AP (1:10 000 dilution) and its substrate BCIP/NBT, giving rise to dark purple hit beads. After incubation, the resins were washed with HCl (pH 2.0) to quench the reaction and then with 0.1% BSA/TBST (5 min \times 3) at 4 °C. The colored hits were

then picked out; washed with 7.5 M guanidine-HCl (pH 2.0), water, DMF, and DCM; and dried under vacuum. Sequencing of the Hits.

Sequencing of the Hits : Edman Degradation

The first round of Edman degradation was performed to remove the click handle that was conjugated to the epitope.³⁵ The hit beads were transferred into a glass vial with 50 μ L of 2.5% PhNCS in pyridine/H₂O (1:1) solution and flushed with Ar for about 15 s. The vial was then placed in a water bath at 50 °C for 30 min, and the solution was removed. The beads were then washed with ethyl acetate (three times) and DCM (once) and air-dried. Subsequently, 100 μ L of TFA solution was added to the vial, flushed with Ar, and left for incubation in the water bath for 10 min at 50 °C. Afterward, the solution was removed, and the beads were washed three times with ethyl acetate and then with DCM. These procedures were repeated for another round of Edman degradation. Later the beads were incubated with a 20% TFA/water solution and heated at 60 °C for 15 min. After 15 min, the solution was removed, and the beads were washed with ethyl acetate and DCM and then air-dried.

Cleavage

After the Edman degradation, individual beads were transferred into a microcentrifuge tube containing 10 μ L of water and 10 μ L of a 0.50 M CNBr/0.2 M HCl solution. The tubes were microwaved for 1 min and dried using a centrifugal vacuum chamber at 45 °C.³⁶

Sequencing by MALDI-TOF MS/MS.

First, 0.55 μL of a 4 mg/mL α -cyano-4-hydroxycinnamic acid (CHCA) solution (50:50 ACN/ water with 0.1% TFA) was added in each microcentrifuge tube. The mixture was spotted on a 384-spot MALDI sample plate and air-dried. The MS/MS spectra were obtained on a SCIEX 5800 mass spectrometer and analyzed using mMass to solve for the sequences.³⁷

FRET Binding Assay

The fluorescein-labeled epitope was incubated with varying concentrations of the rhodamine-tagged cyclic peptides. The final concentration of the Fluo-epitope was kept at 100 nM in all samples. Then, 65 μL of the mixed solution was placed in a Greiner black 384-well low binding plate and incubated for 30 min. The FRET intensities were measured using a Synergy H1 microplate reader. For the competitive FRET assay, the concentrations of the epitope and the rhodamine-tagged cyclic peptide were kept at 100 nM in all samples, and the concentration of the unlabeled cyclic peptide (the competitor) was varied. Furthermore, 65 μL of the mixtures was added into a Greiner black 384-well low binding plate and incubated at room temperature for 30 min. The FRET intensities were measured using a Synergy H1 microplate reader. All of the FRET experiments were performed using individually prepared triplicate samples. The values from the triplicate were averaged and analyzed. Every experiment was independently repeated at least three times on different days, and a consistent trend was observed. Representative experiment results are presented in the paper.

proMMP2 Expression and Purification. The cDNA fragment encoding full-length human proMMP2 was inserted into an in-house expression vector in which it was N-terminally fused to a hexahistidine (His6)-MBP tag and a tobacco etch virus (TEV) protease cleavage site. The resulting plasmid was transformed into BL21(DE3) RIL cells (Novagen Inc.). After the cell density reached an optical density at 600 nm (OD 600) of ~0.8, the protein expression was induced by 0.4 mM isopropyl β -D-1-thiogalactopyranoside (IPTG) and the cells continued to grow at 18 °C overnight. The cells were harvested and lysed in a buffer containing 25 mM Tris-HCl (pH 7.5), 25 mM imidazole, 1 M NaCl, 5% glycerol, and 1 mM PMSF. The proMMP2 fusion protein was first purified using a nickel column and eluted with a buffer containing 25 mM Tris-HCl (pH 7.5), 300 mM NaCl, 5% glycerol, and 300 mM imidazole. Subsequently, the eluted protein sample was supplemented with 5 mM dithiothreitol (DTT) and incubated with TEV protease overnight. The tag-free MMP2 protein was further purified by ion-exchange chromatography on a Q HP column (GE Healthcare) and size-exclusion chromatography on a Hiload 16/600 Superdex 200 pg column (GE Healthcare) preequilibrated with a buffer containing 20 mM Tris-HCl (pH 7.5), 250 mM NaCl, 5% glycerol, and 5 mM DTT. The final protein sample was stored at -80 °C in a freezer before use.

FP Binding Assay

The rhodamine-tagged ligand Rhod-cy- (WPHPY) was mixed with varying concentrations of the recombinant proMMP2 protein in PBS. The final concentration of Rhodcy(WPHPY) was kept at 100 nM in all samples. Then, 65 μ L of the mixture was

added in a Greiner black 384-well low binding plate and incubated at room temperature for 30 min. The fluorescence polarization values were measured with a Synergy H1 microplate reader. For the competitive polarization assay, the concentrations of the recombinant protein and Rhod-cy(WPHPY) were kept at 100 nM in all samples. The concentration of the unlabeled ligand cy(WPHPY) was varied. The mixtures were added into a Greiner black 384-well plate, and the fluorescence polarization values were measured with a Synergy H1 microplate reader. All of the FP experiments were performed in triplicates using individually prepared samples, and the results from the triplicates were averaged and analyzed. Each experiment was repeated at least three times on different days, and consistent trends were observed. Representative results are presented in the paper.

Conformational Search and Molecular Dynamics Simulation

To study the properties of cy(WPHPY) in silico, conformational search and molecular dynamics simulation were performed. The standard amino acid part of the peptide (WPHPY) was parameterized with the protein.ff14SB force field.³⁸ The organic linkage that connects the amino acid was built by Avogadro v1.2.0 and then processed by Antechamber to calculate the AM1-BCC charge and assign the gaff2 force field parameters.³⁹⁻⁴¹ After the amino acids and the small organic fragment were parameterized, they were assembled using xleap from AmberTools18.⁴² The topology and coordinate files for the hybrid peptide were saved as prmtop and inpcrd files, which were converted into counterpart top and crd files, respectively, using the script provided

in the VM2 package.⁴³ The whole peptide was treated as a flexible set to enable a thorough conformational search by using the VM2 package.

For the molecular dynamics simulation, the selected conformation of the peptide was immersed in a rectangular box of TIP3P water molecules with a margin distance of 12.0 Å.⁴³ The solvated box was further neutralized with a Cl⁻ counter ion using the tleap program. The water molecules and the whole system then went through a 3000- step and 5000-step minimization to correct any inconsistencies, respectively. Next, we relaxed the system by slowly heating it up during an equilibrium course of 1 ns at 50, 100, 150, 200, 250, and 298 K. By using the GPU accelerated pmemd.cuda code in Amber18, 20 ns simulations were performed at 298 K in an NPT (isothermal– isobaric) ensemble.⁴⁵ Particle mesh Ewald (PME) was employed to calculate the long-range electrostatic interactions, and the nonbonded energy cutoff was set to 10.0 Å.⁴⁶

Cell Culture

The human metastatic melanoma cell line, WM115, was a gift from Prof. Yinsheng Wang (UC Riverside). It was cultured in Dulbecco's modified Eagle's medium (DMEM, Corning) supplemented with 10% heat-inactivated fetal bovine serum (FBS, Gibco) and 100 U/mL penicillin/streptomycin (Sigma). Cells were cultured under 5% CO₂ in a 37°C incubator. A trypsin-EDTA solution (0.05%, Sigma) was used for passaging once the cells reached 80–90% confluency.

Enzyme-Linked Immunosorbent Assay (ELISA)

A 96-well Nicoated plate was incubated with His-tagged recombinant TIMP2 protein (9 pmol/well) for an hour at room temperature. Afterward, the protein solution was

removed, and the plate was washed three times with PBST (phosphate buffer saline, 0.05% Tween 20). To minimize any nonspecific binding, the plate was blocked with His6 peptide (9 pmol/well) for an hour at room temperature and washed with PBST three times.

WM115 cells were cultured to 80% confluency and then incubated in serum-free media for 24 h. The culture media were collected and concentrated using centrifugal membrane filters (10 kDa cutoff, Amicon). The concentrated media were aliquoted at 200 μ L each. PBS solutions of cy(WPHPY) with varying concentrations of cy(WPHPY) (20 μ L) were mixed with the aliquots. For the positive control, PBS was mixed with the aliquot. The mixtures were added into the above-mentioned 96-well plate. The plate was incubated on an orbital shaker at room temperature for an hour. Then, the wells were washed with PBST, and 100 μ L of MMP2 primary antibody solution (Rabbit mAb, #40994, Cell Signaling Technology, 1:200 in 5% BSA/PBST) was added into each well. The plate was incubated at room temperature for an hour and then washed with PBST three times. Furthermore, 100 μ L of secondary antibody (Goat Anti-Rabbit IgG, HRP-linked, ab97051, Abcam, 1:10 000 in 5% BSA/PBST) was added into each well, and the plate was incubated for another hour at room temperature. To generate luminescence readouts, the wells were washed with PBST three times, and then a luminol substrate was added into the wells (SuperSignal West Pico PLUS Chemiluminescent Substrate, Thermo). The luminescence was quantified using a SYNERGY H1 microplate reader (Biotek) after 5 min of additional incubation. For each cy(WPHPY) concentration, three individually prepared replicates were used, and the luminescence values were averaged and reported.

To ensure reproducibility, this ELISA experiment was independently repeated three times with a different plate each time, and consistent results were observed.

Fluorogenic Substrate Assay

WM115 cells were cultured in full media to 80% confluency. Afterward, the media were replaced by serum-free media, and the cells were cultured for another 24 h. The media were then collected and concentrated with centrifugal membrane filters (10 kDa cutoff, Amicon). Once concentrated, the total protein content was quantified using a bicinchoninic acid (BCA) assay kit (Thermo) and normalized. In a 96-well microplate, 10 μL (1 $\mu\text{g}/\mu\text{L}$ protein content) of the media was mixed with 90 μL of a tenascin C (TNC) assay buffer (50 mM Tris base, 0.15 M NaCl, 10 mM CaCl₂, pH 7.5) and 10 μL of cy(WPHPY) (varying concentrations in PBS). For the positive control sample, 10 μL of the TNC assay buffer was added in place of cy(WPHPY). The plate was left for 5 min at 37 °C for equilibration, and 100 μL of MMPspecific substrates (Sigma, 3 μM) was added in the mix.⁴⁷ The plate was then incubated at 37 °C for 20 min. The fluorescence was measured using a SYNERGY H1 microplate reader with an excitation wavelength of 325 nm and an emission wavelength of 393 nm.

For the experiment shown in Figure 2.38c, the same procedure was followed as that described above. The difference was that an additional 10 μL of the recombinant TIMP2 (1 $\mu\text{g}/\mu\text{L}$ in PBS) was added to all of the mixtures.

For the experiment shown in Figure 2.38e,f, WM115 cells were cultured in full media to 80% confluency. Afterward, the media were changed to serum-free media containing varying concentrations of cy(WPHPY), and the cells were cultured for 24 h. The control

sample contained no cy(WPHPY). The media were then collected, concentrated, and quantified as described above. In a 96-well microplate, 10 μL (1 $\mu\text{g}/\mu\text{L}$ protein content) of the media was mixed with 90 μL of the TNC assay buffer and 100 μL of MMP-specific substrates (Sigma, 3 μM). The plate was then incubated at 37 $^{\circ}\text{C}$ for 20 min, and the fluorescence was measured as described above.

In every fluorogenic substrate experiment, three individually prepared replicates were used for each cy(WPHPY) concentration (including control), and the averaged values from the replicates were reported. To ensure reproducibility, all experiments were independently repeated three times, using fresh substrate each time. Consistent trends were observed.

Gelatin Zymography

In a 6-well plate, 600 k cells were seeded in full DMEM medium containing 10% FBS and 1% PS. After 8 h, each well was washed twice with serum-free media. Then, 2 mL of serum-free media containing different concentrations of cy(WPHPY) was added into the wells. For the positive control, no cy(WPHPY) was added. The plate was kept in the 5% CO₂ incubator at 37 $^{\circ}\text{C}$ for 24 h. Afterward, the media were collected and concentrated using centrifugal membrane filters (10 kDa cutoff, Amicon). The protein content in each of the samples was quantified using a BCA assay kit (Thermo), and the solutions were normalized accordingly to reach a concentration of 10 $\mu\text{g}/\text{mL}$ in each sample. A 7.5% acrylamide gel was prepared using 2 mL of gelatin (4 mg/mL in water) and a 1 mm electrophoresis plate. Then, 10 μL of the sample (10 $\mu\text{g}/\text{mL}$ protein content) was added into each well, and a standard protocol was followed for running the gel.⁴⁸ After the run,

the gel was washed (2×30 min) with washing buffer (pH 7.5, 2.5% Triton X-100, 50 mM Tris-HCl, 5 mM CaCl₂, 1 μ M ZnCl₂) at room temperature and then kept in the incubation buffer (1% Triton X-100, 50 mM Tris-HCl, 5 mM CaCl₂, 1 μ M ZnCl₂) for 10 min at 37 °C. Later the buffer was replaced with a new incubation buffer and was kept in the incubator at 37 °C for 20 h. After incubation, the gel was washed using a washing buffer and was stained using a 0.3% Coomassie blue water solution (containing 4% methanol and 1% acetic acid) for 30 min at room temperature. Afterward, the gel was washed with H₂O to remove the excess coloring. Then, the gel was incubated in the destain solution (4% methanol and 1% acetic acid in H₂O) until the bands on the gel became clear. Following this process, we carried out three independent experiments. All three experiments showed similar results. A representative result is presented in Figure 2.38d.

Western Blot

WM115 cells were treated with different concentrations of the ligand in serum-free media for 24 h. For the positive control, PBS was added instead of the ligand. After preparing the samples, western blot was carried out following standard protocols.⁴⁹ The antibodies (#13132, Cell Signaling Technology; ab97051, Abcam) were used at 1:1000 and 1:10000 dilutions, as recommended by the manufacturers. The resulting membrane was developed using SuperSignal West Pico PLUS chemiluminescent substrate (Thermo Scientific), and the image was taken using an Odyssey Fc imaging system (LI-COR Biosciences, Lincoln, NE). We followed this process to run three independent western blots, with freshly collected medium samples from new batches of cells each time. All

three experiments showed similar results, and a representative one is presented in Figure 2.38d.

Immunofluorescence and Confocal Imaging

WM115 cells were cultured in 6-well plates in full media until reaching the desired confluency. For cy(WPHPY)-treated cells, cy(WPHPY) was added to reach a final concentration of 10 nM, and the cells were incubated for 15 h. The cells were fixed using 4% paraformaldehyde at room temperature for 15 min. Note that no membrane permeabilizer (such as Triton X-100) was used here because we wanted to assess membrane-associated MMP2. Subsequently, fixed cells were washed with PBS (three times) and blocked in a blocking buffer (PBS + 5% normal goat serum) for 1 h at room temperature. Afterward, cells were incubated with a 1:500 dilution of anti-MMP2 (#40994, Cell Signaling Technology) in the blocking buffer overnight at 4 °C and washed with PBS (three times). Then, cells were incubated with a 1:2000 dilution of Alexa Fluor 594-conjugated goat anti-rabbit IgG (#8889, Cell Signaling Technology) in the blocking buffer for 2 h at room temperature and washed thoroughly with PBS.

To image the cells, a Zeiss 880 inverted confocal laser scanning microscope (Carl Zeiss, Germany) was used. Image acquisition and analyses were carried out using the manufacturer's software (ZEN, Carl Zeiss). Quantification of fluorescence intensity in single cells was performed using Fiji software. Thirty single cells were analyzed for each image. The experiment was repeated three times, with different WM115 cells each time. Consistent results were observed, and the representative images are presented in Figure 2.38.

Scratch Wound-Healing Assay. The scratch assay was performed in 6-well plates. To coat the wells with gelatin, 2 mL of a 0.1% gelatin/H₂O solution was added into each well, and the plates were incubated at 37 °C for 2 h. Afterward, the gelatin solution was removed, and the wells were washed with PBS three times. WM115 cells were seeded into the wells and cultured in media containing 0.3% FBS. When the cells reached 90% confluency, 3 µg/mL mitomycin C (Sigma-Aldrich) was added and incubated for 3 h to stop cell proliferation. A 10 µL pipet tip was used to create scratch wounds in a straight line. The wells were then washed three times with serum-free media. Subsequently, serum-free media containing different concentrations of cy(WPHPY) were added in the wells. For a positive control, no cy(WPHPY) was added. The cell images were immediately taken (0 h). During the imaging process, once a spot was selected, the area was marked so that the same spot could be located and imaged after 24 h. The cells were incubated at 37 °C for 24 h, and the images were retaken at the marked locations. This process was followed to carry out three independent scratch assays, all of which showed similar results. The representative result is presented in Figure 2.45b.

Cell Migration and Invasion Assay

The 24-well plates with inserts were purchased from Corning (8.0 µm, pore size; 6.5 mm, diameter; and 0.33 cm², growth area) and the ECM gel from SigmaAldrich. The cell culture insert was coated with 100 µL of the ECM gel (2 mg/mL) and left in the 5% CO₂ incubator at 37 °C for 30 min. The excess gel solution was removed carefully, and the insert was washed gently with serum-free media twice. Then, 100 µL of the WM115 cell suspension (200 k cells in serum-free media) was added into the gel-coated insert. Full

medium with 10% FBS was added to the lower chamber, and the insert was placed into the wells. Furthermore, 100 μ L of the cy(WPHPY) solution in serum-free media was added into the insert chamber. For a positive control, serum-free medium with no ligand was added to the chamber. The assembly was kept in the cell incubator for 24 h. The insert was then removed from the well and washed three times with PBS. The cells were fixed with a 4% paraformaldehyde solution in PBS (10 min at room temperature). After the removal of the paraformaldehyde solution, the insert was washed three times with PBS. The insert was then incubated in methanol for 20 min at room temperature and then washed three times with PBS. After that, a 0.2% crystal violet/ methanol solution was added, and the insert was incubated for 15 min at room temperature. The staining solution was removed, and the insert was washed three times with PBS. Cells above the membrane (noninvasive cells) were scraped off, and the cells beneath the membrane were imaged using an inverted microscope. Three independent experiments were performed to ensure reproducibility, and individually prepared triplicate samples were used in each experiment. All of the experiments showed similar results, and a representative result is shown in Figure 2.45d.

Data and Statistical Analysis

Results from the triplicate measurements are reported as average \pm standard deviation. The binding assay (FRET and FP) results were processed using OriginPro 2019 software. A Hill function was used for fitting the binding curves and calculating the K_d . For the single-cell immunofluorescence analysis, the p-value was calculated using a Mann–Whitney test.

2.3 Results and Discussion

Epitope-Targeted Library Screening Generated Hit Sequences

To identify compounds that can bind to the D570- A583 epitope, we performed a high-throughput screening using a one-bead–two-compound monocyclic/linear peptide library.^{26,50} We constructed this library through five iterations of split-and-pool processes, using 18 natural amino acids as building blocks (Figure 2.4a). We used Cu-catalyzed alkyne– azide cyclization and installed an extra N-terminal alkyne group (Figure 2.5).^{26,50} We removed the sequences that nonspecifically bound to a panel of dyes and proteins and screened this precleared library against a biotinylated D570-A583 epitope bearing an azide group (Figures 2.6 and 2.7). A strong binding between the synthetic epitope and a peptide sequence would promote a proximity-induced click reaction, allowing for hit identification through the biotin tag (Figure 2.7). The hit sequences were then determined by mass spectrometry, following established protocols.^{26,50} This screening generated 15 hit sequences, including four leucine/isoleucine isomers (Figure 2.4b).

To validate the identified hits, we conjugated the hits to rhodamine B (Rhod) and the epitope to fluorescein (Fluo) (Figures 2.8–2.23). Binding between the cyclic peptide and the epitope would bring the two fluorophore tags into proximity, which would generate a Förster resonance energy transfer (FRET) signal. Therefore, we could evaluate binding affinities by titrating Fluo-epitope with Rhod-peptide and analyzing the FRET signals. As shown in Figure 2.4c, 7 of the 15 sequences bound to the epitope with low micromolar affinities (Figure S22). We chose Rhod-cy(WPHPY) for further studies because it showed the highest binding affinity (Figure 2.4d).

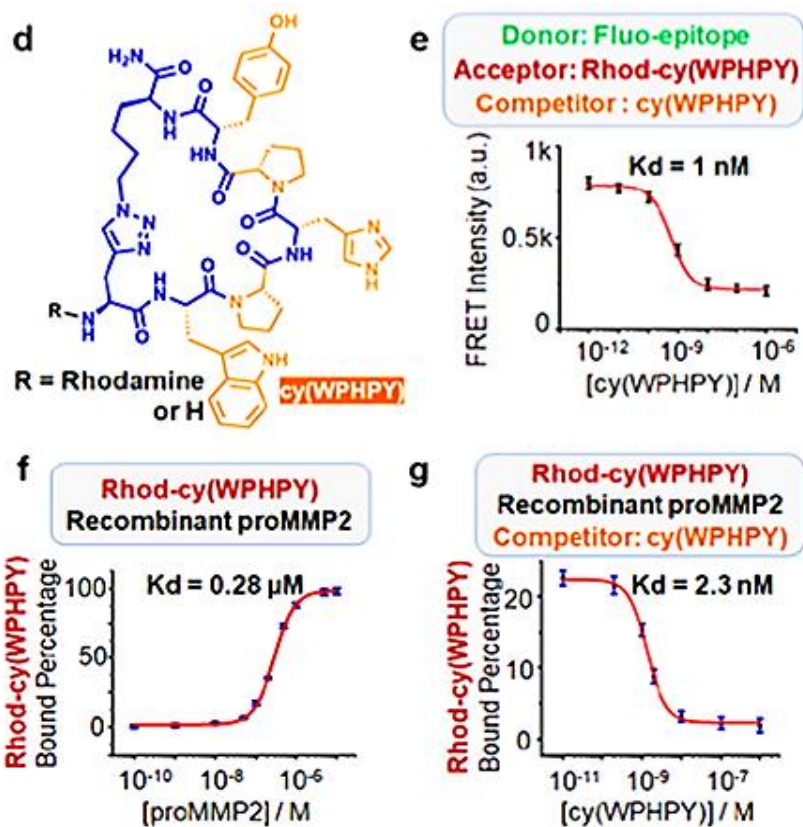
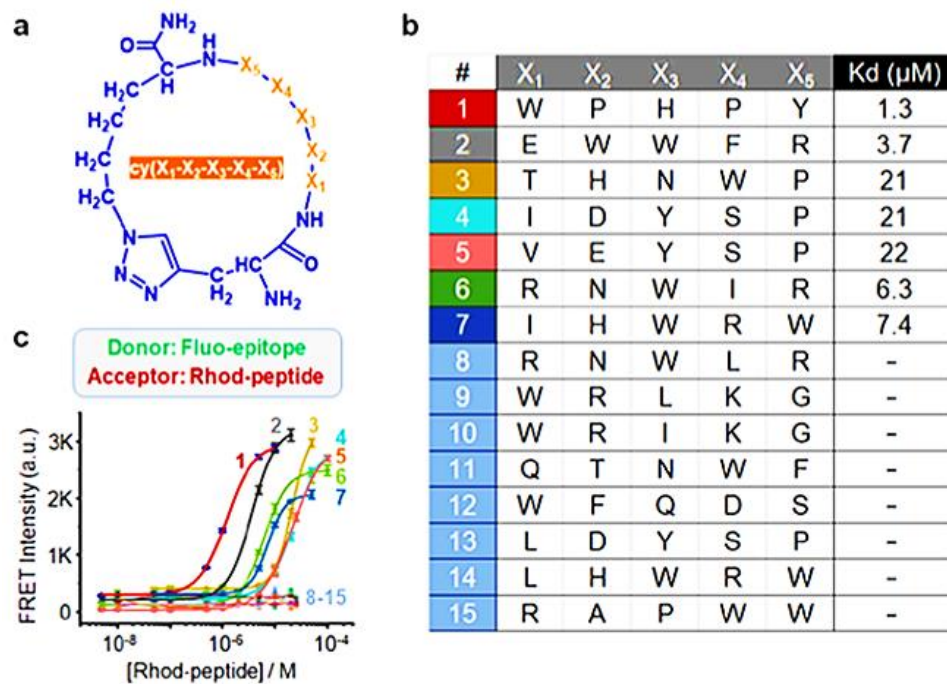


Figure 2.4. Validation of the hit sequences generated from library screening. (a) Generic structure of the cyclic peptide library. (b) Identified hits from the screening. (c) Förster resonance energy transfer (FRET) signals generated from the binding between 100 nM fluorescein-labeled epitope (Fluo-epitope) and varying concentrations of rhodamine B-modified ligand (Rhod-peptide). (d) Structure of cy(WPHPY) with and without the rhodamine B tag. (e) Competitive FRET results obtained using 100 nM Fluo-epitope, 100 nM Rhod-cy(WPHPY), and varying concentrations of cy(WPHPY) as the donor, acceptor, and competitor, respectively. The interaction between unlabeled cy(WPHPY) and Fluo-epitope displaced Rhod-cy(WPHPY), causing decreased FRET signals. (f) Fluorescence polarization (FP) assay results demonstrating the binding affinity between Rhod-cy(WPHPY) (100 nM) and the full-length recombinant proMMP2. (g) Competitive FP results demonstrating the binding between the unlabeled cy(WPHPY) and recombinant proMMP2 (100 nM). Here, the unlabeled cy(WPHPY) displaced Rhod-cy(WPHPY) (100 nM) and led to decreased FP values.

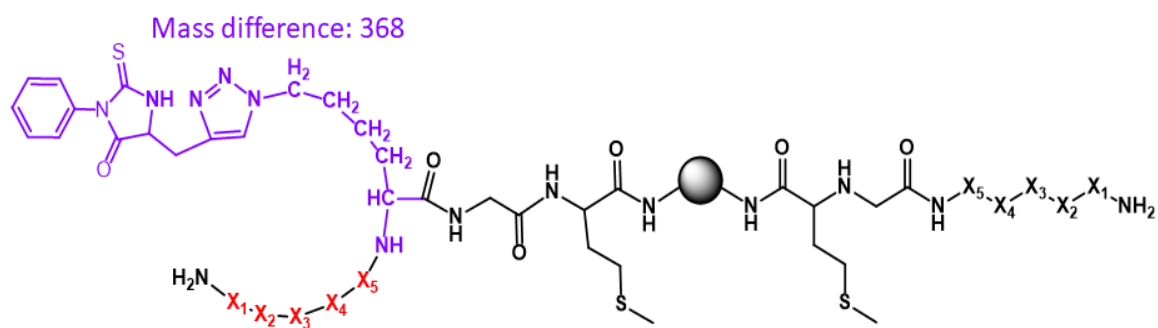
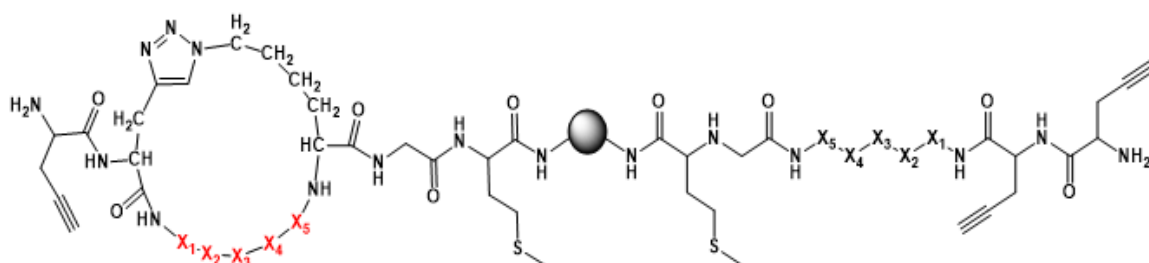


Figure 2.5. (Top) The generic structure of the one-bead-two-compound 80% Cyclic and 20% linear peptide library. X1-X5: comprehensive 18 natural L-amino acids, excluding Cys and Met. The library was built using 90 μm -sized TantaGel® S-NH₂ resins. Lower) After two steps of Edman degradation, the cyclic sequence contains a PTH moiety, while the linear one does not. A mass difference of 368 can be observed on the corresponding MS spectrum.

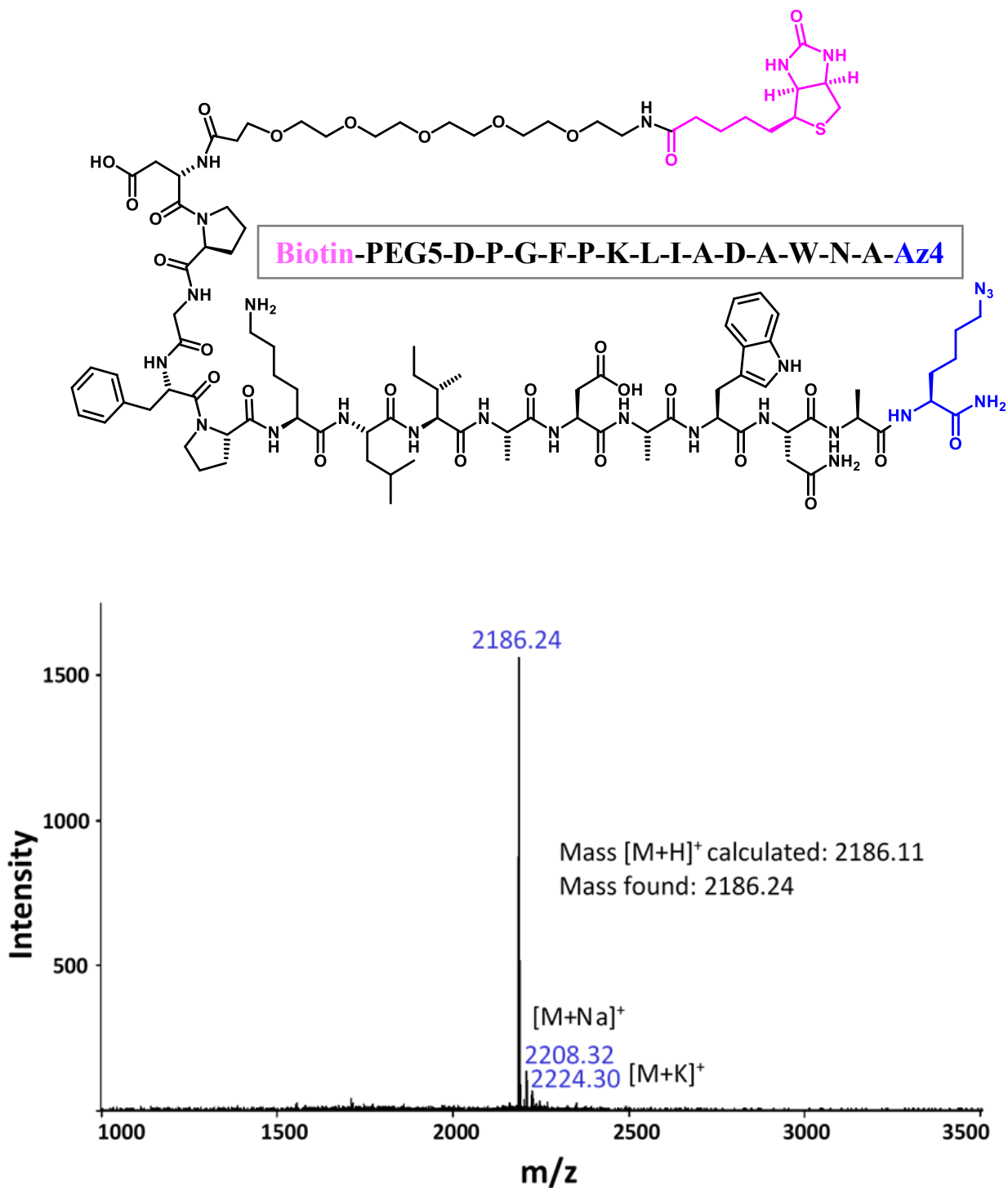


Figure 2.6. Structure and MALDI-TOF mass spectrum of the biotinylated epitope used in the library screening (Az4: L-azidolysine).

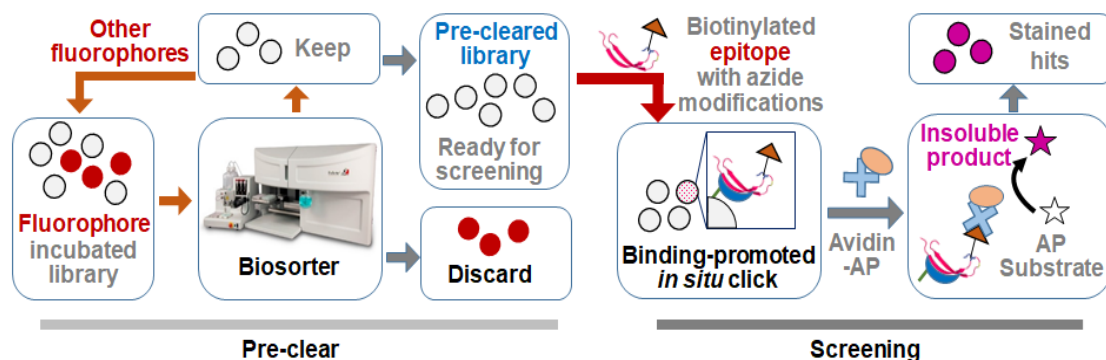


Figure 2.7. Schematic illustration of the automated pre-clear procedure and epitope targeting library screening strategy. The library was pre-cleared using a fluorescence-activated BioSorter® and a panel of fluorophores and fluorescently labeled proteins. The pre-cleared library was then screened against the biotinylated epitope. A binding between the epitope and the hit sequences promoted an in situ click reaction, which anchored biotin tags on the resin. The hits were then identified through the biotin tag by using the avidin-alkaline phosphatase (AP) and its colorimetric substrate BCIP (5-bromo-4-chloro-3'-indolyphosphate p-toluidine salt) /NBT (nitroblue tetrazolium chloride). The stained hits were picked out and processed for sequencing.

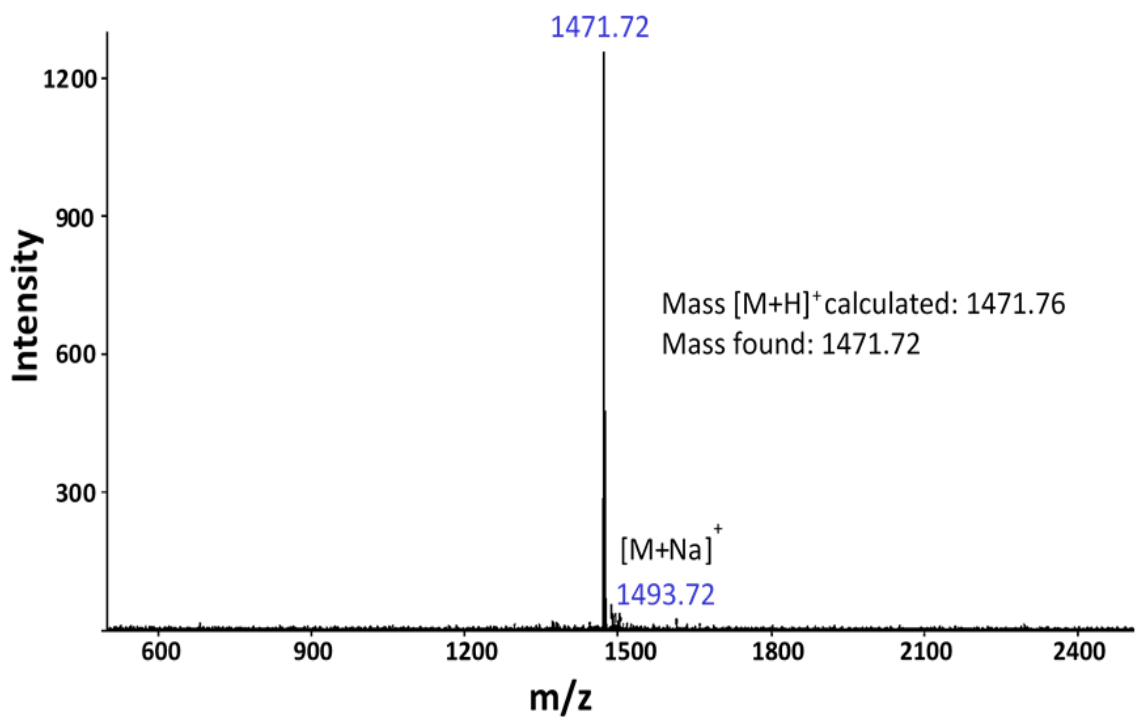
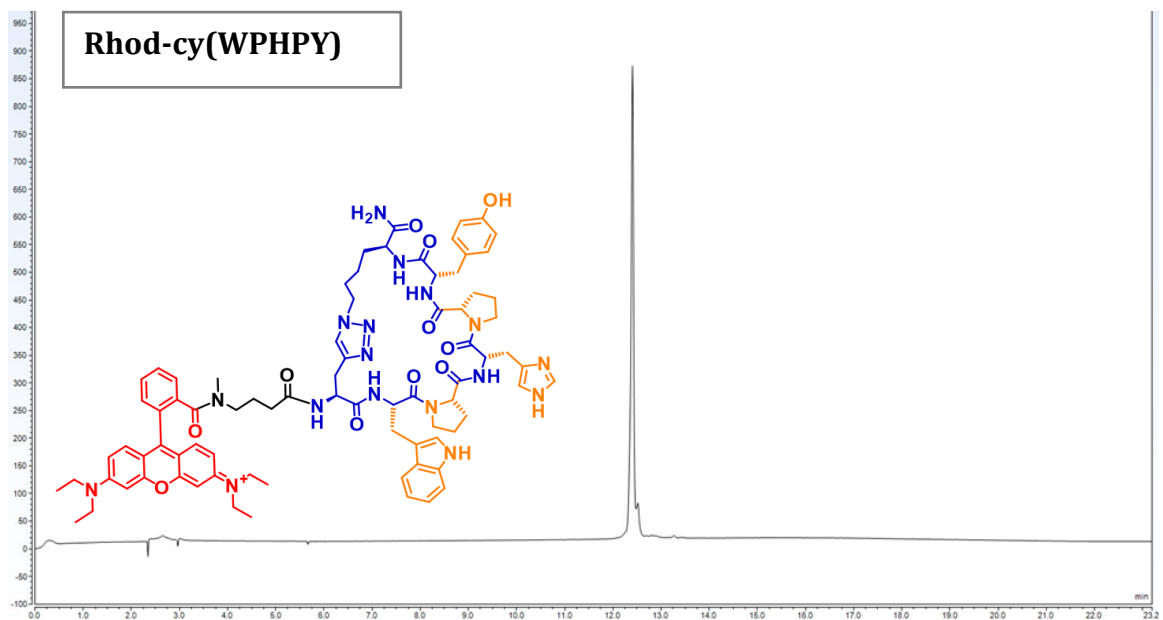


Figure 2.8. HPLC chromatogram (560 nm absorption) and MALDI-TOF mass spectrum for Rhod-cy(WPHPY).

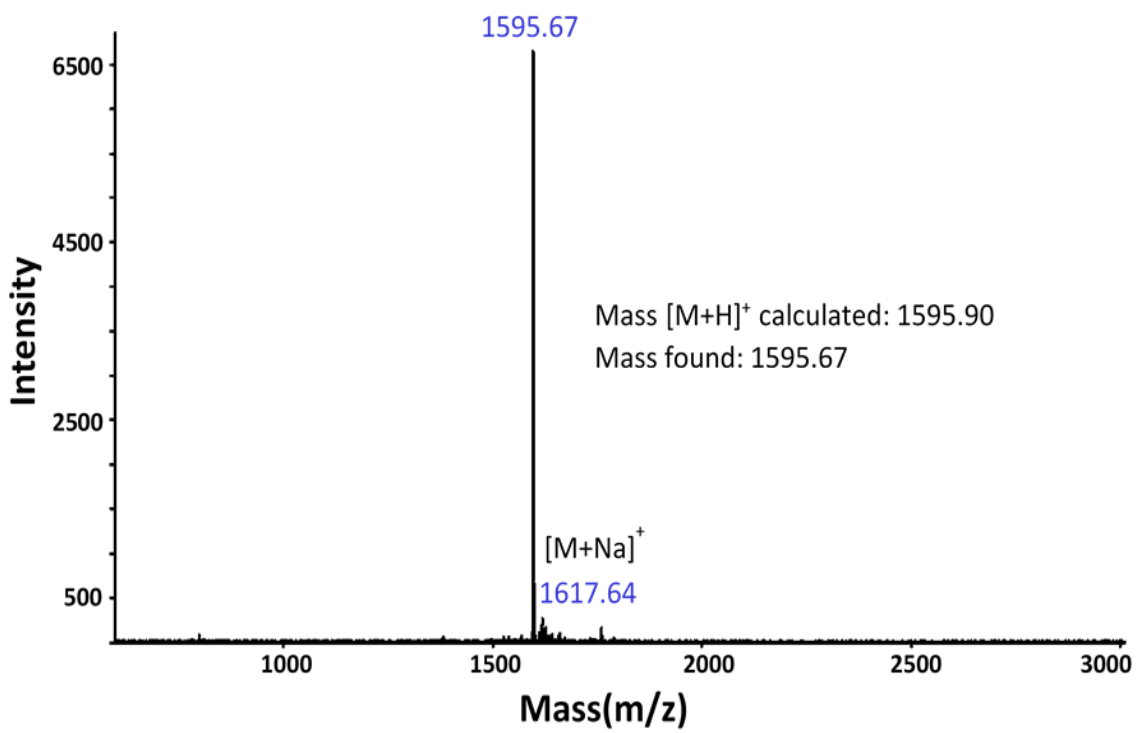
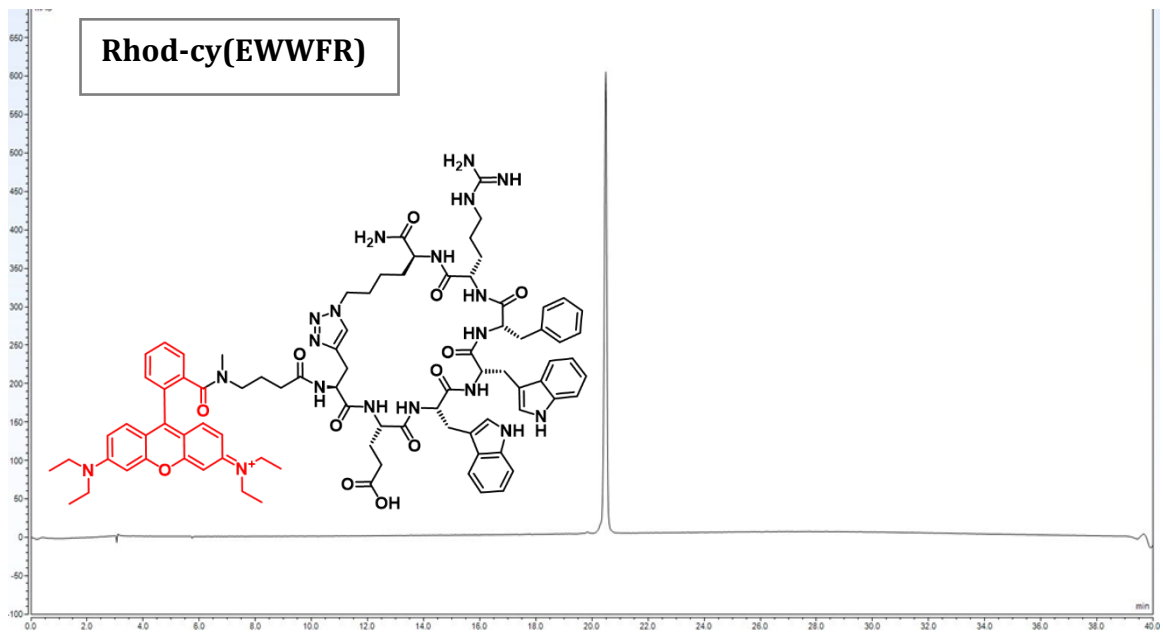


Figure 2.9. HPLC chromatogram (560 nm absorption) and MALDI-TOF mass spectrum for Rhod-cy(EWWFR).

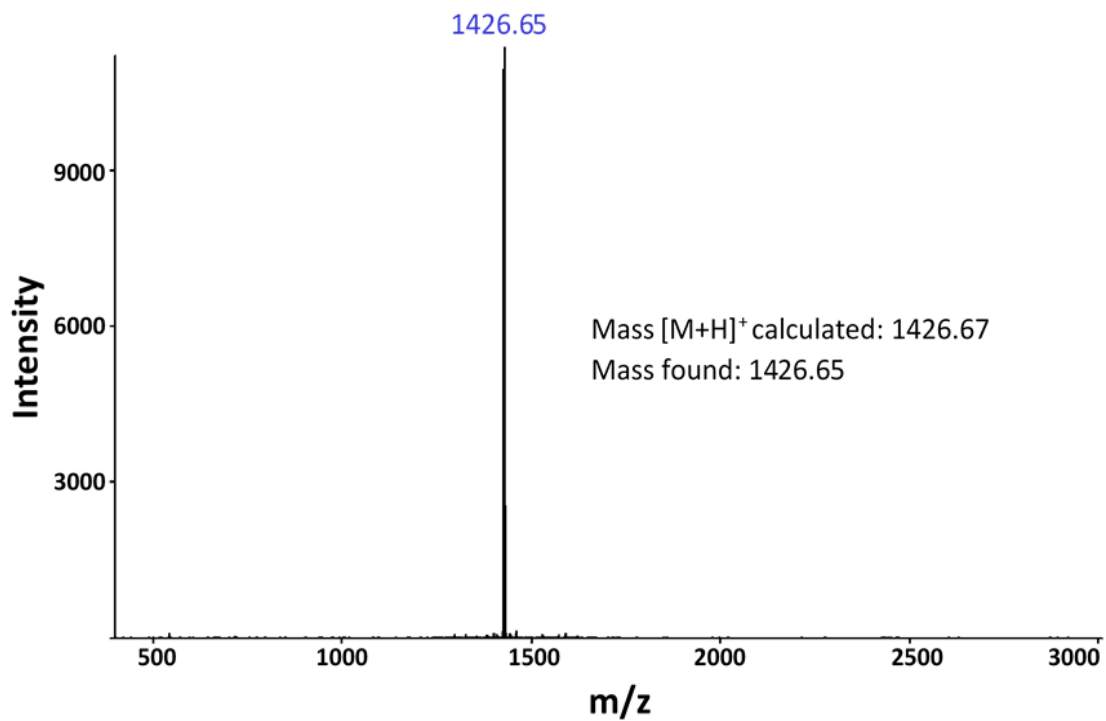
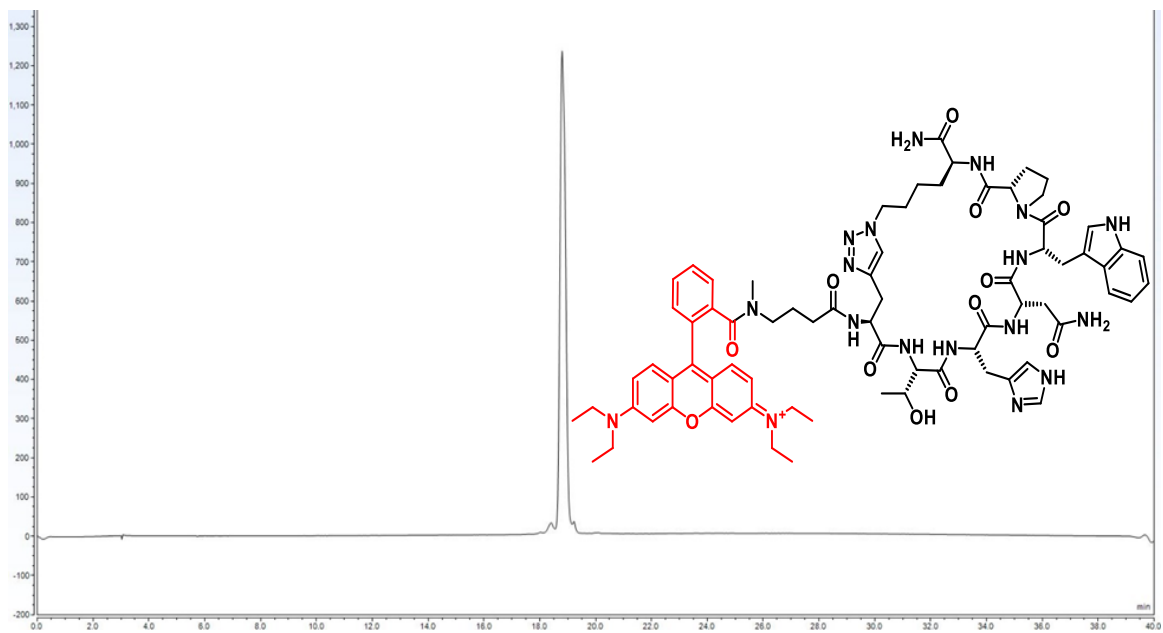


Figure 2.10. HPLC chromatogram (560 nm absorption) and MALDI-TOF mass spectrum for Rhod-cy(THNWP).

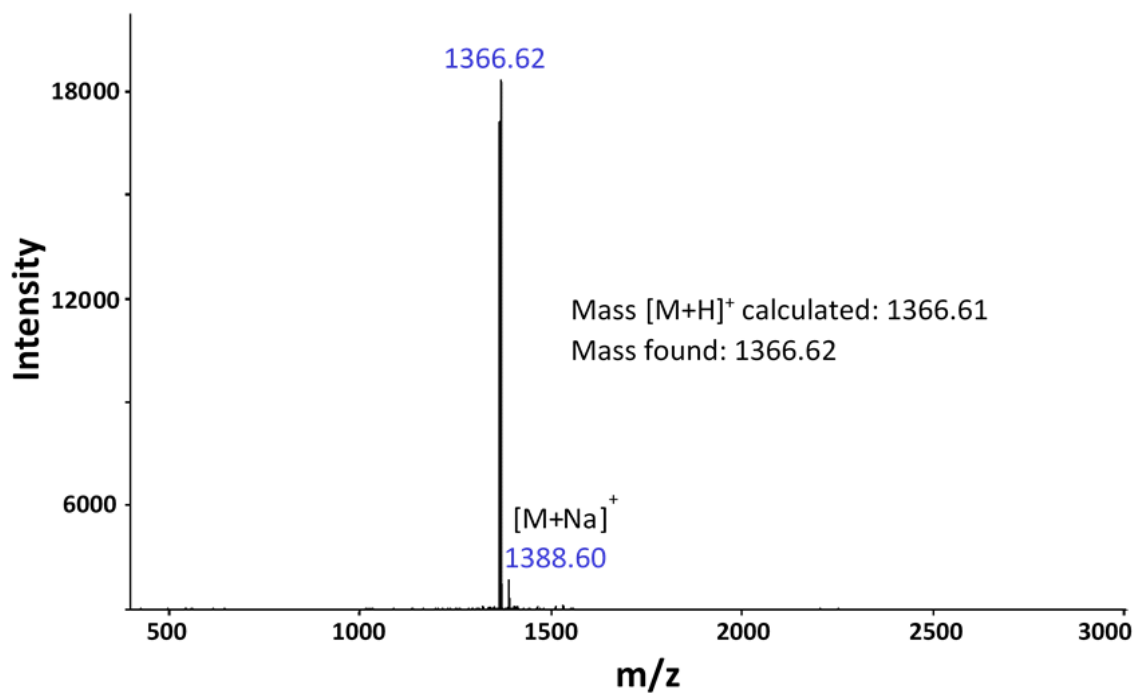
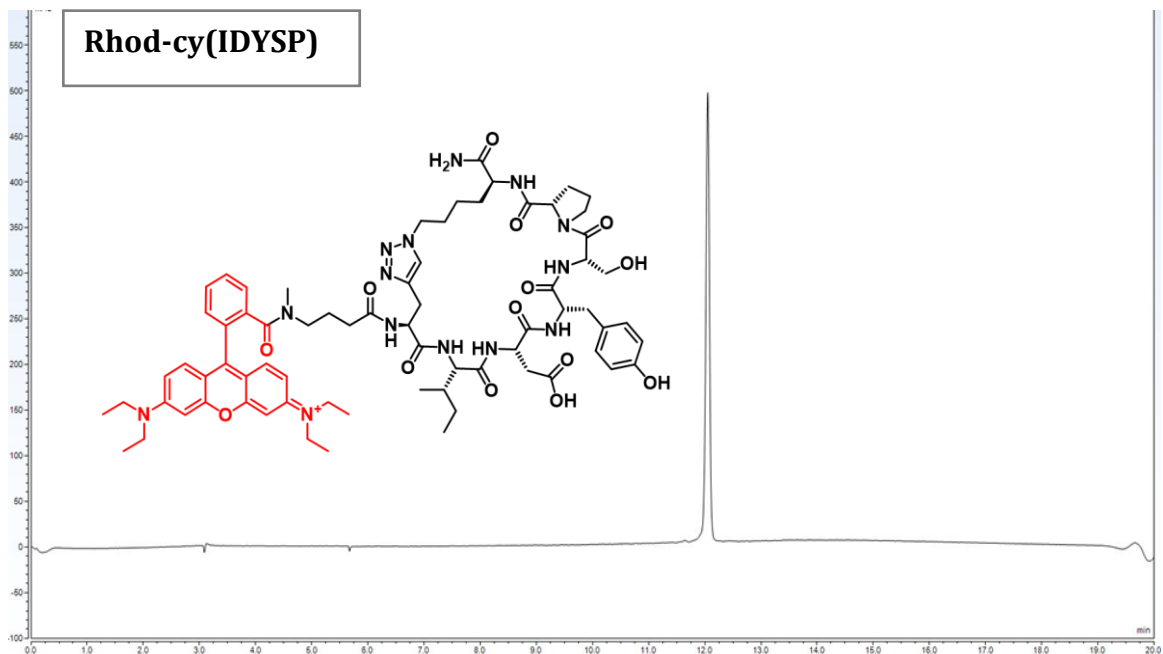


Figure 2.11. HPLC chromatogram (560 nm absorption) and MALDI-TOF mass spectrum for Rhod-cy(IDYSP). The bump at the end of the chromatogram is because of the sudden change in the flow rate.

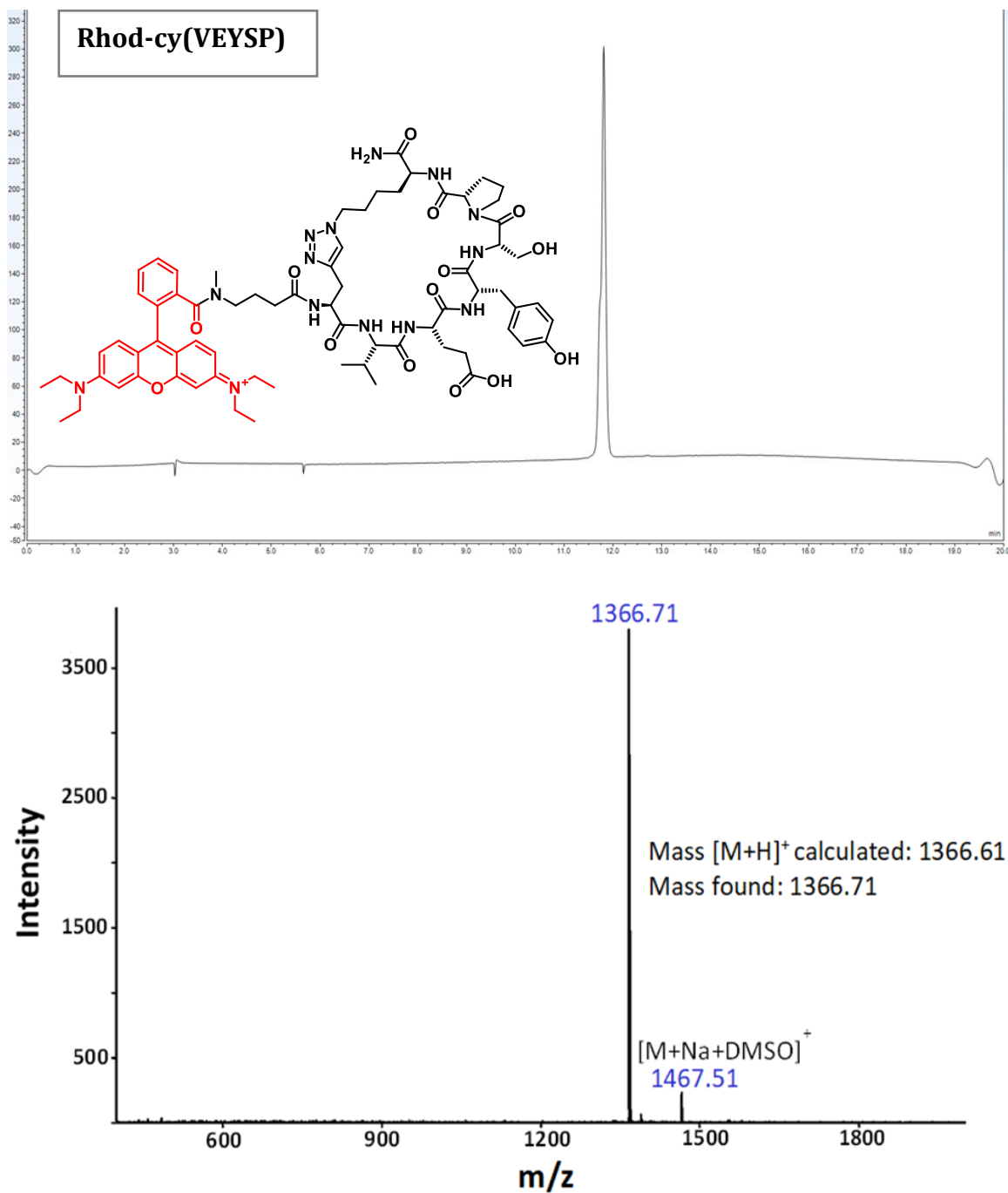


Figure 2.12. HPLC chromatogram (560 nm absorption) and MALDI-TOF mass spectrum for Rhod-cy(VEYSP). The bump at the end of the chromatogram is because of the sudden change in the flow rate.

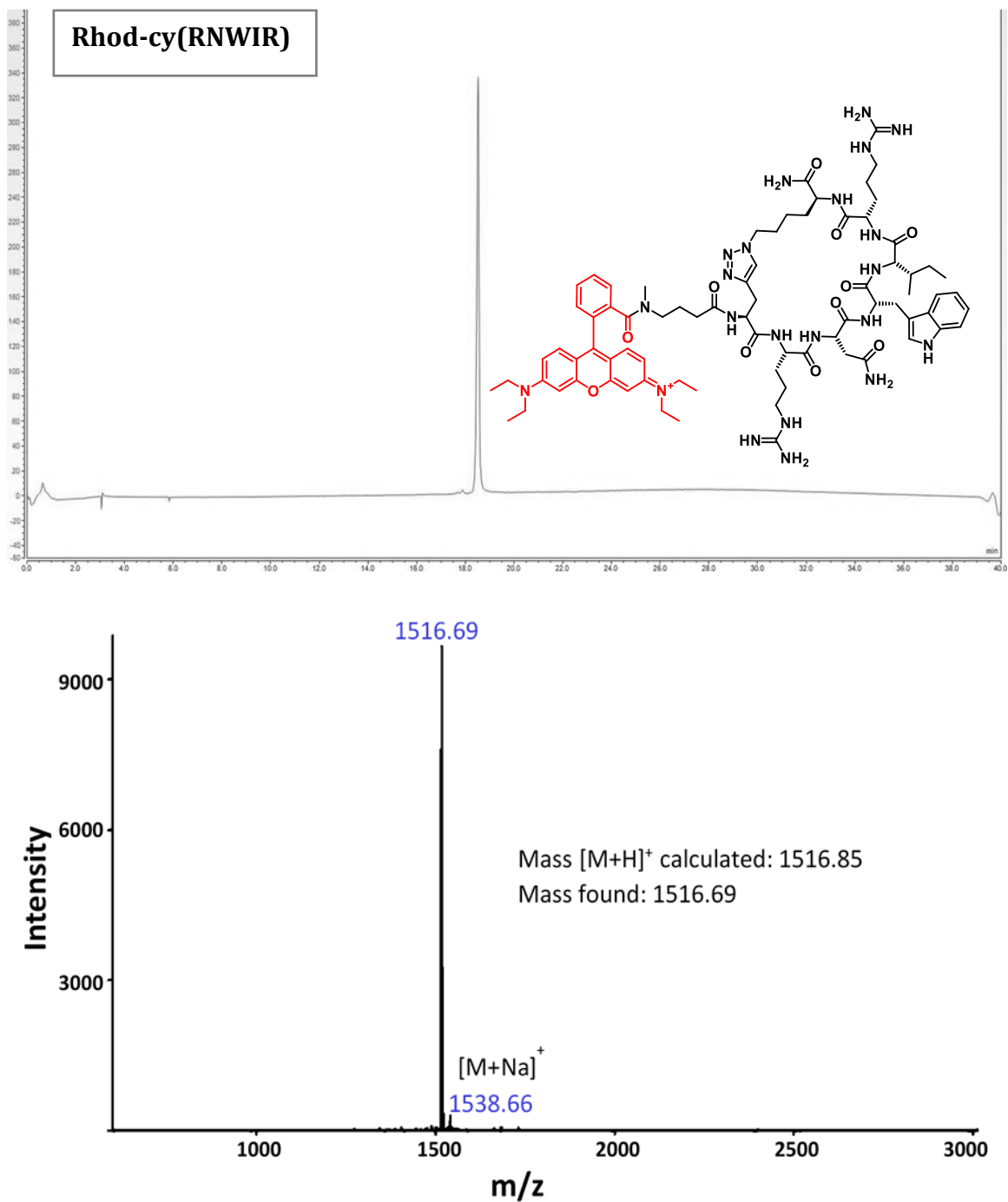


Figure 2.13. HPLC chromatogram (560 nm absorption) and MALDI-TOF mass spectrum for Rhod-cy(RNWIR). The bump at the end of the chromatogram is because of the sudden change in the flow rate.

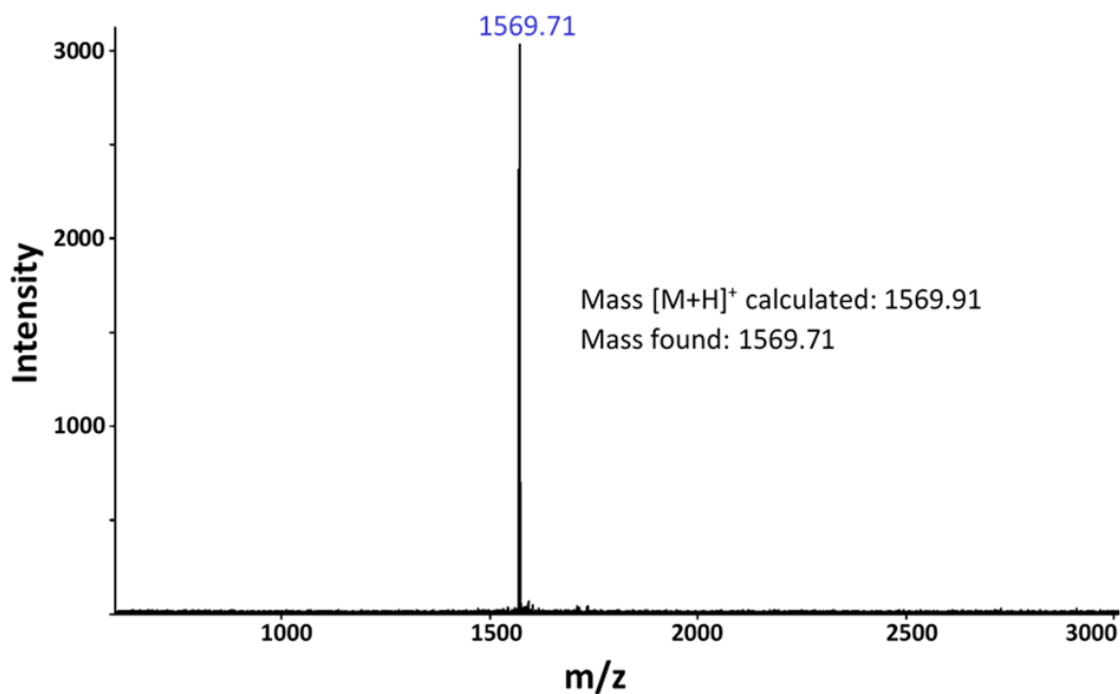
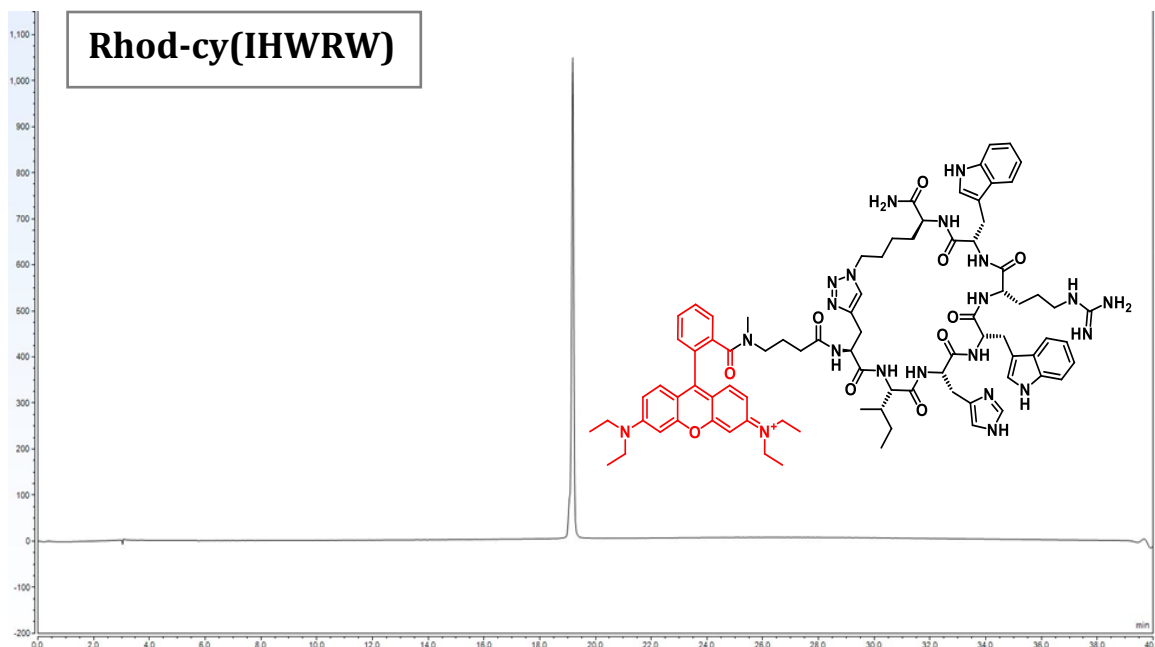


Figure 2.14. HPLC chromatogram (560 nm absorption) and MALDI-TOF mass spectrum for Rhod-cy(IHWRW). The bump at the end of the chromatogram is because of the sudden change in the flow rate.

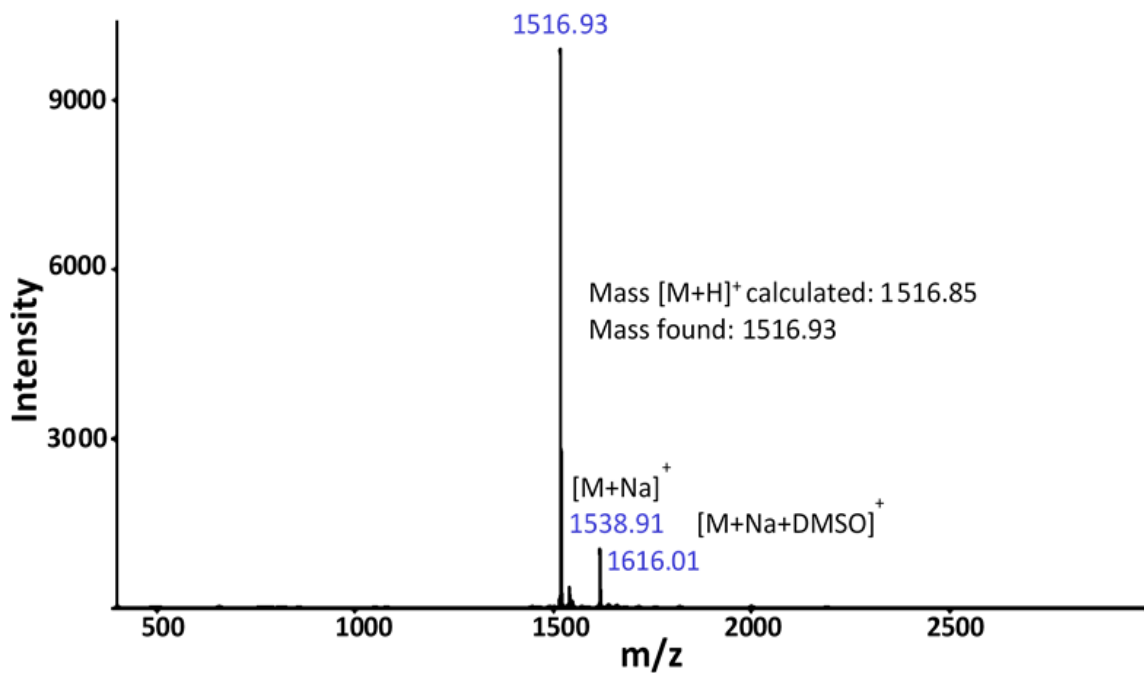
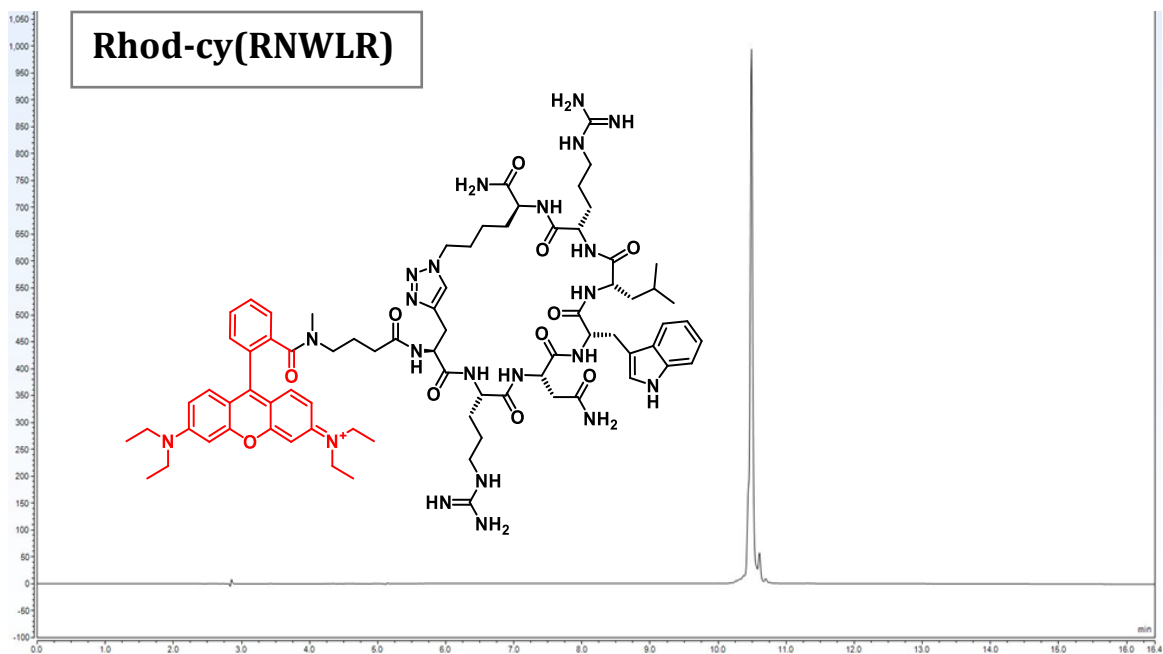


Figure 2.15. HPLC chromatogram (560 nm absorption) and MALDI-TOF mass spectrum and for Rhod-cy(RNWLR).

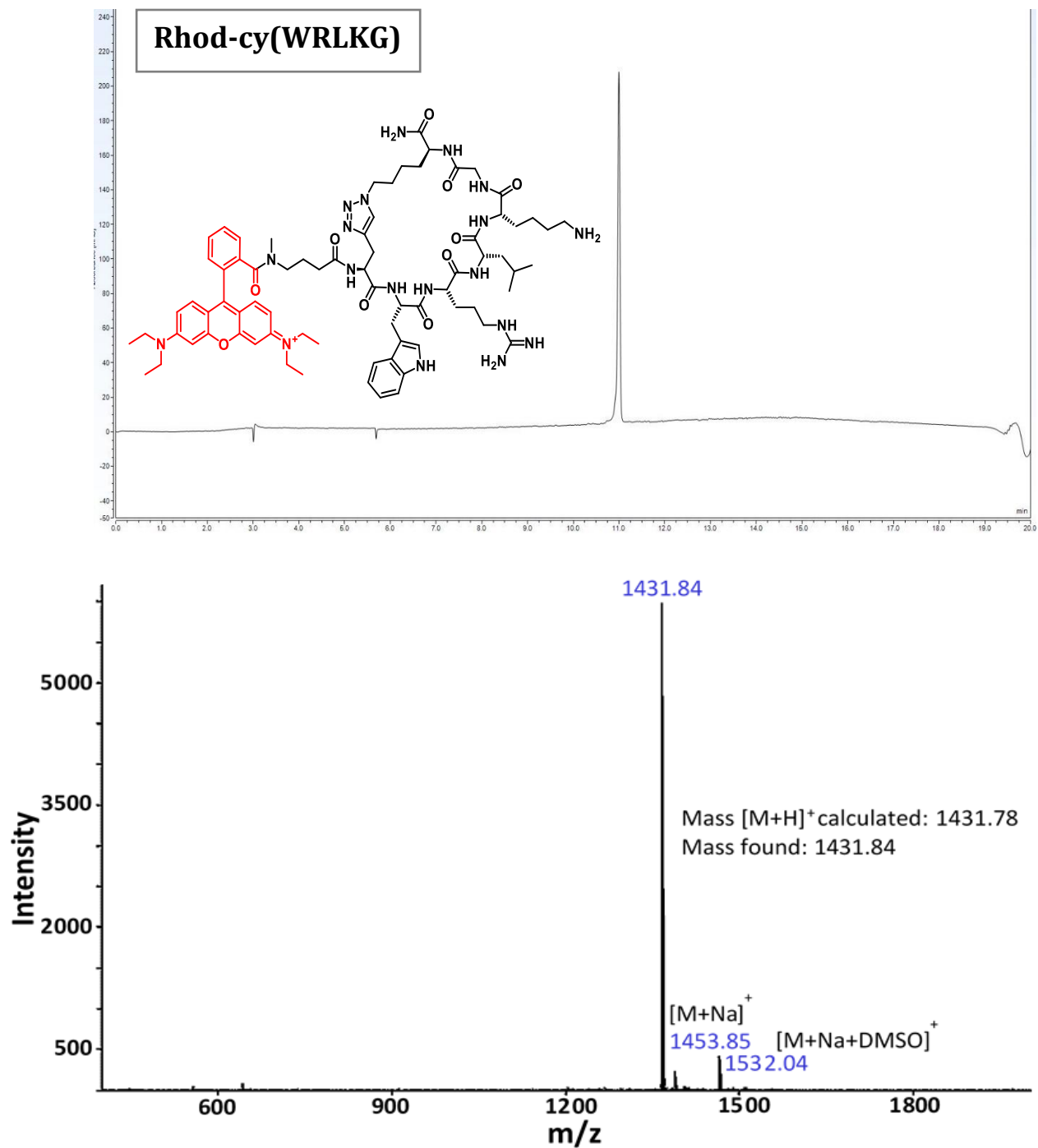


Figure 2.16. HPLC chromatogram (560 nm absorption) and MALDI-TOF mass spectrum for Rhod-cy(WRLKG). The bump at the end of the chromatogram is because of the sudden change in the flow rate.

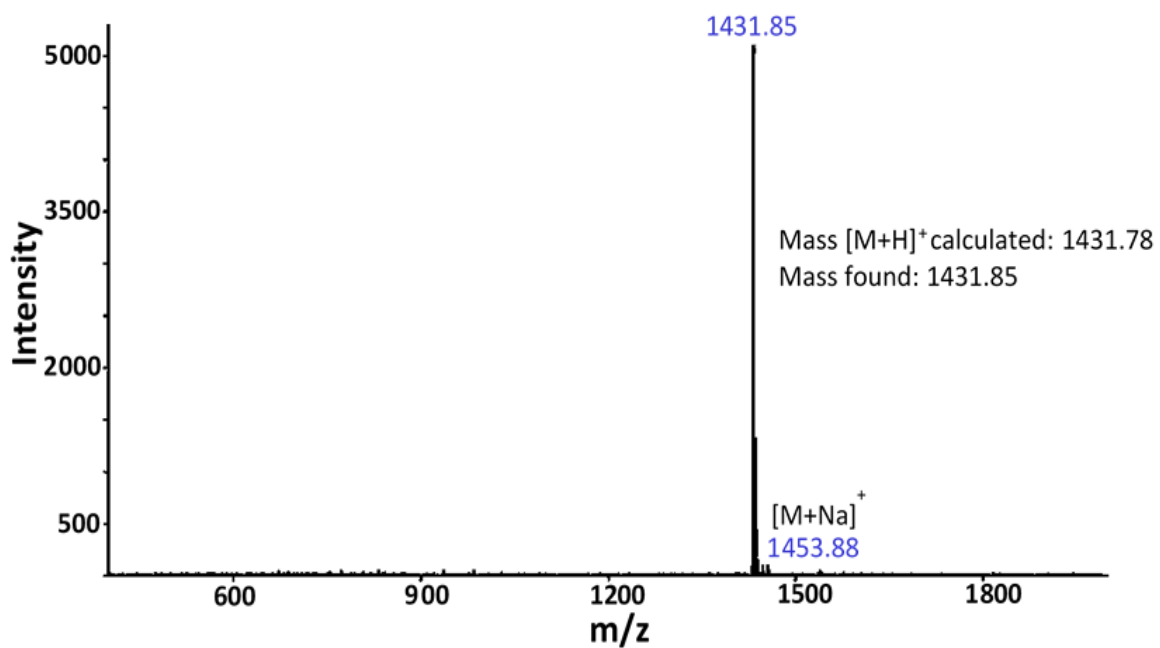
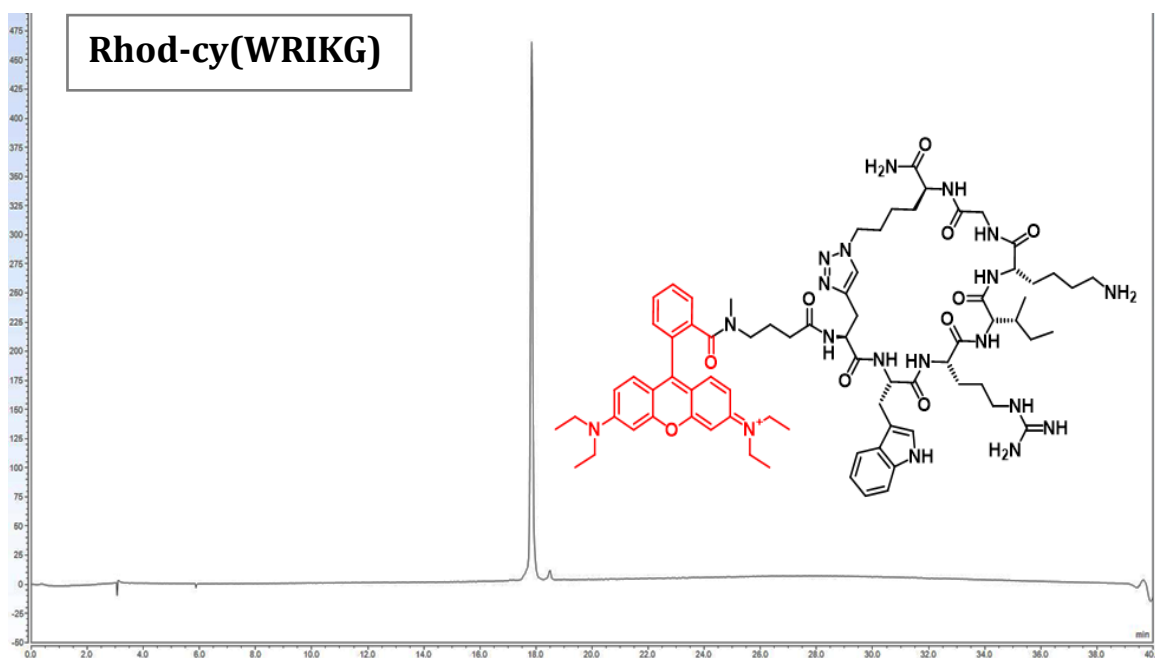


Figure 2.17. HPLC chromatogram (560 nm absorption) and MALDI-TOF mass spectrum for Rhod-cy(WRIKG).

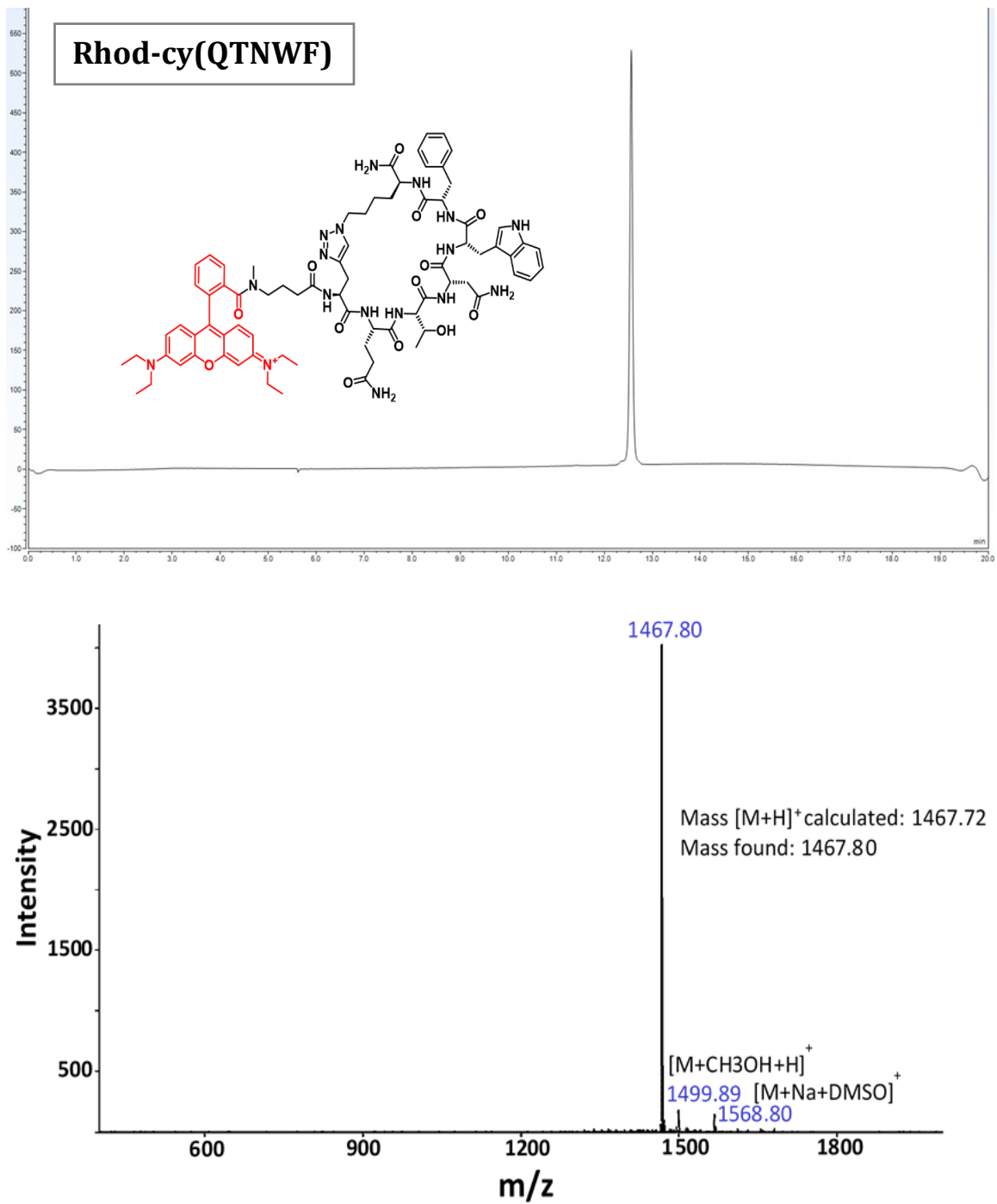


Figure 2.18. HPLC chromatogram (560 nm absorption) and MALDI-TOF mass spectrum for Rhod-cy(QTNWF).

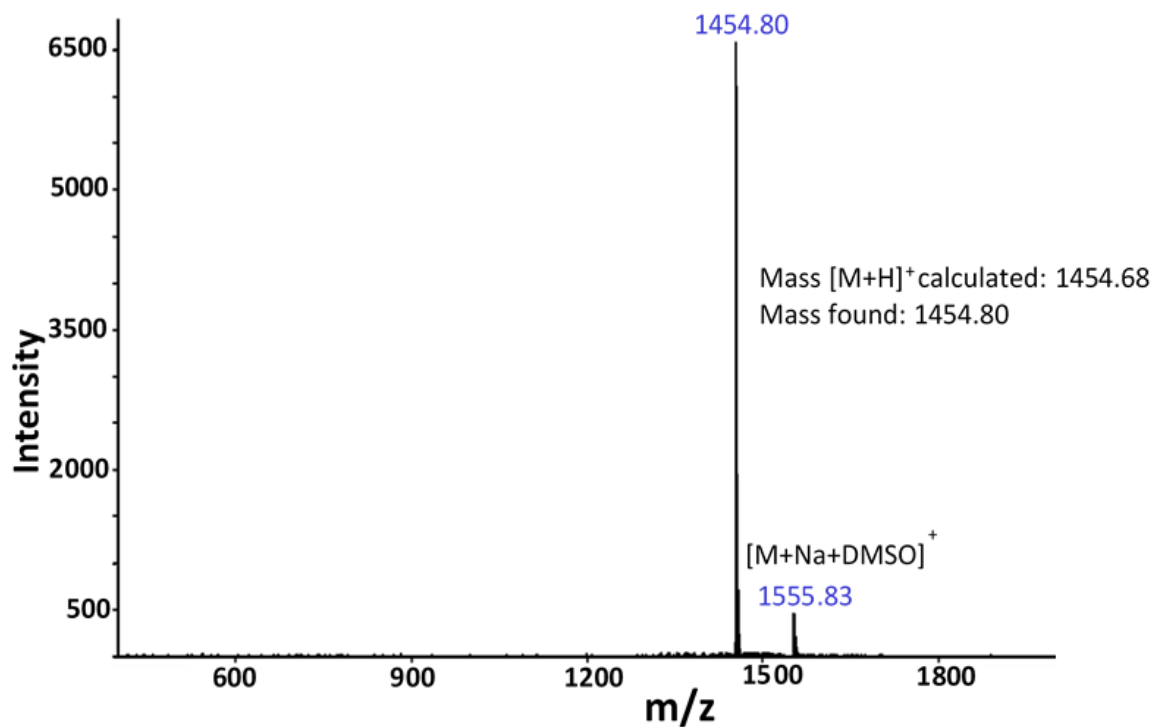
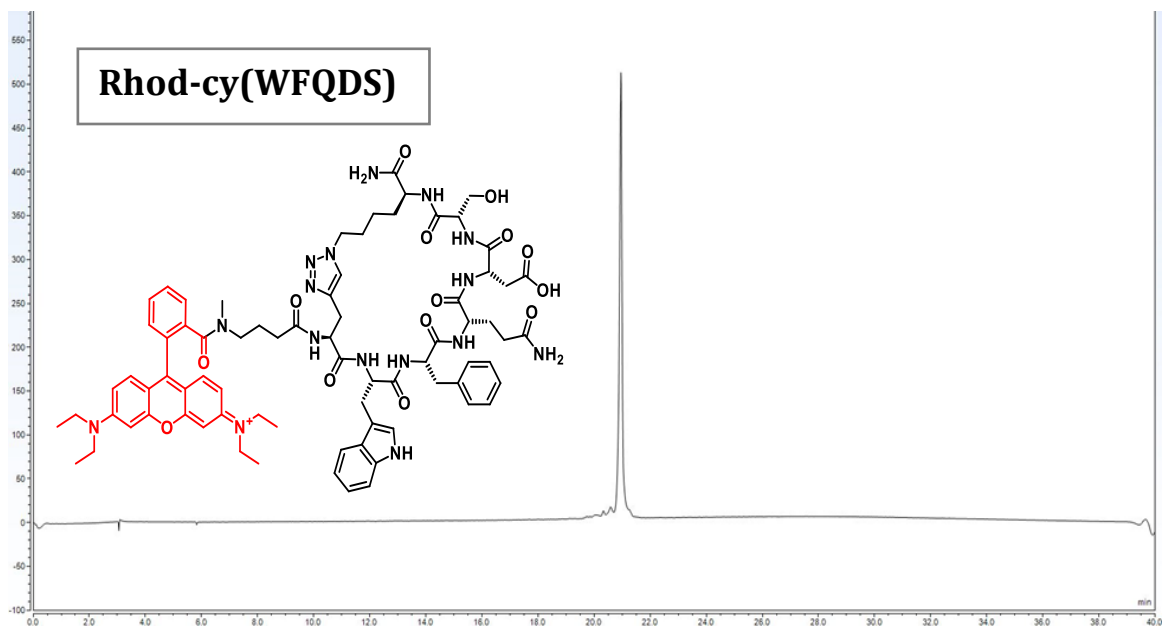


Figure 2.19. HPLC chromatogram (560 nm absorption) and MALDI-TOF mass spectrum for Rhod-cy(WFQDS).

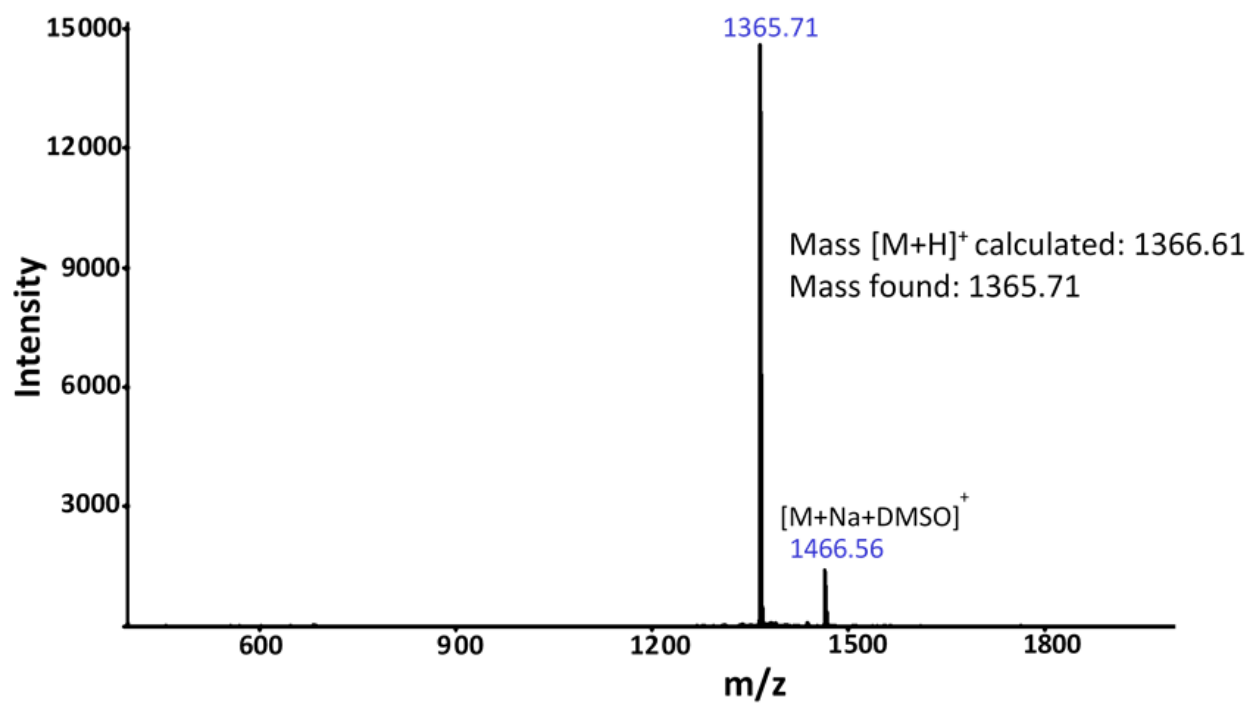
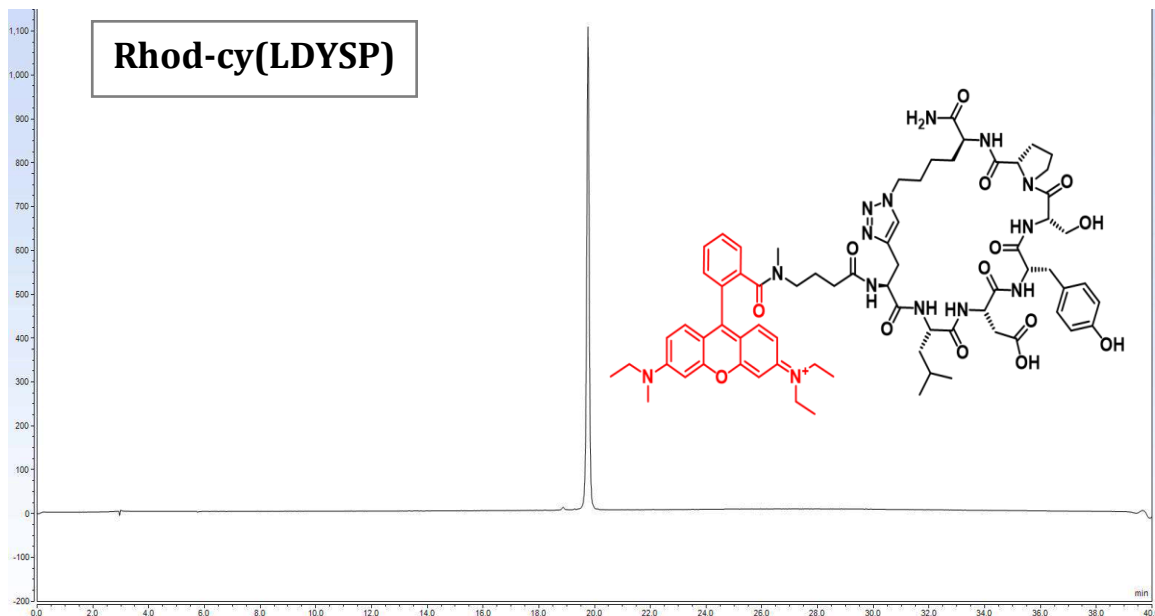


Figure 2.20. HPLC chromatogram (560 nm absorption) and MALDI-TOF mass spectrum and for Rhod-cy(LDYSP).

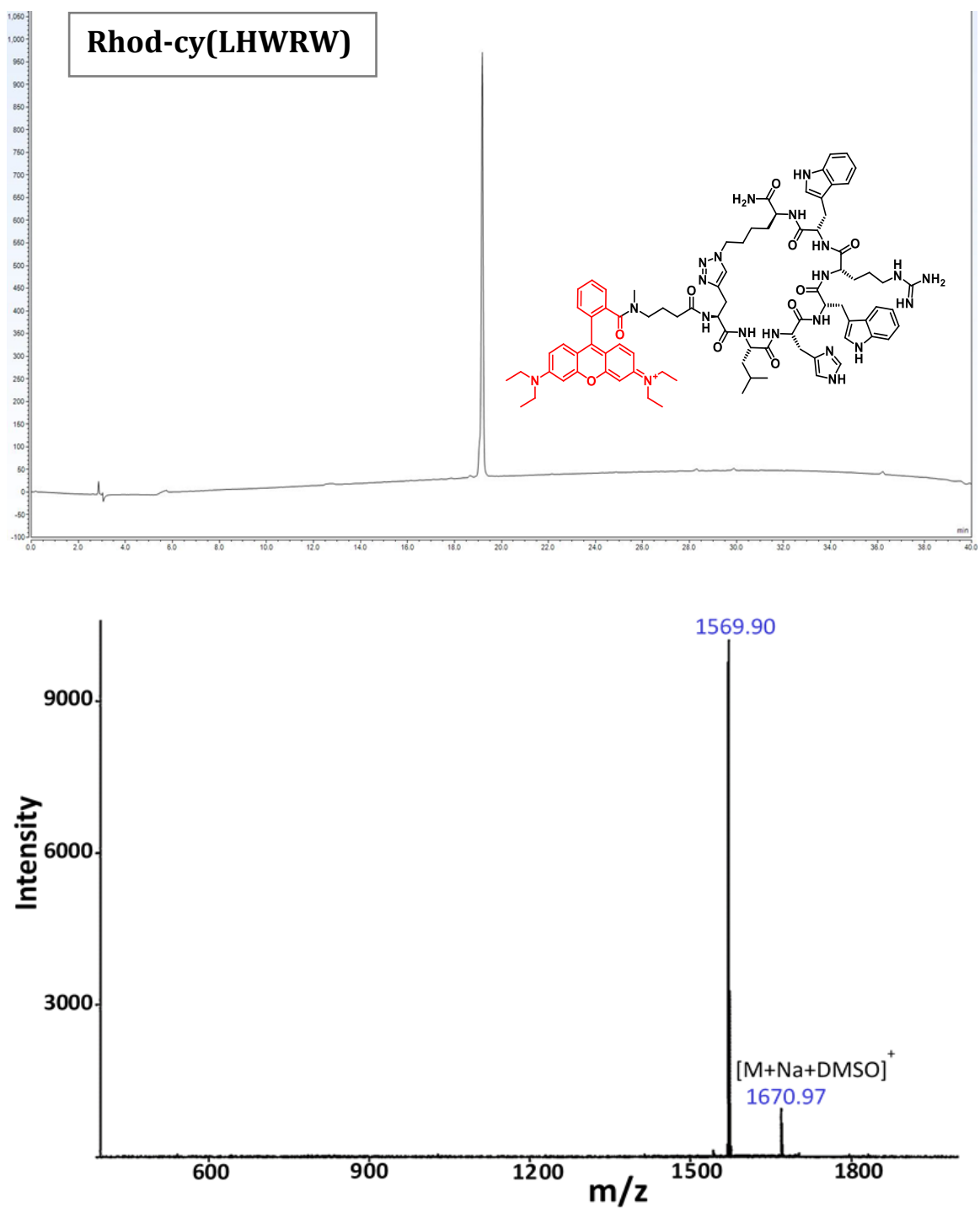


Figure 2.21. HPLC chromatogram (560 nm absorption) and MALDI-TOF mass spectrum for Rhod-cy(LHWRW).

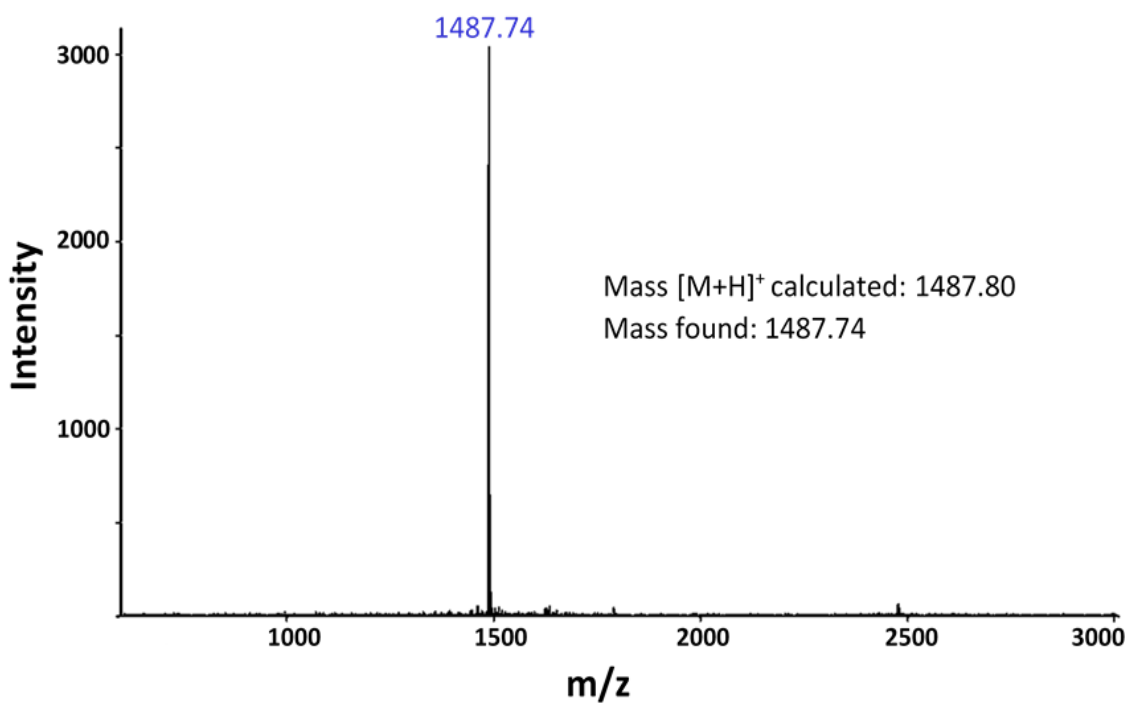
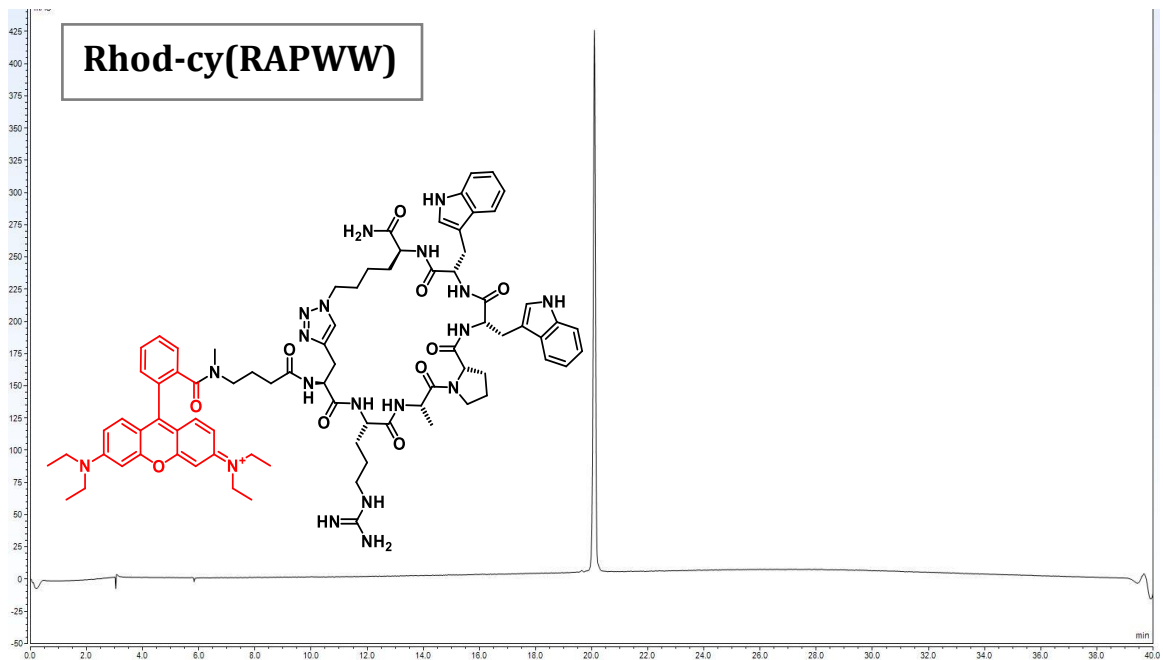


Figure 2.22. HPLC chromatogram (560 nm absorption) and MALDI-TOF mass spectrum for Rhod-cy(RAPWW).

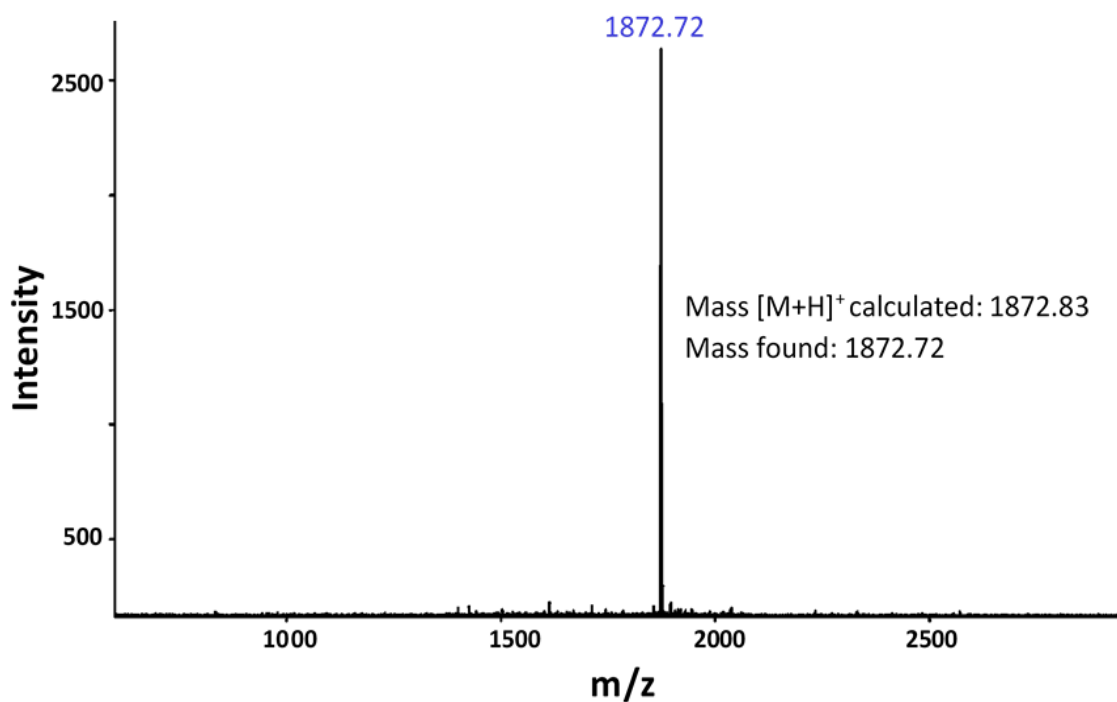
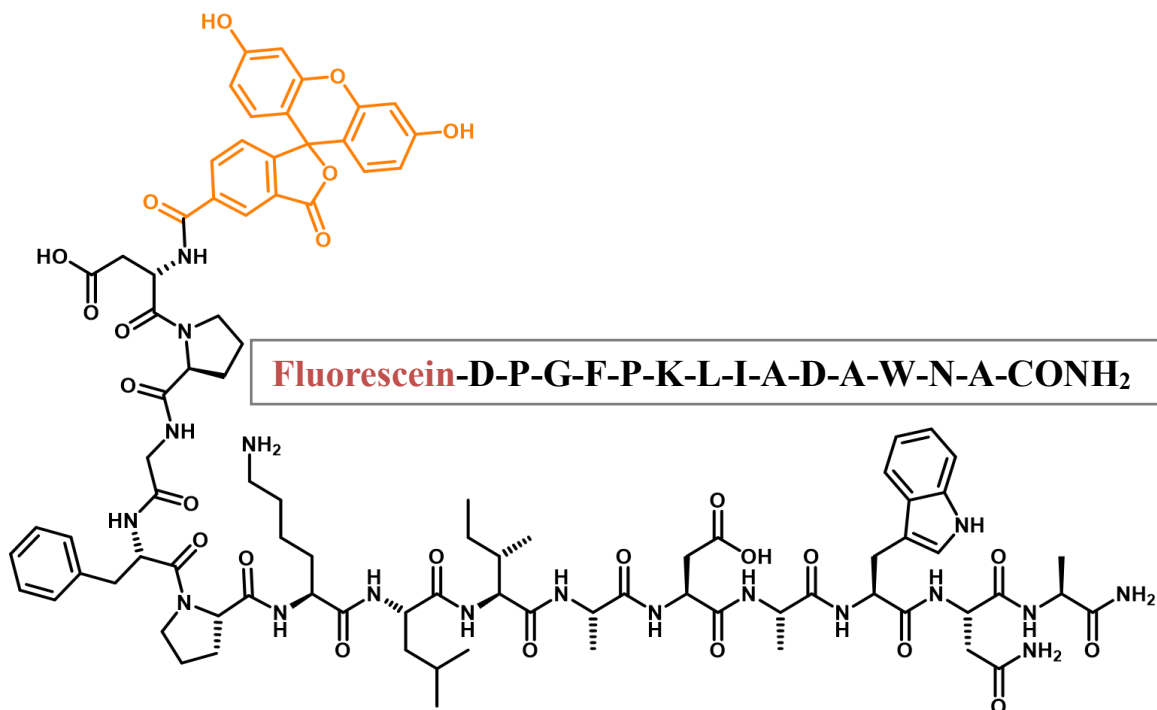
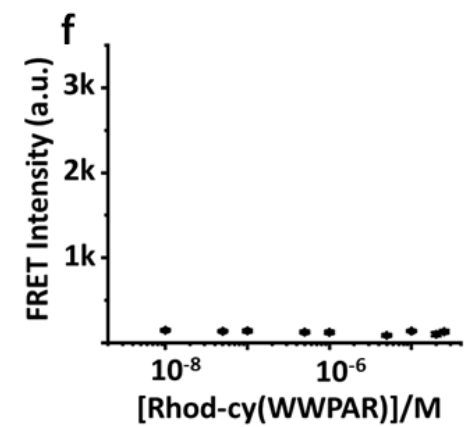
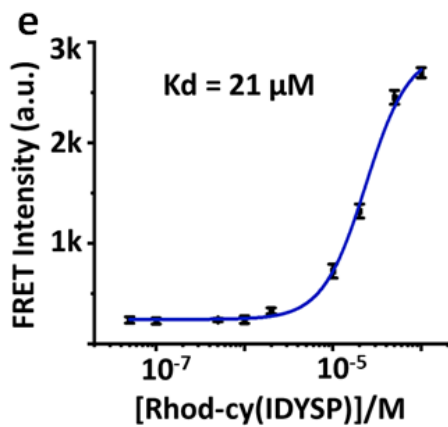
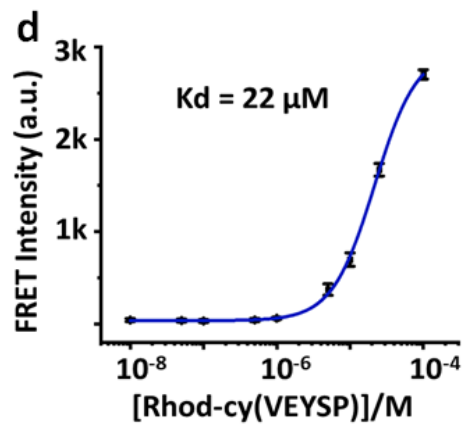
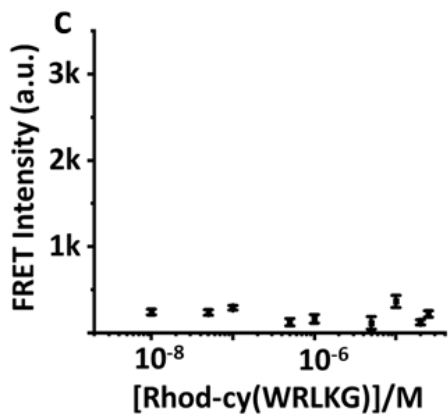
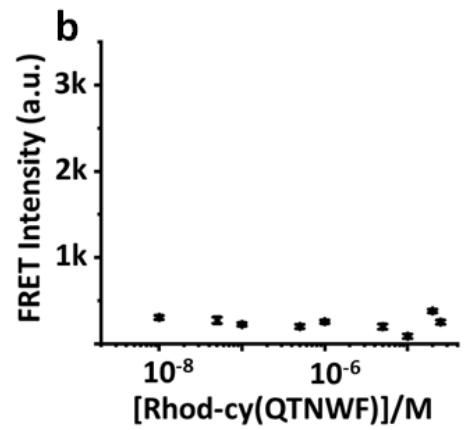
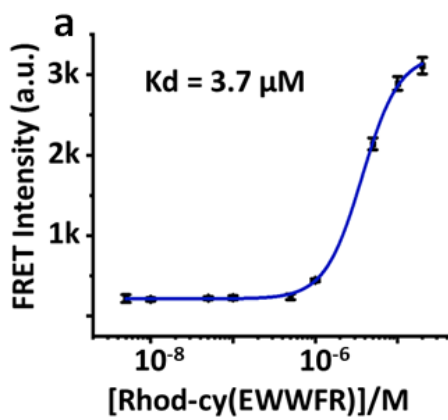
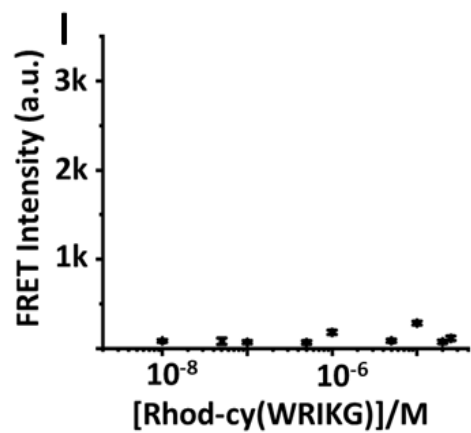
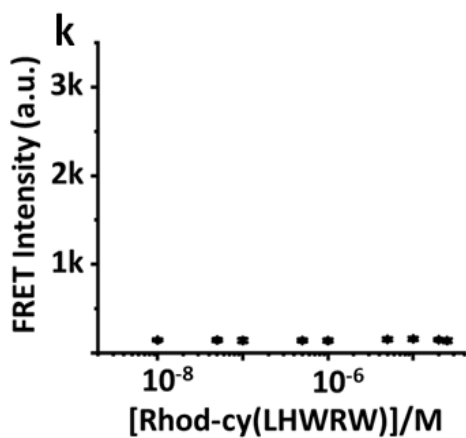
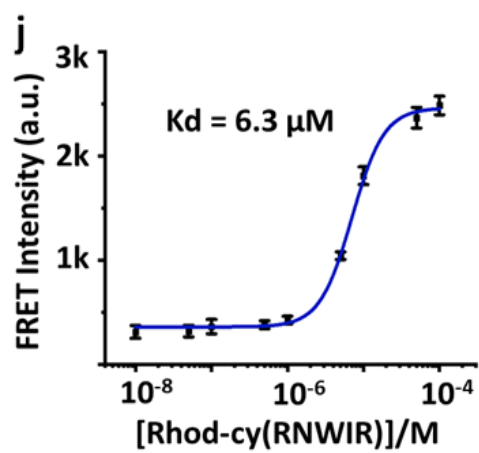
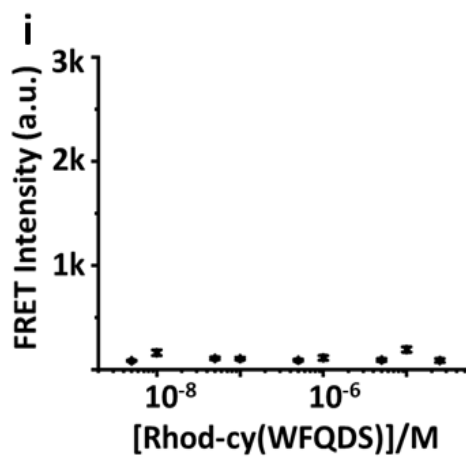
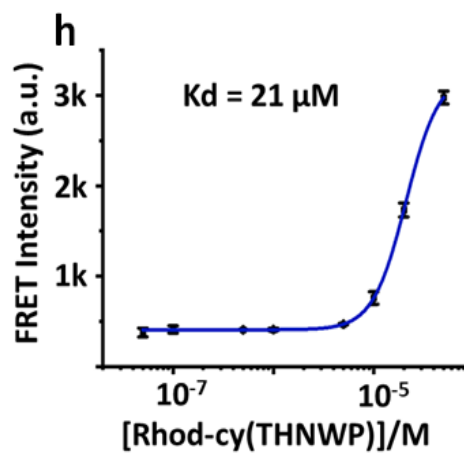
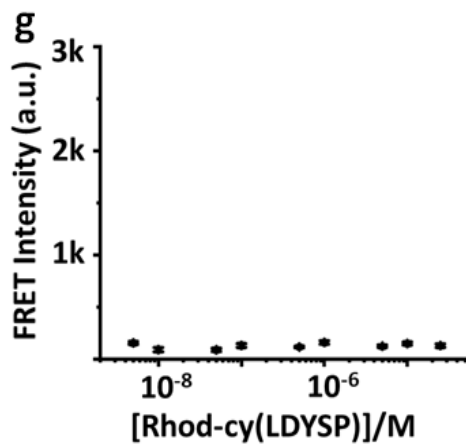


Figure 2.23. MALDI-TOF mass spectrum for the fluorescein-labeled epitope.





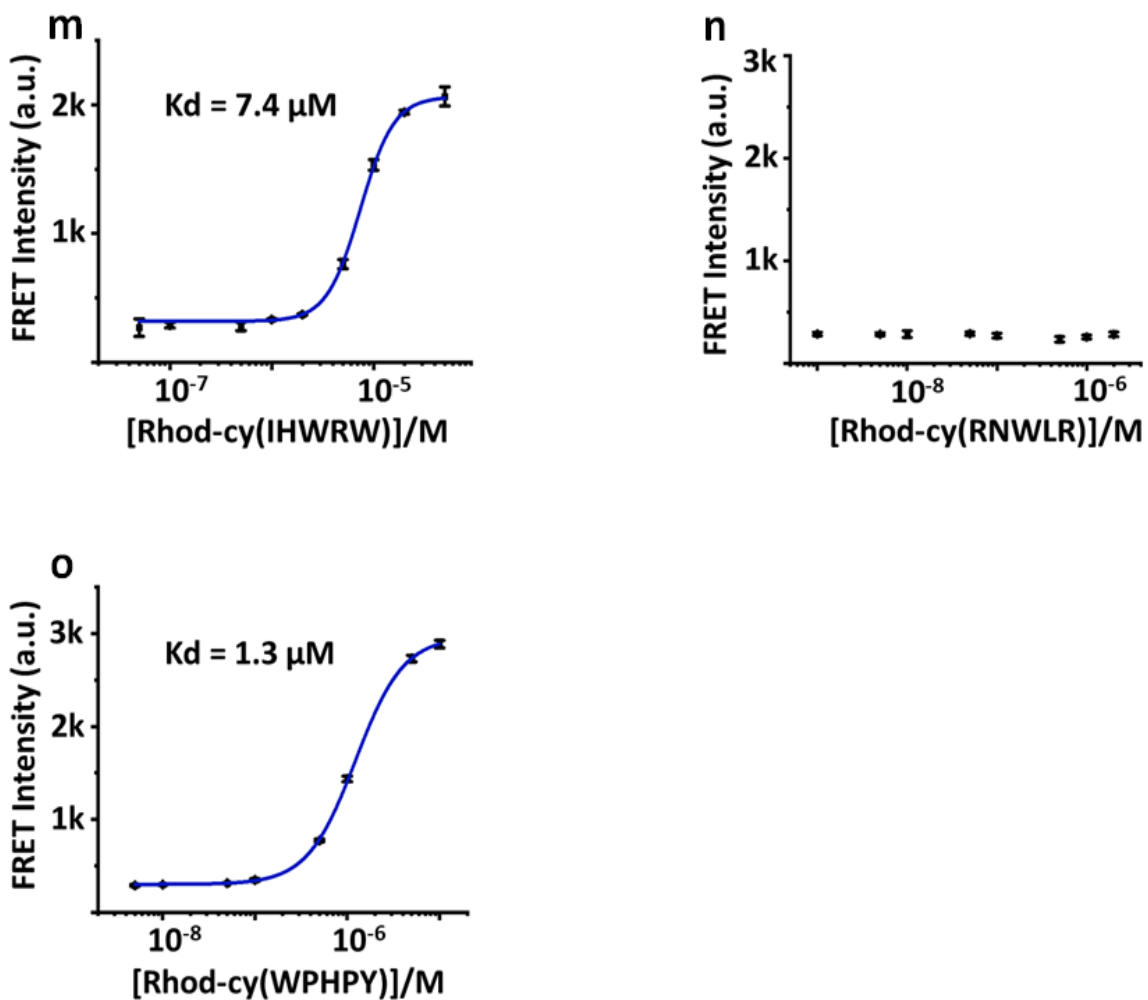


Figure 2.24. a-o. Varying concentrations of rhodamine B-conjugated hit peptides were mixed with 100 nM of the fluorescein-labeled epitope, and the FRET intensities were measured. The curves were fitted using a Hill function to obtain the K_d values.

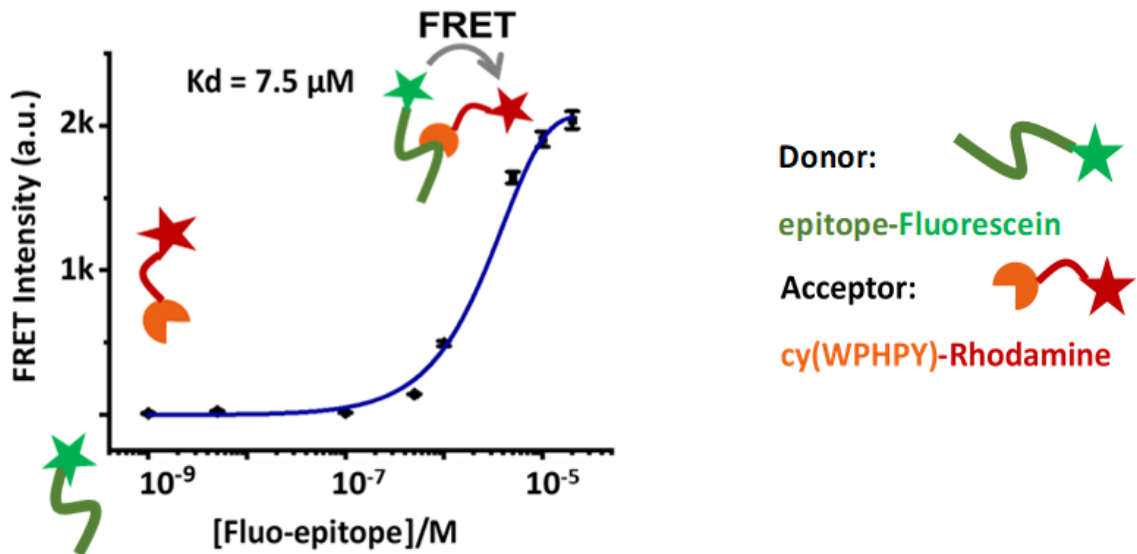


Figure 2.25. FRET signal obtained from the binding between 100 nM of rhodamine B-labeled ligand (Rhod-cy(WPHPY)) and varying concentrations of the fluorescein-labeled epitope (Fluo-Epitope). The binding affinity obtained was similar to the original one (Fig 2.24, o).

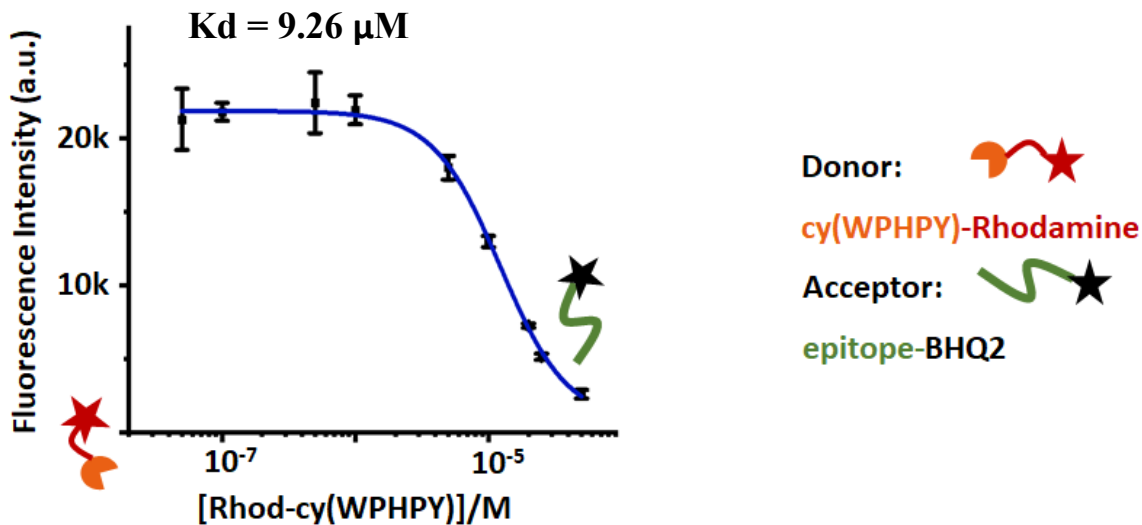


Figure 2.26. Residual fluorescence as a result of the binding between 100 nM of BHQ2-modified epitope and Rhod-cy(WPHPY). The dark quencher BHQ2 quenched the rhodamine fluorescence through a FRET mechanism.

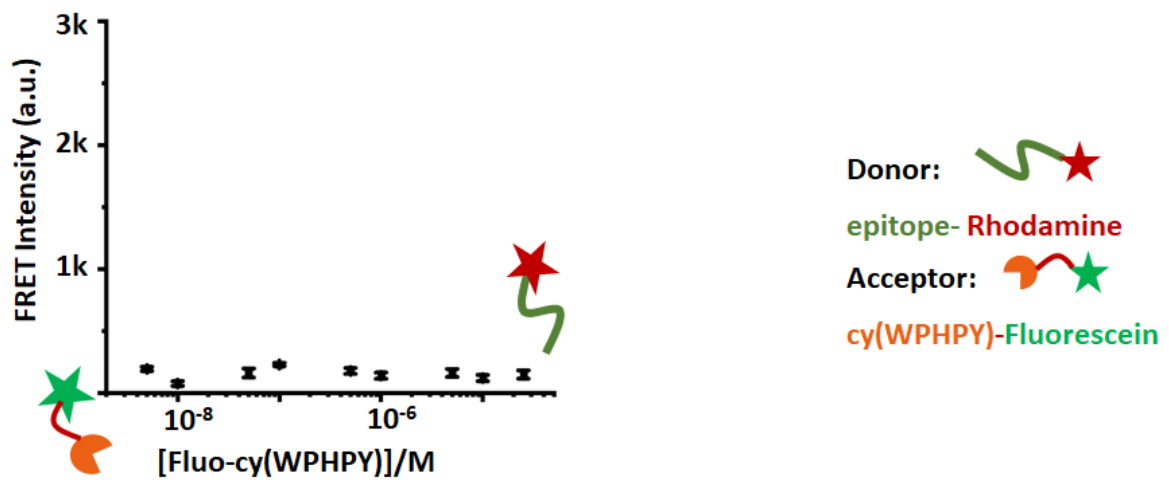


Figure 2.27. FRET signal obtained from the binding between 100 nM of Rhod-Epitope and varying concentrations of fluorescein-labeled ligand (Fluo-cy(WPHPY)). Changing the tag on the ligand resulted in a total loss of binding.

cy(WPHPY) Binds to proMMP2 with a Low nM Affinity

Because FRET-based titration experiments frequently suffer from artifacts such as microenvironment-induced quantum yield changes, we carried out more experiments to validate the binding between Rhod-cy(WPHPY) and the epitope. We found that the binding was insensitive to the titrant designation or the tag identity on the epitope (Figures 2.25 and 2.26). Conjugating cy(WPHPY) to a different fluorophore, however, destroyed the binding (Figure 2.27), indicating that N-terminal modifications to cy(WPHPY) could affect the binding significantly. Based on this result, we removed the N-terminal rhodamine B tag and tested its binding to the epitope using a competitive FRET approach (Figure 2.28). Here, cy(WPHPY) was used to titrate a mixture of Rhod-cy(WPHPY) (100 nM) and Fluo-epitope (100 nM). The cy(WPHPY)–epitope binding would disrupt the Rhodcy(WPHPY)–Fluo-epitope interaction and therefore lower the FRET signal. To our surprise, the result (Figure 2.4e) showed that the unconjugated cy(WPHPY) bound to the epitope with a much higher affinity ($K_d = 1$ nM) compared with Rhodcy(WPHPY).

To test if the observed cyclic peptide–epitope binding could translate to cyclic peptide–protein binding, we expressed and purified recombinant full-length proMMP2 and performed fluorescence polarization (FP) experiments to validate the binding. As shown in Figure 2.4f, Rhod-cy(WPHPY) was able to recognize recombinant proMMP2 with a high nM affinity ($K_d = 280$ nM), which was consistent with the epitope binding assay. This validated binding allowed us to implement a competitive FP assay to further test the binding between unmodified cy(WPHPY) and recombinant proMMP2. Here, we

used unlabeled cy(WPHPY) to titrate a solution of Rhodcy(WPHPY) and recombinant proMMP2. Similar to the competitive FRET assay described above, cy(WPHPY) was expected to replace Rhod-cy(WPHPY) on proMMP2, causing decreased FP values. The result proved that the unmodified cy(WPHPY) peptide bound strongly to proMMP2 ($K_d = 2.3$ nM, Figure 2.4g), which also agreed with the epitope binding assay results.

Structure–Activity Relationship Analysis

We sought to elucidate the structure–activity relationship. The existence of two proline residues pointed to prominent backbone rigidity, which was expected to confer entropic advantages and contribute to enhanced binding affinities by providing privileged conformations.⁵¹ To evaluate the backbone rigidity, we performed molecular dynamics simulations of cy(WPHPY). We found that the two proline residues caused a unique kink in the backbone structure, which significantly limited the range of motion of the W, H, and Y residues (Figure 2.30a and Tables 2.1– 2.2, Figure 2.29). Substituting either of the two proline residues with alanine caused complete loss of binding to proMMP2, as demonstrated by the competitive FP results (Figure 2.30b,c). Also, alanine substitution at the W, H, and Y residues abolished the binding. These results indicated that both the identity and the orientation of the side-chain groups on cy(WPHPY) were critical to its binding affinity to proMMP2.

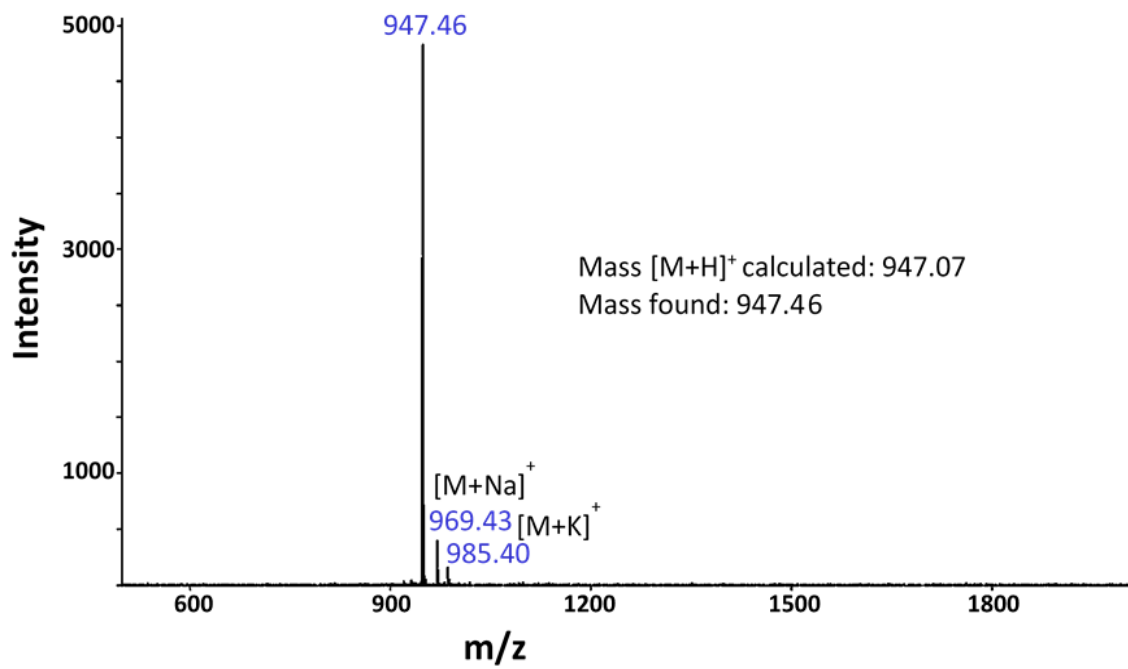
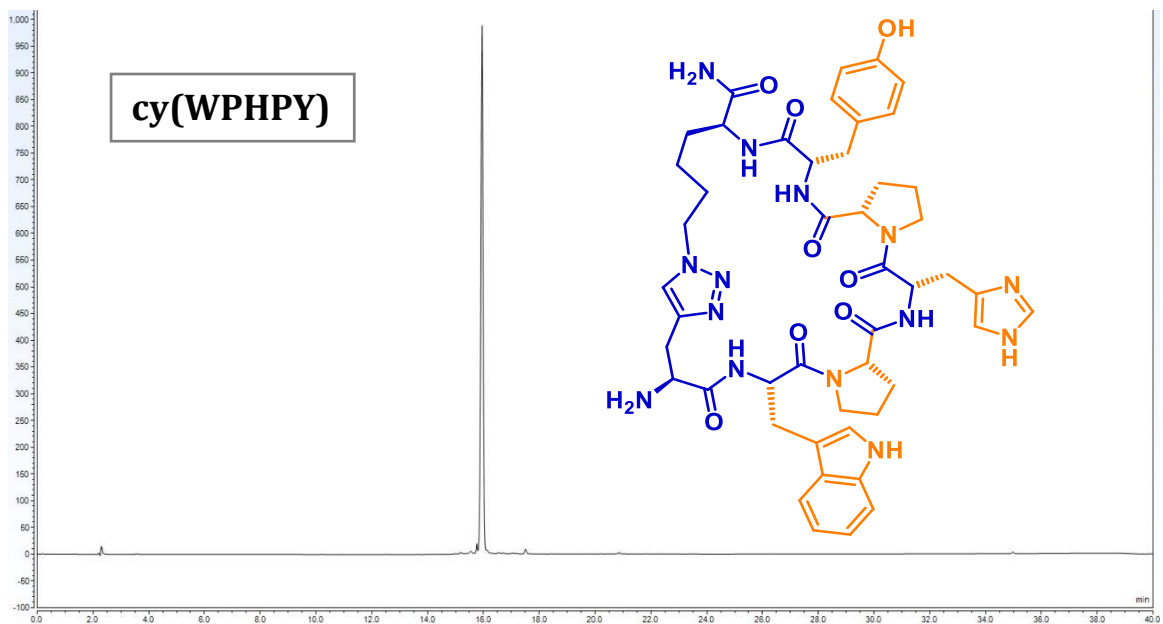


Figure 2.28. Analytical HPLC chromatogram (280 nm absorption) and MALDI-TOF mass spectrum and for the unmodified cyclic peptide ligand cy(WPHPY).

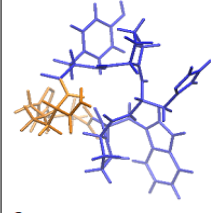
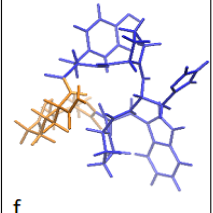
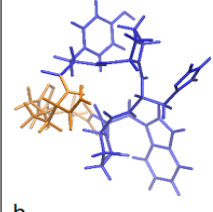
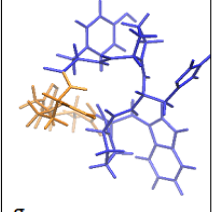
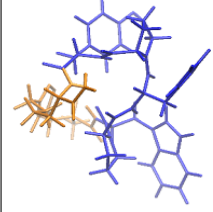
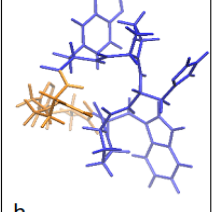
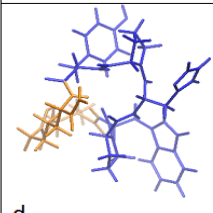
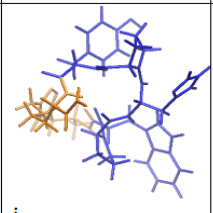
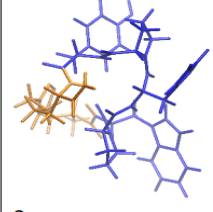
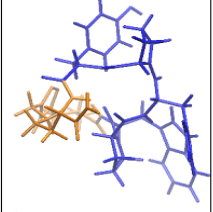
Conformation	Free Energy (kcal/mol)	Conformation	Free Energy (kcal/mol)
 a	226.37	 f	227.527
 b	226.38	 g	227.534
 c	227.401	 h	227.63
 d	227.404	 i	227.65
 e	227.41	 j	227.93

Table 2.1. The most stable conformations of cy(WPHPY) obtained from free energy calculations. Top 10 most stable conformations from a total of 546 conformations are shown in stick representation with orange and blue color representing two linkages. Conformational search and free energy calculations were performed with VM2 using the implicit solvation model.

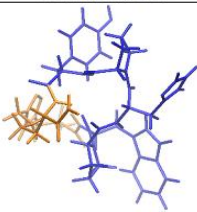
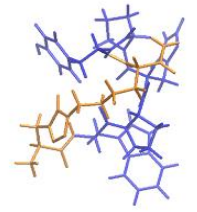
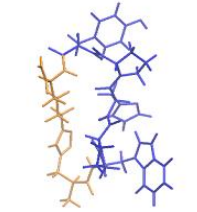
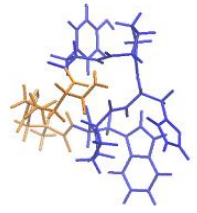
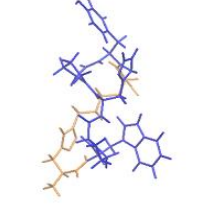
Conformation	Free Energy (kcal/mol)
 1	226.37
 2	227.93
 3	228.08
 4	228.86
 5	229.54

Table 2.2. Five manually selected conformations with the most significant changes in the dihedral angle in the peptide backbone or sidechain were taken as the initial conformations to start MD simulation in an explicit water model. Free energy is in kcal/mol.

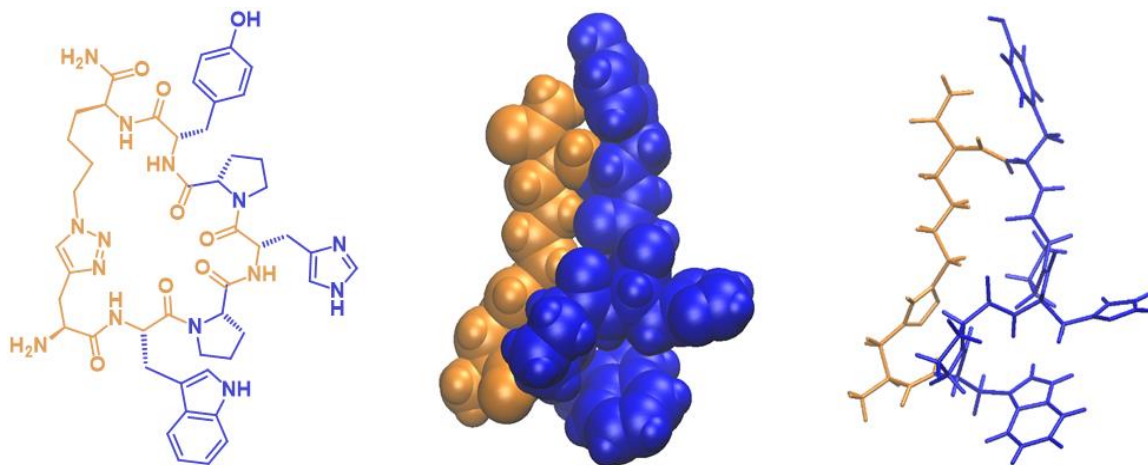
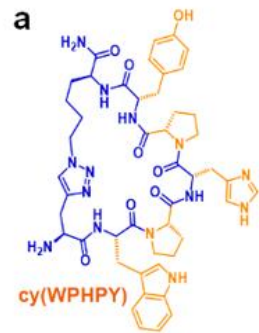
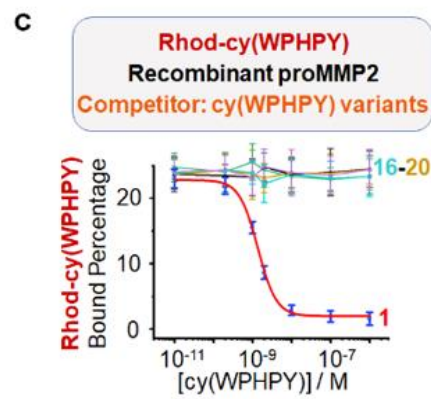
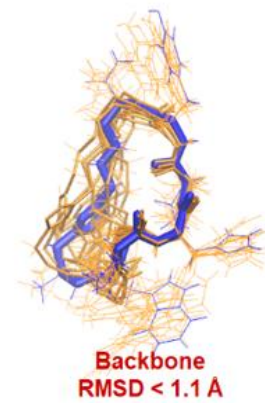


Figure 2.29. The representative conformation of an MD run for cy(WPHPY) is shown in van der Waals (middle) and stick (right) representations. This conformation constitutes 57.7% conformations of a 20-ns long MD trajectory. The RMSD of the MD calculation is 1.066 angstrom. The average total energy for 20 ns is -15250.89 kcal/mol, the average kinetic energy is 3571.86 kcal/mol, and the average potential energy is -18822.76 kcal/mol. $E_{\text{total}} = E_{\text{kinetic}} + E_{\text{potential}}$ is used. This energy is for the whole system (cy(WPHPY) + water + one Cl⁻).



b

#	X ₁	X ₂	X ₃	X ₄	X ₅
1	W	P	H	P	Y
16	W	P	H	P	A
17	W	P	H	A	Y
18	W	P	A	P	Y
19	W	A	H	P	Y
20	A	P	H	P	Y



d

Original : Fluo-NH-D-P-G-F-P-K-L-I-A-D-A-W-N-A-CONH₂
C5 : Fluo-NH-D-P-G-F-P-K-L-I-A-A-N-A-W-D-CONH₂
M5 : Fluo-NH-D-P-G-F-I-A-K-P-L-D-A-W-N-A-CONH₂
N5 : Fluo-NH-P-F-D-P-G-K-L-I-A-D-A-W-N-A-CONH₂

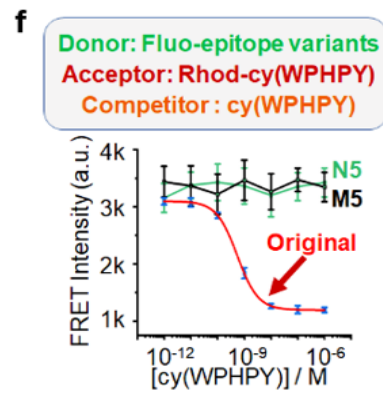
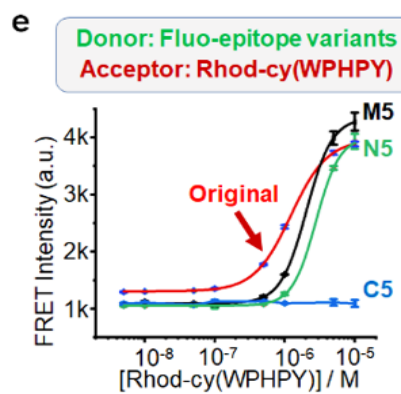


Figure 2.30. Analysis of the structure–activity relationship. (a) Optimal conformations of cy(WPHPY) as calculated using molecular dynamics (MD) approaches. The blue wire is the most representative conformation generated from the conformation search. The orange wires illustrate the conformations that were evenly extracted every 2 ns from the MD simulation trajectory. (b) Alanine scanning variations of cy(WPHPY). (c) Competitive FP results obtained using alanine-substituted cy(WPHPY) variations. The competitive FP results of cy(WPHPY) were included as a reference (red line, peptide 1). (d) Partially scrambled epitope sequences in comparison with the original epitope. (e) FRET signals generated from the binding between 100 nM Fluo-epitope variations and varying concentrations of Rhod-cy(WPHPY). The result from the original Fluo-epitope was included as a reference. C5 was not able to bind to Rhod-cy(WPHPY), while M5 and N5 retained the binding affinity. (f) Competitive FRET assay results demonstrating the lack of binding affinity between the unlabeled cy(WPHPY) and the partially scrambled epitopes (M5 and N5). Unlabeled cy(WPHPY) could not displace Rhod-cy(WPHPY) from the epitope; therefore, the FRET intensities did not change. The result from the original Fluo- epitope was included as a reference.

To map the critical interaction sites on the epitope, we synthesized partially scrambled epitopes and evaluated their binding affinities to the cy(WPHPY) peptide using the aforementioned FRET approach (Figures 2.30d and 2.31–2.34). The results showed that altering the C terminal of the epitope caused a loss of binding (Figure 2.30e), while scrambling the middle and N-terminal segments retained the binding to Rhodcy(WPHPY). Interestingly, we also found that preserving the C terminal alone could not maintain the binding to Rhodcy(WPHPY) (Figure 2.35). These results suggested that Rhod-cy(WPHPY) interacted with multiple segments on the epitope, and this interaction was slightly more dependent on the C terminal.

We further evaluated the binding between the unlabeled cy(WPHPY) and the scrambled epitopes, using the competitive FRET method. Even though M5 and N5 were able to bind to Rhod-cy(WPHPY), they were not able to recognize the unlabeled cy(WPHPY) (Figure 2.30f). Since the original and partially scrambled epitopes all lack secondary structures (Figures 2.31–2.34), these results hinted that the whole epitope participated in the binding, perhaps by adopting a favored conformation that was induced by the cyclic peptide ligand. In addition, we found that the cy(WPHPY)–epitope interaction caused an increase of Trp fluorescence (Figures 2.36 and 2.37), while the alanine-substituted peptide, cy(WAHPY), did not. Because Trp fluorescence is sensitive to local environments, this increase was likely due to the epitope conformation change.⁵²

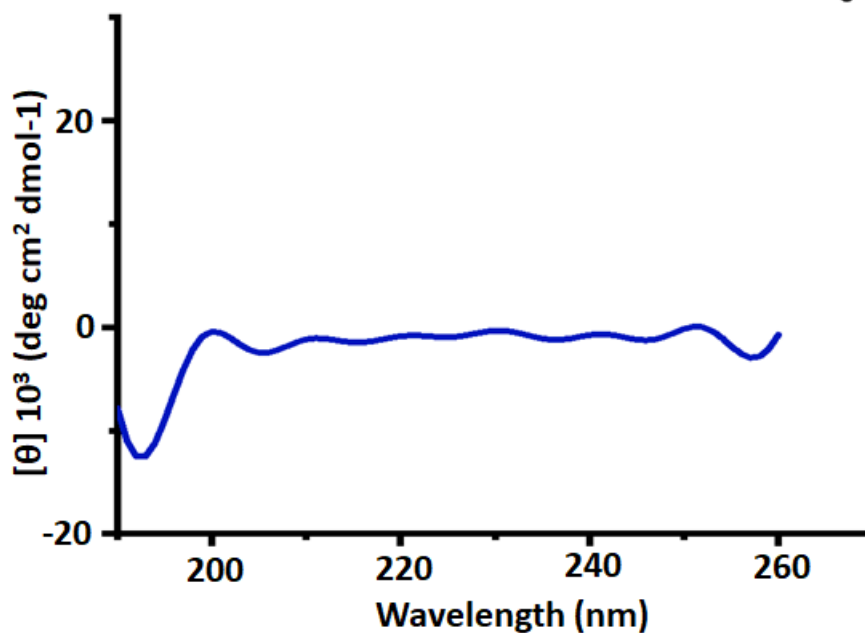
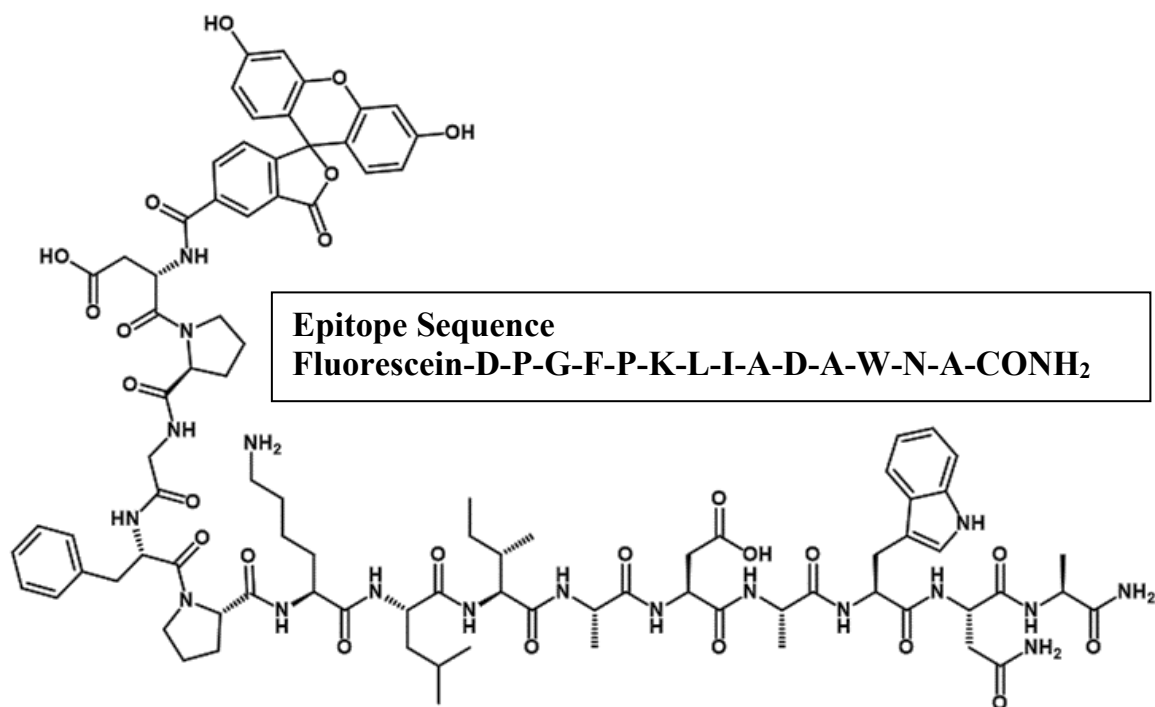


Figure 2.31. Circular dichroism (CD) spectrum of 20 μM of the fluorescein-labeled epitope (D₅₇₀-A₅₈₃) in PBS. No apparent secondary structure was observed, and the epitope appeared to be a random coil.

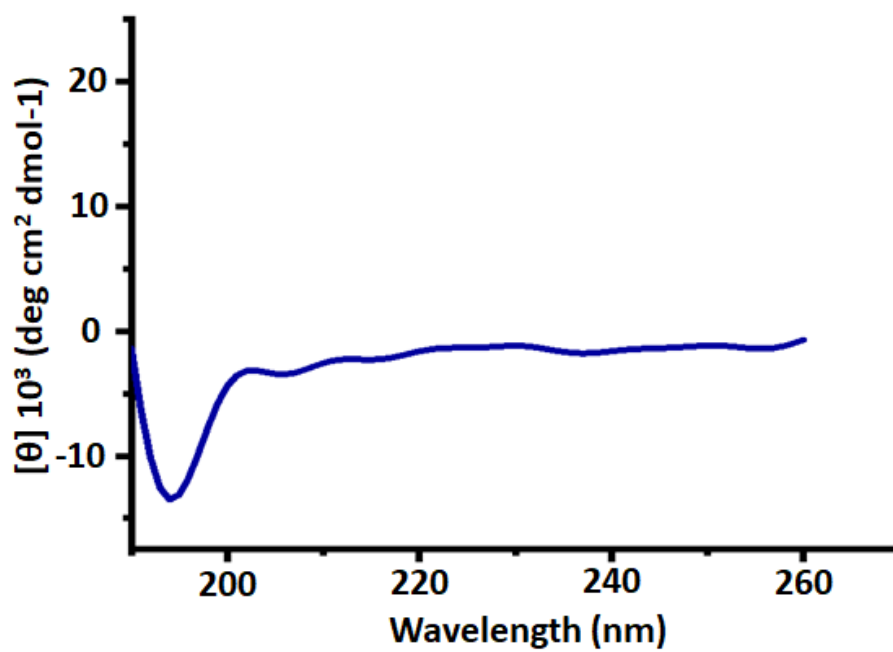
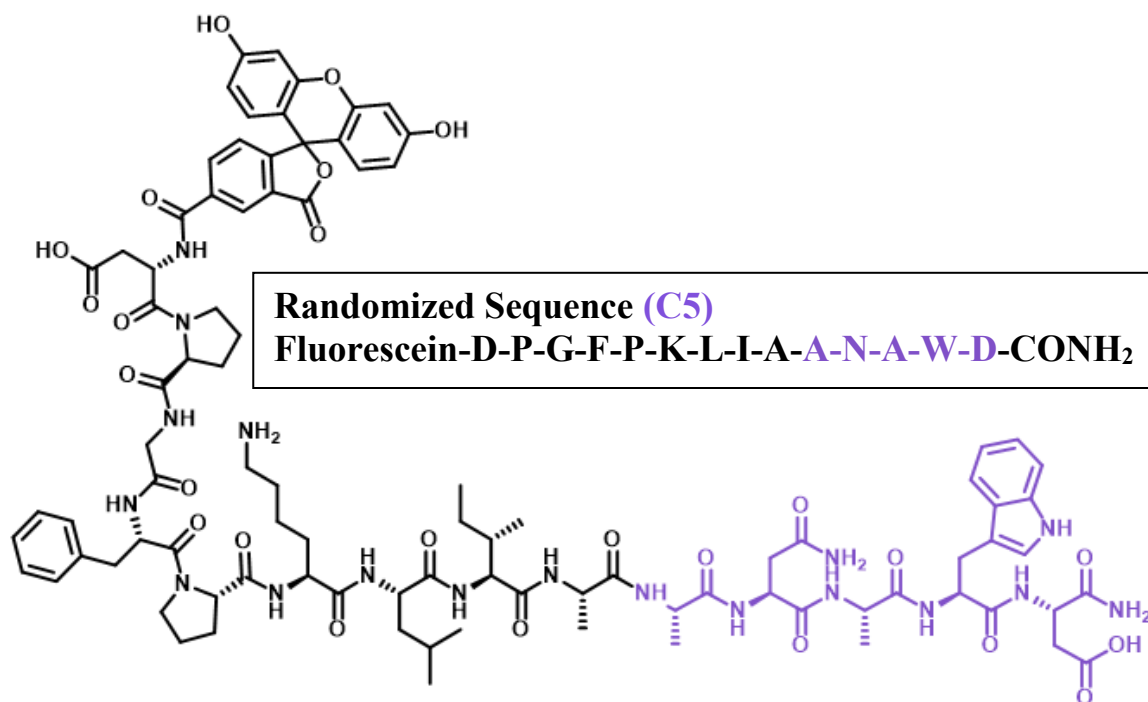


Figure 2.32. Circular dichroism (CD) spectrum of 20 μM of the fluorescein-labeled randomized epitope (C5) in PBS. No apparent secondary structure was observed.

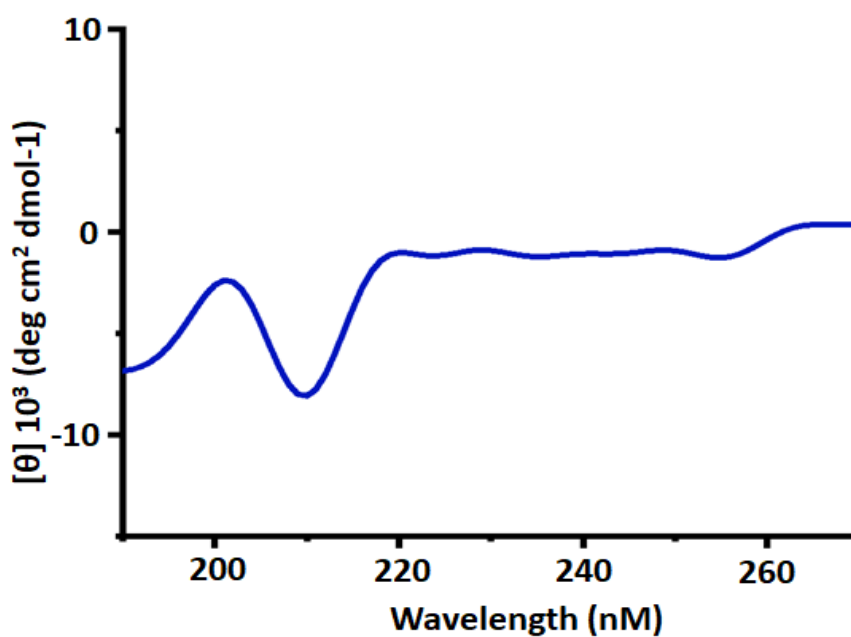
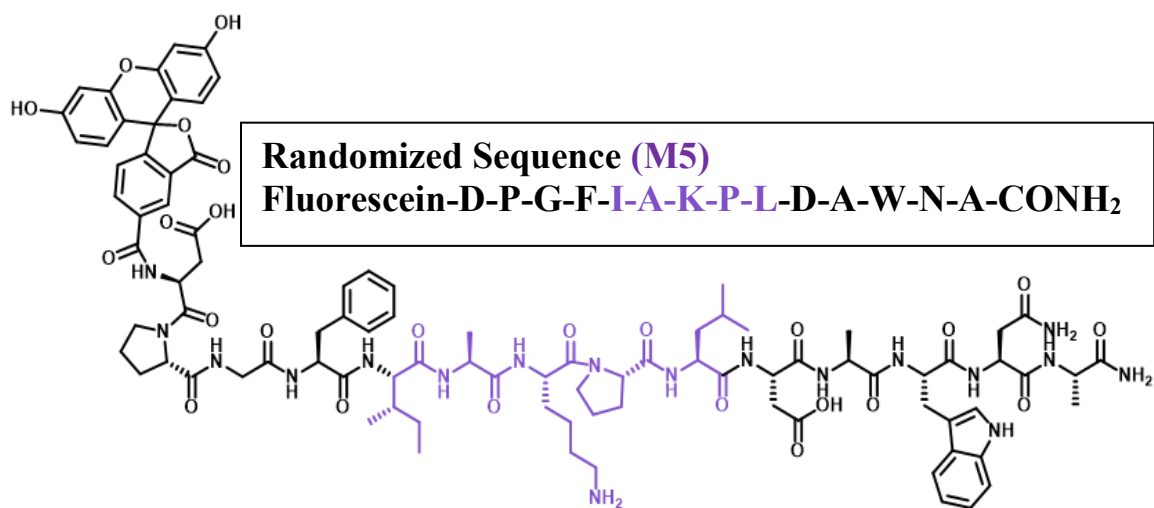


Figure 2.33. Circular dichroism (CD) spectrum of 20 μM of the fluorescein-labeled randomized epitope (M5) in PBS. No apparent secondary structure was observed.

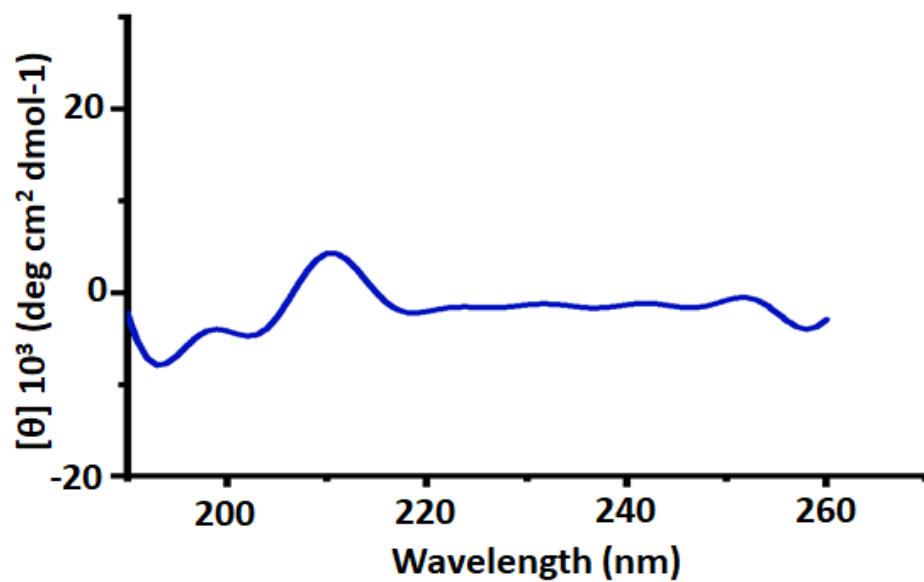
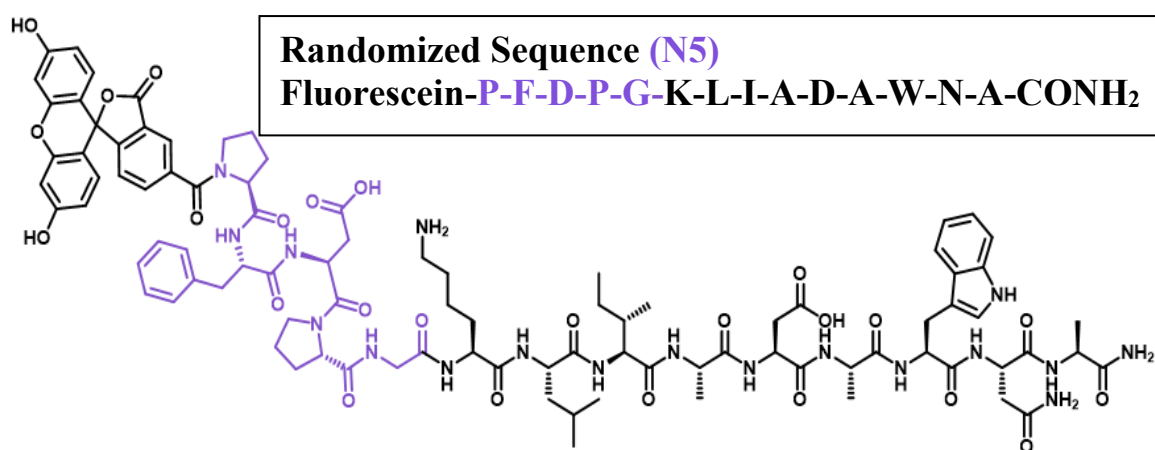


Figure 2.34. Circular dichroism (CD) spectrum of 20 μM of the fluorescein-labeled randomized epitope (N5) in PBS. No apparent secondary structure was observed.

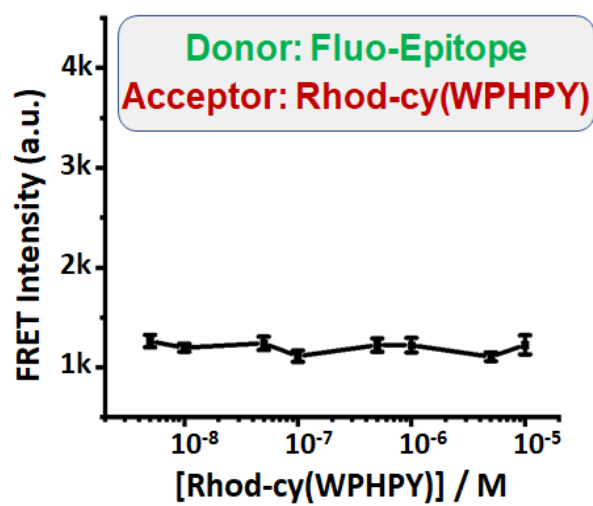
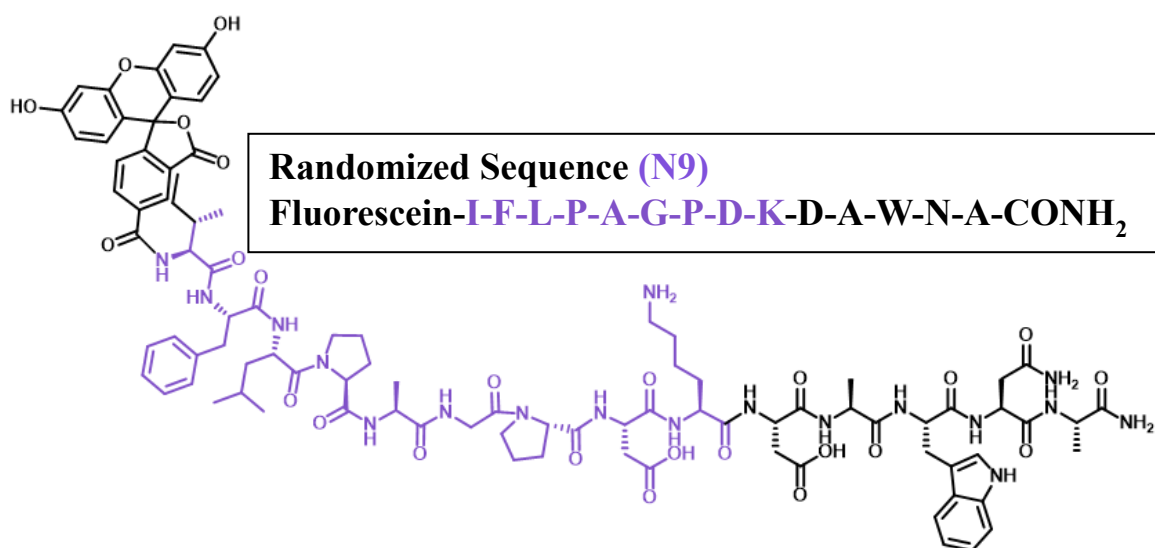


Figure 2.35. Since changing C5 showed a total loss of binding, this time we kept the first five amino acids at the C terminal unchanged and randomized the last nine amino acids. We ran a FRET assay using this epitope (N9) and rhodamine tagged ligand which also showed loss of binding.

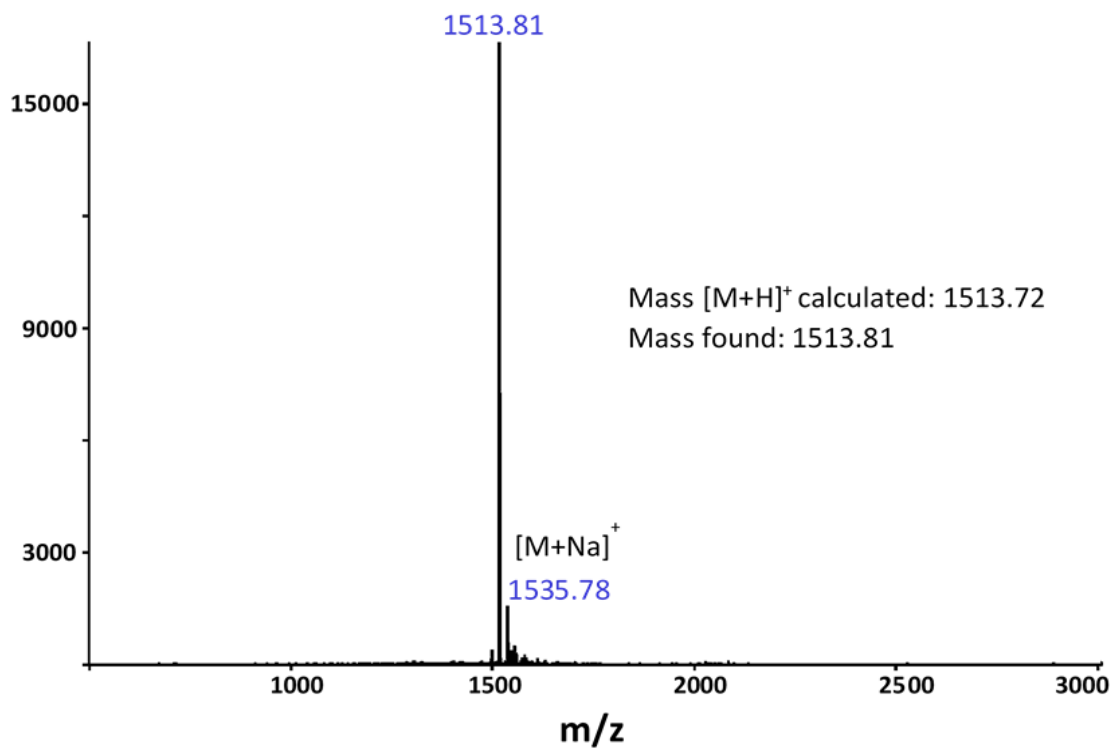
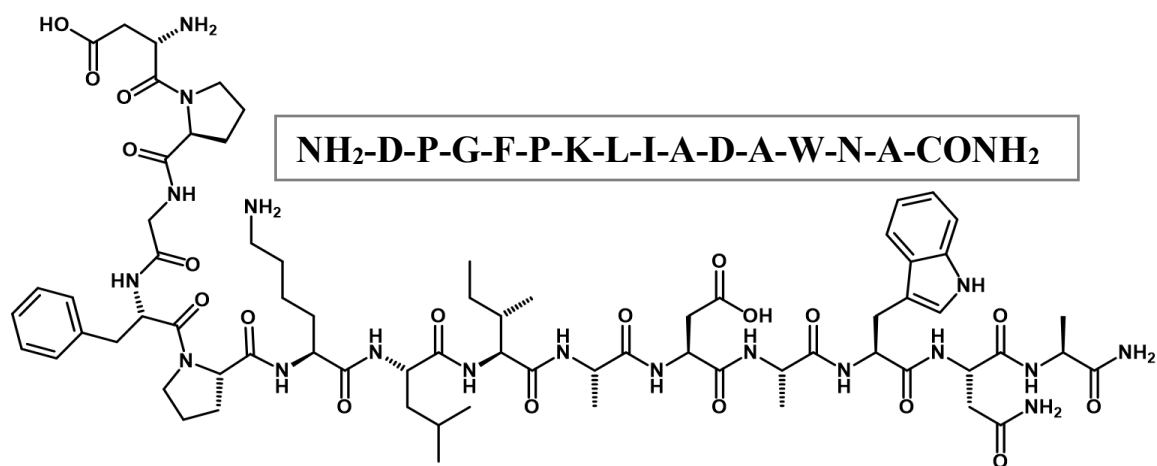


Figure 2.36. MALDI-TOF mass spectrum of the unmodified epitope.

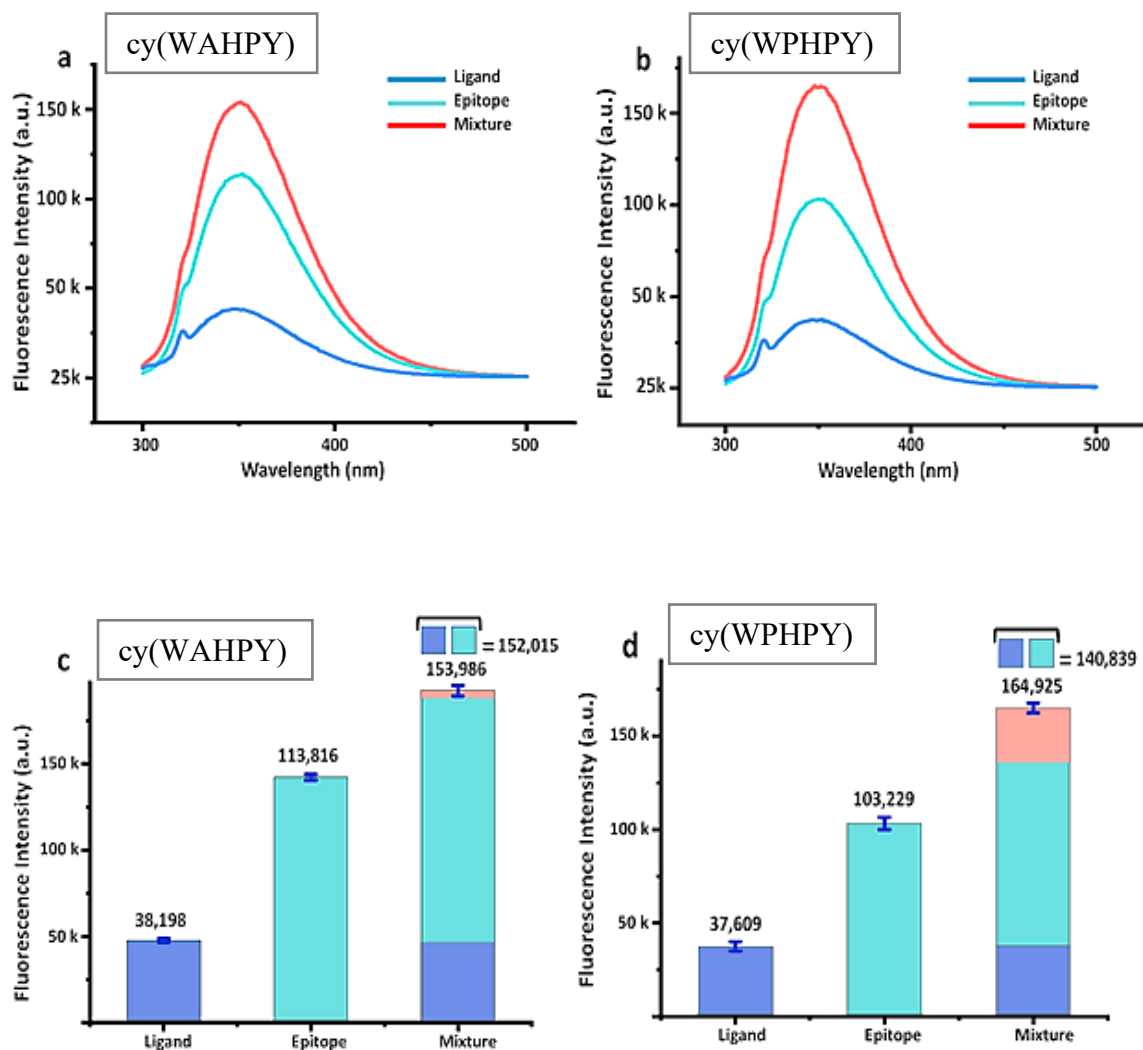


Figure 2.37. a. Emission spectra of the mutated ligand cy(WAHPY) (10 μ M), the epitope (10 μ M), and a mixture containing both. The spectra were obtained using an excitation wavelength of 288 nm. b. Similar emission spectra obtained using cy(WPHPY) (10 μ M), the epitope (10 μ M), and their mixture. c,d. Bar graph representations of a and b showing the fluorescence intensities at 350 nm. Only the cy(WPHPY)-epitope interaction led to an increased Trp fluorescence intensity.

cy(WPHPY) Inhibits the TIMP2–MMP2 Interaction through Binding to the MMP2 Hemopexin Domain

The TIMP2-binding region on the hemopexin domain remains intact during MMP2 activation. Therefore, we expected that cy(WPHPY) could bind to both pro- and active MMP2. To validate if cy(WPHPY) could interfere with the TIMP2–MMP2 protein–protein interaction, we performed a competitive binding test based on enzyme-linked immunosorbent assay (ELISA). WM115 cells (a human metastatic melanoma cell line) were cultured in serum-free media, which were used as a source of MMP2.⁵⁰ As shown in Figure 4a, surface immobilized recombinant TIMP2 was able to pull down MMP2 (pro- and active) from culture media, and cy(WPHPY) addition led to decreased MMP2 levels in a concentration dependent manner. These results agreed with our hypothesis that cy(WPHPY) could inhibit the PPI between TIMP2 and MMP2.

In addition to the hemopexin domain shared by pro- and active MMP2, the catalytic domain of active MMP2 is also a TIMP2 target. This alternative PPI is the basis of TIMP2- mediated MMP2 inhibition. Therefore, we must rule out the possibility that cy(WPHPY) was interfering with the TIMP2–MMP2 (catalytic domain) interaction.^{23,54-}

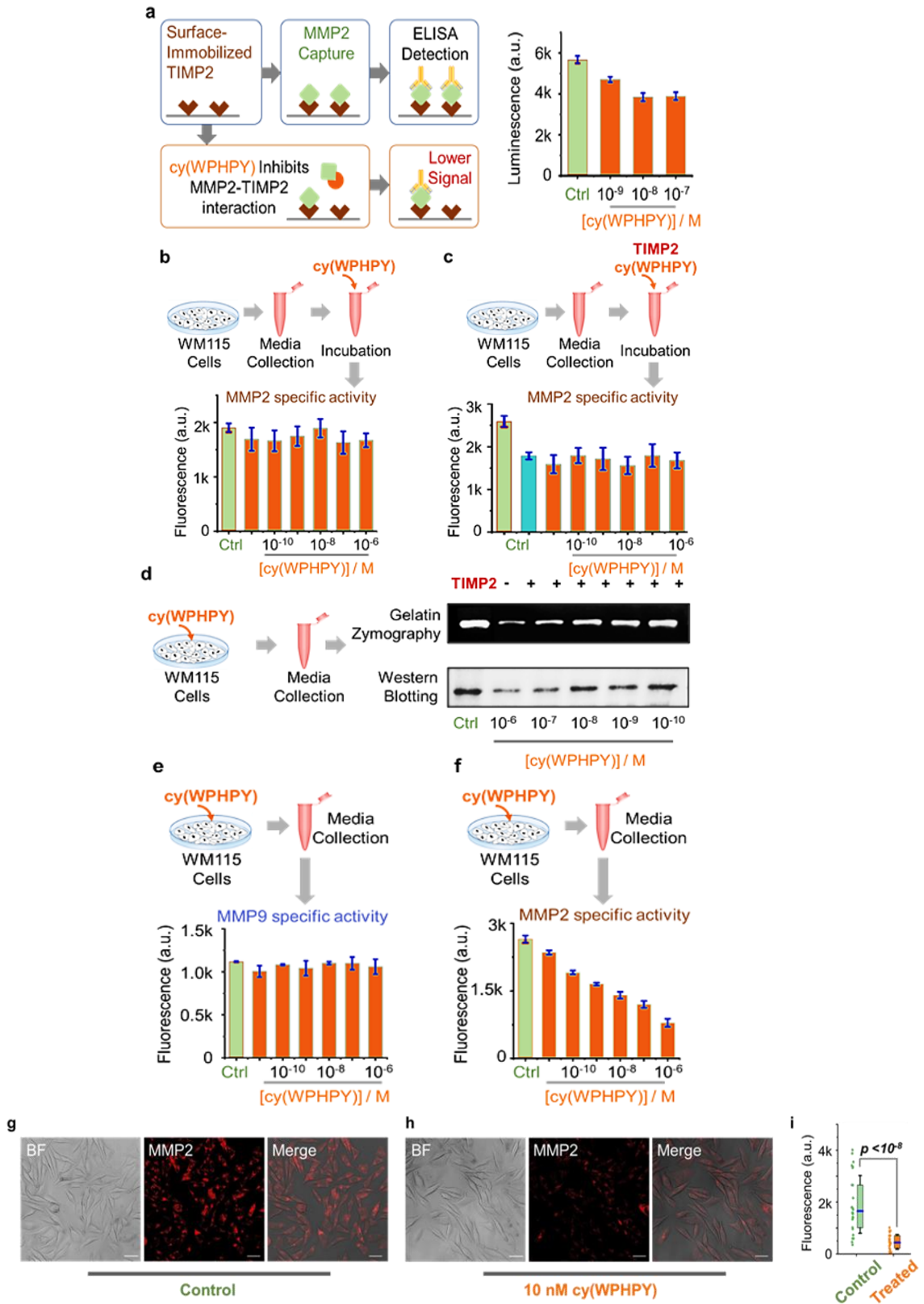
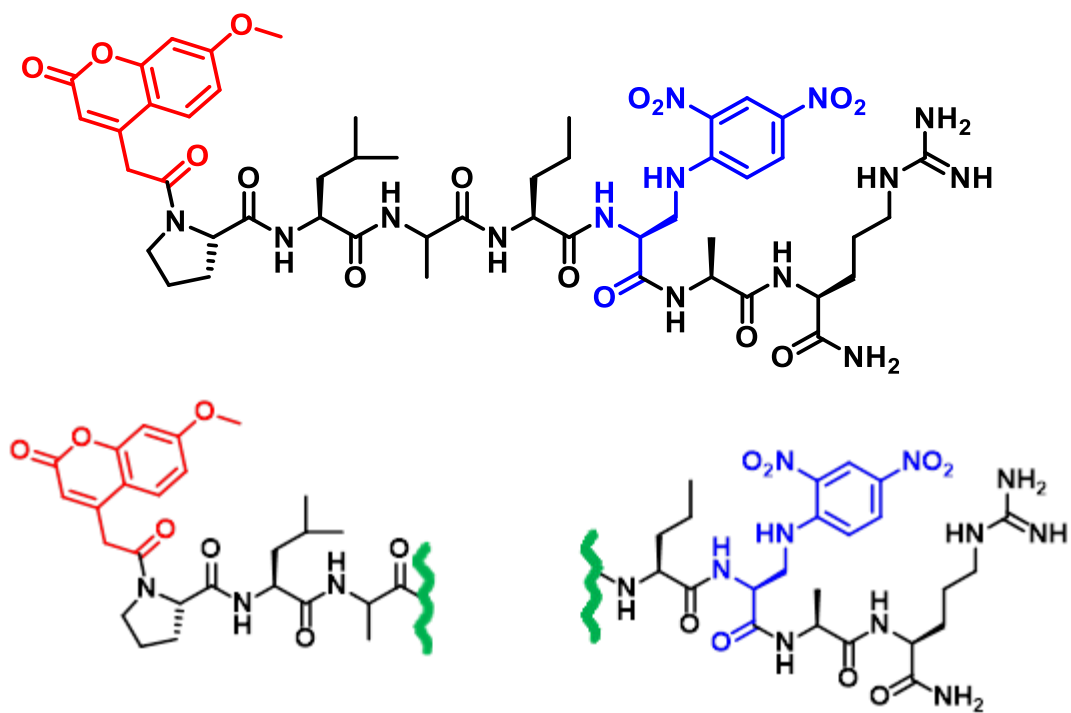


Figure 2.38. cy(WPHPY) inhibited the TIMP2–proMMP2 interaction and prevented proMMP2 activation. (a) Principle and results of the ELISA-based competitive binding assay. Surface-immobilized recombinant TIMP2 can pull down MMP2 from the solution, while cy(WPHPY) binds to MMP2 and blocks this interaction. Phosphate-buffered saline (PBS) was used in place of cy(WPHPY) in the control sample. (b–f) Schematic illustration and results of the *in vitro* bioactivity assay evaluating the function of cy(WPHPY). (b) Media from WM115 cell culture were collected and incubated with varying concentrations of cy(WPHPY). The corresponding MMP2 activities were analyzed using an MMP2-specific fluorogenic substrate. The assay buffer was used in place of cy(WPHPY) in the control sample. (c) WM115 culture media were incubated with TIMP2 and cy(WPHPY), and the corresponding MMP2 activities were evaluated. For the control samples, the assay buffer was used in place of cy(WPHPY) and TIMP2. (d–f) WM115 cells were cultured with varying concentrations of cy(WPHPY), and the corresponding media were collected for subsequent analyses. Serum-free media without cy(WPHPY) were used for the control samples. (d) Gelatin zymography and western blotting results demonstrate that cy(WPHPY) inhibited the MMP2 activity in the WM115 cell culture. (e, f) Enzymatic activity assays show that cy(WPHPY) was highly specific to MMP2 activities and did not affect MMP9. (g, h) Confocal microscopy images of WM115 cells showing membrane-bound MMP2 immunofluorescence. The scale bars are 10 μm . Media without cy(WPHPY) were used in the control sample. (i) Comparison of the single-cell MMP2 immunofluorescence signals extracted from the confocal images. A total of 30 single cells were analyzed for each image. The boxes denote the middle two quartiles, and the horizontal blue bars represent median values. The whiskers show the standard deviation values.

To address this concern, we first mixed the WM115 culture media with different concentrations of cy(WPHPY) and then used an MMP2-specific fluorogenic substrate to evaluate the corresponding MMP2 activity (Figure 2.39). Because cy(WPHPY) did not interact with the fluorescent substrate (Figure 2.40), our result proved that cy(WPHPY) did not affect MMP2 activity (Figure 4b). Nevertheless, because the size of cy(WPHPY) was small, even if it bound to the catalytic domain, it might not block the substrate's access to the catalytic center. To further validate our hypothesis, we introduced recombinant TIMP2 into the same experiment. Here, we found that cy(WPHPY) was not able to rescue the MMP2 activity from TIMP2 inhibition (Figure 4c), which proved that the PPI of TIMP2–MMP2 at the MMP2 catalytic domain was not affected. Taken together, these results supported our hypothesis that cy(WPHPY) specifically acted on the TIMP2–MMP2 interaction through the MMP2 hemopexin domain.



MCA-P-L-A-Nva-Dap(DNP)-A-R-NH₂

Figure 2.39. The structure of the MMP2-specific fluorogenic peptide substrate. Green lines highlight the MMP cleaving sites.

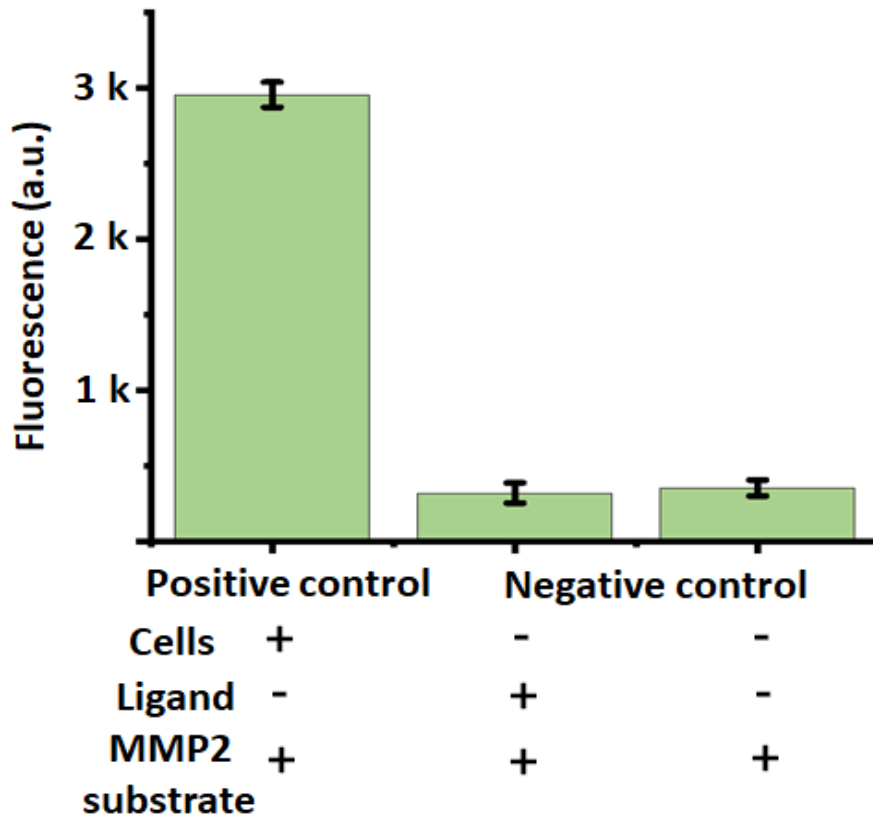


Figure 2.40. Positive and Negative controls used in the MMP2 specific substrate assay using MCA-P-L-A~Nva-Dap(DNP)-A-R-NH₂. The positive control consists of the serum-free media collected from WM115 cells. This media was then concentrated with a centrifugal membrane filter (10 kDa cut-off, Amicon). Once concentrated, the total protein content was quantified using a BCA assay kit (Thermo). In a 96 well microplate, 10 μ l (1 μ g/ μ l protein content) of the media was mixed with 90 μ l of TNC assay buffer (50 mM Tris base, 0.15 M NaCl, 10 mM CaCl₂, pH 7.5). The plate was left for 5 min at 37 °C for equilibration, and then 100 μ L of MMP2 specific substrate (3 μ M) was added. The plate was then incubated at 37 °C for 20 min. The fluorescence was measured using a SYNERGY H1 microplate reader. One of the negative controls has the ligand (1 μ M) in the serum-free media in which later the 3 μ M substrate was added, and the other one is the MMP2 specific substrate by itself in the serum-free media. The fluorescence was measured with a SYNERGY H1 microplate reader.

cy(WPHPY) Specifically Inhibits proMMP2 Activation In Vitro

We then moved on to test our hypothesis that disturbing the TIMP2–MMP2 interaction through the hemopexin domain will prevent proMMP2 activation. We treated WM115 cells with different concentrations of cy-(WPHPY) and analyzed the MMP2 content in the corresponding culture media. We first used gelatin zymography to evaluate how cy(WPHPY) affected MMP2 activity. As shown in Figure 4d, cy(WPHPY) treatment caused decreased MMP2 activity in the culture media, and the effect was dependent on the cy(WPHPY) concentration. To rule out the possibility that the observed decrease was due to cy(WPHPY) inhibiting MMP2 catalytic activity, we performed western blotting to quantify the amount of active MMP2 in the media. As expected, we observed a similar trend (Figure 4d). Based on the band intensity on the gel, we estimated an IC_{50} value of ~20 nM (Figure 2.41), which was consistent with the K_d value obtained from binding assays (Figure 2.4g). These results supported our proposed mechanism of action that cy-(WPHPY) inhibited proMMP2 activation.

Because our strategy targeted the unique D570-A583 epitope, which shares little homology with other MMPs, the inhibition was expected to be highly specific. To test this hypothesis, we used enzyme-specific fluorogenic substrates to analyze the activities of MMP2 and its most similar gelatinase relative, MMP9, in the culture media (Figures 2.39, 2.42, and 2.43). As shown in Figure 4e,f, cy(WPHPY) specifically acted on MMP2 and did not affect MMP9. In addition, we found that the linear sequence, WPHPY, showed no inhibition effect on MMP2 in the same experiment (Figure 2.44).

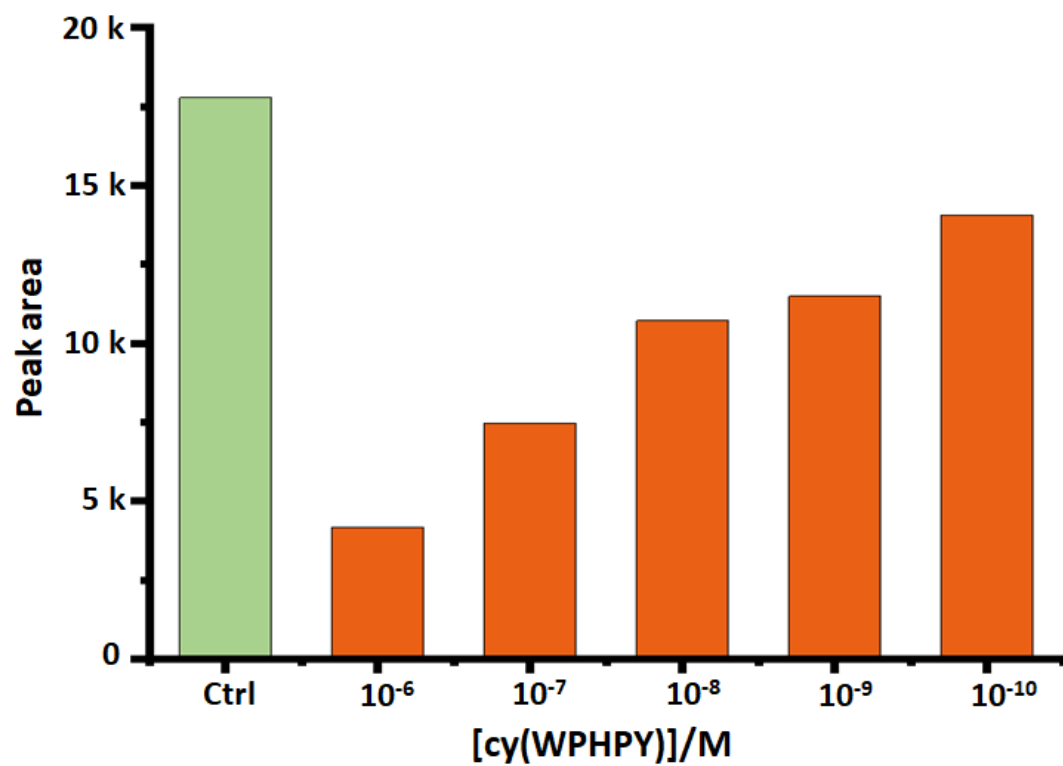
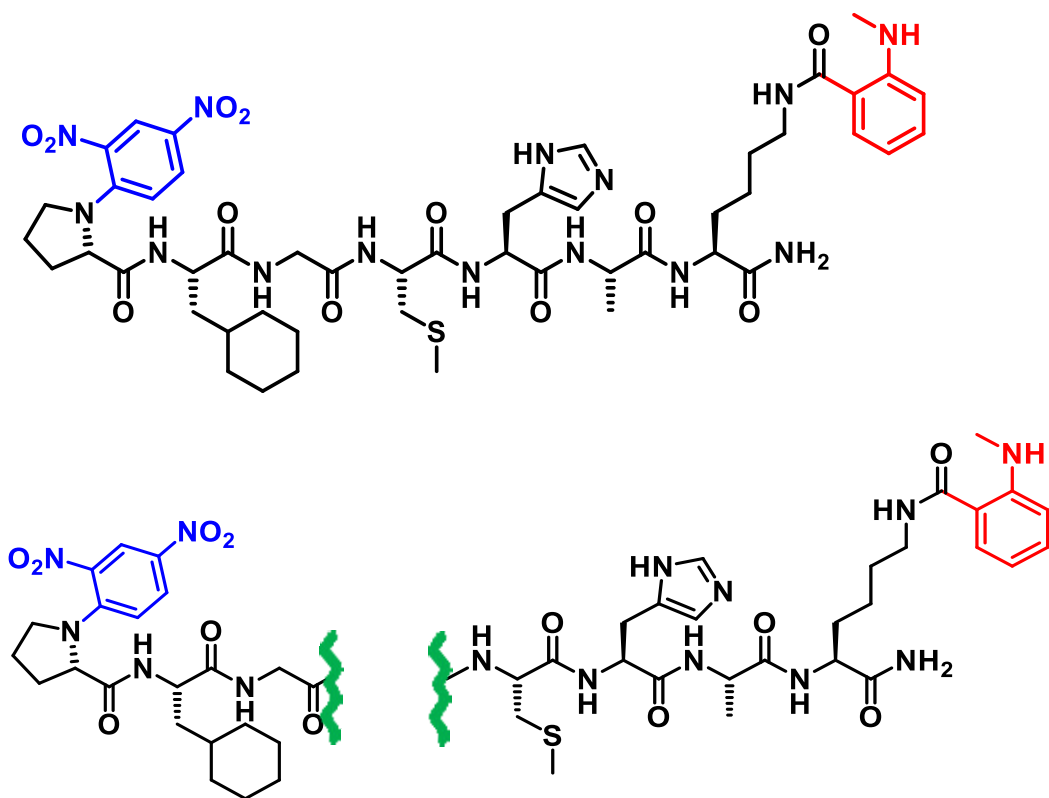


Figure 2.41. The intensities of the gelatin zymogram bands were measured using ImageJ software and plotted. The IC₅₀ value was estimated to be around 20 nM.



DNP-P-Cha-G-C(Me)-H-A-K(N-Me-Abz)-NH₂

Figure 2.42. The structure of the MM9-specific fluorogenic peptide substrate. Green lines highlight the MMP cleaving sites.

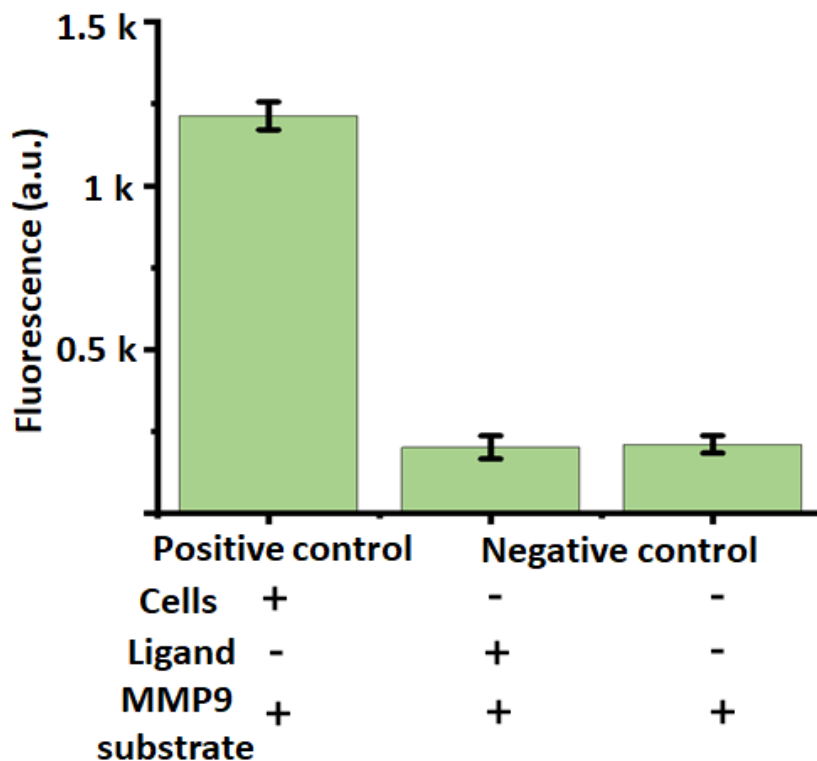


Figure 2.43. Positive and Negative controls used in the MMP9 specific substrate assay using DNP-P-Cha-G~C(Me)-H-A-K(N-Me-Abz)-NH₂. The positive control consists of the serum-free media collected from WM115 cells. This media was then concentrated with a centrifugal membrane filter (10 kDa cut-off, Amicon). Once concentrated, the total protein content was quantified using a BCA assay kit (Thermo). In a 96 well microplate, 10 μ l (1 μ g/ μ l protein content) of the protein solution was mixed with 90 μ l of TNC assay buffer (50 mM Tris base, 0.15 M NaCl, 10 mM CaCl₂, pH 7.5). The plate was left for 5 min at 37 °C for equilibration, and then 100 μ L of MMP9 specific substrate (3 μ M) was added. The plate was then incubated at 37 °C for 20 min. The fluorescence was measured using a SYNERGY H1 microplate reader. One of the negative controls has the ligand (1 μ M) in the serum-free media in which later the 3 μ M substrate was added, and the other one is the MMP9 specific substrate by itself in the serum-free media. The fluorescence was measured with a SYNERGY H1 microplate reader.

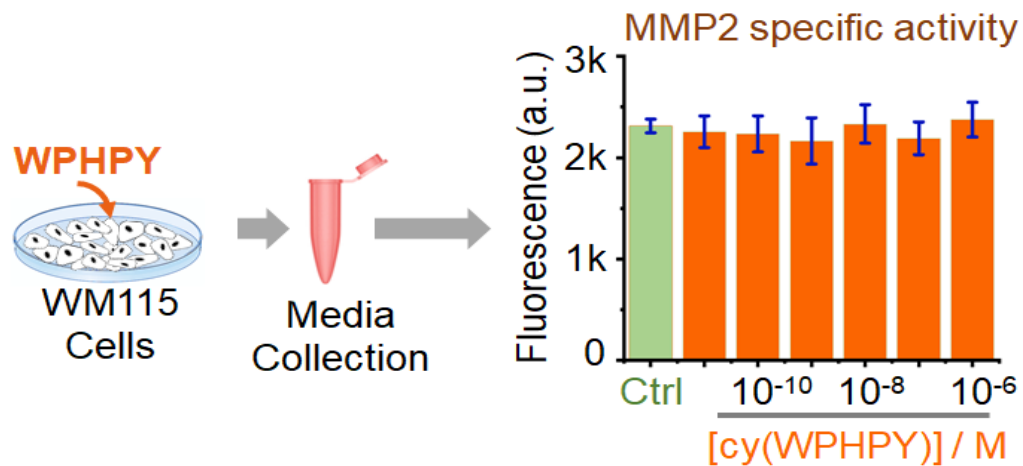


Figure 2.44. The linear sequence WPHPY was synthesized to see if it shows any inhibition efficiency. WM115 cells were cultured in full media to 80% confluency and then changed to serum-free media containing varying concentrations of the linear sequence. The culture media was then taken out, and the active MMP2 specific fluorogenic substrate was added to it. No significant change in the intensity was observed.

According to our proposed mechanism of action, cy- (WPHPY) was expected to prevent the cell membrane association of proMMP2. To visualize such an effect, we performed confocal microscopy experiments. We treated WM115 cells with cy(WPHPY) for 15 h and subsequently fixed the cells using paraformaldehyde. We then stained MMP2 using anti-MMP2 antibodies and evaluated the corresponding immunofluorescence. Because no permeabilizer was used, the majority of the fluorescence signal came from surface-bound MMP2. We found that cy(WPHPY) treatment led to decreased MMP2 signals (Figure 2.38g,h), which proved that fewer copies of MMP2 were associated with the cell surface. By extracting single-cell immunofluorescence data from the confocal images, we also validated that the observed MMP2 signal difference was statistically significant (Figure 2.38i).

cy(WPHPY) Inhibits Cell Migration

To validate if the inhibitory effect of cy(WPHPY) can translate into decreased cell mobility, we performed a wound-healing scratch assay. We used a micropipette tip to create artificial wounds on the cell culture and incubated the cells with cy(WPHPY) for 24 h (Figure 2.45a). Because these cells were pretreated with a mitotic inhibitor (mitomycin C), cells that appeared in the wound were due to cell migration. As shown in Figure 2.45b, cy(WPHPY) treatment led to decreased cell numbers in the wound region, demonstrating its ability to inhibit cell mobility.

To further validate our findings in a more quantitative manner, we carried out a transwell cell invasion assay using a two-chamber apparatus.⁵⁷ In the inner chamber, we cultured WM115 cells on Matrigel in serum-free media. A porous membrane separated this inner chamber from the outer chamber, which contained full media. To access the full media, cells must secrete MMP2 to digest the Matrigel and migrate to the other side of the membrane (Figure 2.45c). We found that cy(WPHPY) treatment led to fewer cells on the full media side of the membrane, indicating that it inhibited cell migration (Figure 2.45d). This effect was consistent with the observation from the wound-healing experiment. In addition, the inhibition ability matched the K_d and IC₅₀ values from previous assays (Figures 2g and 2.41), supporting our proposed mechanism of action.

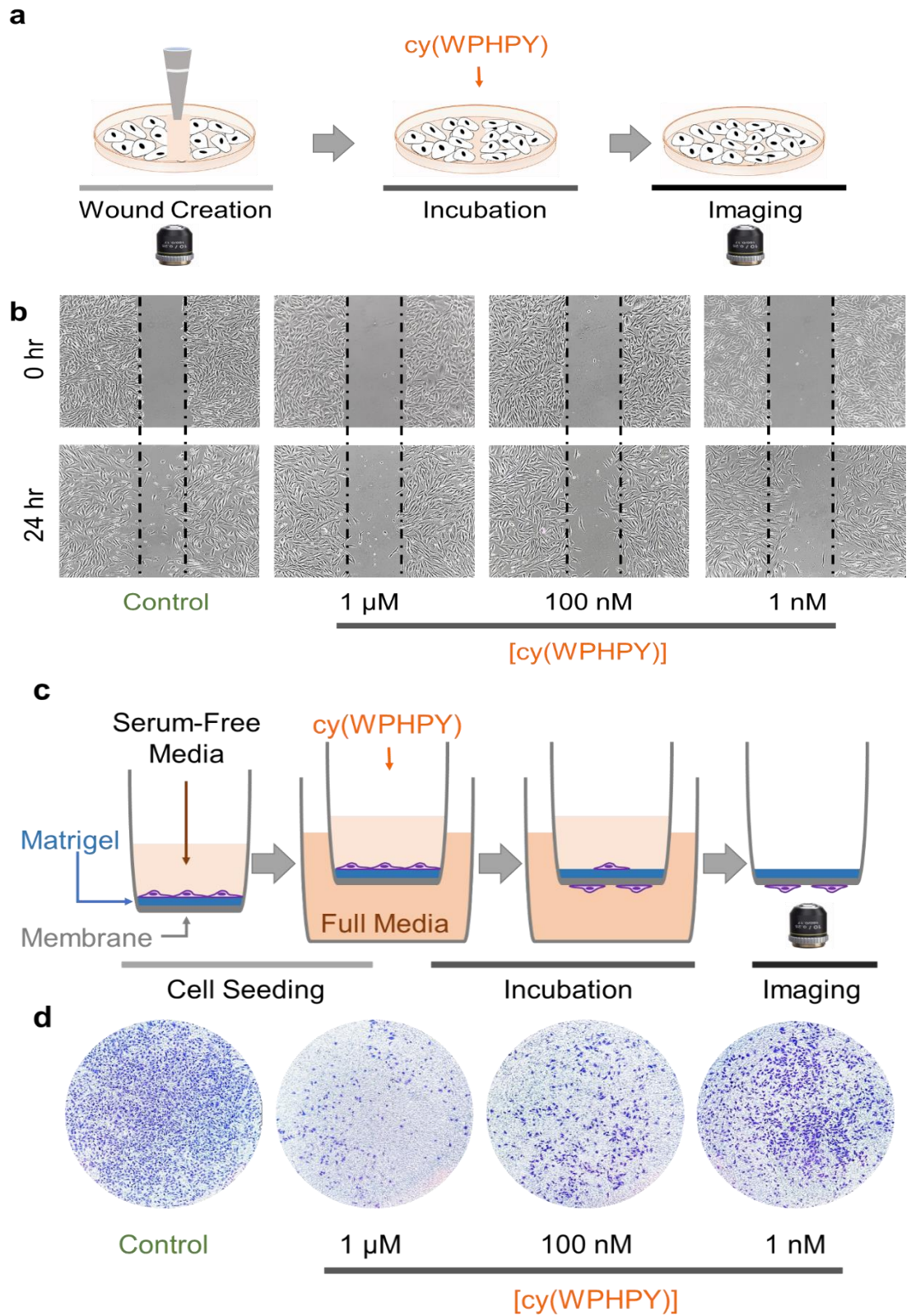


Figure 2.45. cy(WPHPY) inhibited cell migration. (a) Schematic illustration of the scratch wound-healing experiment. (b) Results of the scratch wound healing experiment demonstrate that cy(WPHPY) treatments led to fewer cells migrating to the scratch wound. (c) Schematic illustration of the trans-well cell invasion assay. Active MMP2 was required for the cells to digest the Matrigel and invade through the porous membrane. Before the final imaging stage, cells were fixed and stained with crystal violet. (d) Results of the trans-well assay demonstrate that cy(WPHPY) significantly inhibited cell invasion. Images were taken after 24 hours of incubation.

Discussion

Inhibiting MMP2 activities has profound therapeutic implications. Unfortunately, a clinically viable drug remains elusive, despite more than 3 decades of research efforts. Results from the failed clinical trials have underscored the need of developing highly specific MMP2 inhibitors. However, this is substantially challenging because of the prevalent structural similarities among the catalytic domain of different MMPs.¹⁶ Consequently, targeting the enzymatic activity of MMP2 has become a less-favored approach.¹⁷ Evidently, research interests have shifted toward alternative strategies, such as inhibiting the zymogen activation process involving the proMMP2/TIMP2/ MT1-MMP ternary complex.¹⁷⁻²⁰ Pioneering work has focused on membrane-tethered MT1-MMP, as represented by the development of DX2400 and 9E8 antibodies.^{19,20} These studies have demonstrated the feasibility of achieving MMP2 inhibition by preventing proMMP2 activation. Nevertheless, therapeutic development based on these antibody leads faces significant obstacles, such as the lack of functional specificity of DX2400 and the murine origin of 9E8 mAb.²⁰

On the other hand, targeting the interaction between proMMP2 and TIMP2 remains underexplored. The structural basis for this PPI involves two epitopes on proMMP2, the Cterminal fourth blade of the hemopexin domain and the loop between the third and

fourth hemopexin blades.²⁵ Because the fourth hemopexin blade exhibits very high sequence homology to many other proteins (Figure 2.46), it is not a suitable target for drug development. In contrast, the second epitope has a unique amino acid sequence. Nevertheless, this second epitope is structureless, which makes it a challenging target for developing high-affinity binders. Although studies on inhibiting a related PPI, i.e., between proMMP9 and TIMP1, have been successful,^{58,59} it is largely because that many parts of the proMMP9 hemopexin domain are structurally distinct and easier to target.⁶⁰ Therefore, it was unclear whether proMMP2 could be targeted similarly. To this end, our results provide the first demonstration of blocking the proMMP2–TIMP2 interaction to inhibit proMMP2 activation, proving the feasibility of this long-sought strategy.

In this study, removing the rhodamine tag improved the binding affinity by 100-fold. Such a result may seem astonishing if one puts peptides and proteins in the same therapeutics category. However, the cyclic peptide presented here has a molecular weight less than 1 kDa, which makes it more similar to a small molecule than large biologics. Considering that the rhodamine tag size is more than half of the cyclic peptide size, it is expected that this tag would significantly affect the binding affinity. Besides, because a structureless loop was targeted, it was expected that this binding would be sensitive to structure variations. The alanine scanning and the epitope randomization results (Figure 2.30) further demonstrated this point. On the other hand, it was to our surprise that the epitope-based competitive FRET results matched extremely well with the recombinant protein-based competitive FP data. Although the target epitope resides at the peripheral region of the protein and its structureless nature is conserved in the full-length protein,

neighboring epitopes and the protein's tertiary structure could influence the peptide-epitope interaction in an unforeseeable manner. Therefore, it is always crucial to validate the binding using full-length proteins. Nevertheless, this extra effort does not diminish the feasibility or application of the epitope-targeted screening approach, which has been demonstrated in many studies.^{26,50,61}

MMP-2 catalytic domain	Homology	Protein name
	64%	MMP-9 (3-157)
RKPKW DKNQITYRIIGYTPDLDPETVDDAFARAF	64%	MMP-13 (6-164)
QVWSDV TPLRFSRIHDGEADIMINFG RWEHGDG	59%	MMP-3 (2-162)
Y PFDGK DGLLAHAFAPGTGVGGDSHFDDDELWS	58%	MMP-12 (3-159)
L GKG VGYSLFLVAAHEFGHAMGLEHSQDPGALM	58%	MMP-20 (2-159)
A PIYTYTKNFRLSQDDIKGIQELYGASP	56%	MMP-8 (6-163)
	58%	MMP-10 (8-165)
	55%	MMP-1 (7-164)

Figure 2.46. Sequence alignment and homology search result for the TIMP2 binding epitope on the 4th hemopexin blade of proMMP-2 using protein BLAST®. The epitope sequence is placed in the first line (navy background). The other MMPs with the sequence homology found from the search are shown in rows 2-7. Empty boxes represent completely mismatched residues.

Our results also shed light on the structural biology of the TIMP2–MMP2 interaction. Instead of facilitating MMP2 activation, a more well-known role of TIMP2 is inhibiting active MMP2. The detailed mechanism of this inhibition is elusive, as the structure of the active MMP2–TIMP2 complex has not been solved. The current hypothesis is that the N-terminal domain of TIMP2 can bind to the catalytic domain of MMP2, thereby blocking the substrate entrance to the catalytic center.^{25,62} Moreover, an auxiliary binding between TIMP2 and the MMP2 hemopexin domain is believed to stabilize the interaction further.⁶⁰ However, it is unclear if this interaction involves the same hemopexin epitope

as the one implicated in proMMP2 activation. Because the hemopexin domain on proMMP2 is conserved through its activation process, the cy(WPHPY) peptide is expected to bind to both pro- and active MMP2. Our results (Figure 4c) demonstrated that binding of cy(WPHPY) to active MMP2 did not interfere with the inhibitory TIMP2–MMP2 interaction. Based on these data, we believe that the inhibitory PPI between TIMP2 and MMP2 does not involve the loop between the third and fourth hemopexin blades on MMP2.

Aside from the TIMP2/MT1-MMP-mediated process, other mechanisms of proMMP2 activation also exist. For instance, in human astrocytic tumor cases, prominent correlations exist among the MT2-MMP expression level, the MMP2 activity, and the tumor grade.⁶¹ These observations are consistent with the in vitro result that MT2-MMP can activate proMMP2 without help from MT1-MMP.⁶⁴ Other types of TIMPs can also bind to proMMP2 to facilitate its activation.⁶² Therefore, our method of directly targeting proMMP2, rather than TIMP2 or MT1-MMP, promises more generalization potential. The uncertainty here is whether our targeted epitope on the hemopexin domain is also involved in these alternative MMP2 activation routes. As a natural extension to this work, we are currently testing the efficacy of cy(WPHPY) in MT1-MMP- and TIMP2-deficient models. The result will provide structural insights into how proMMP2 interacts with other types of MT-MMPs and TIMPs.

2.4 Conclusion

The work presented here, together with recent reports from other groups and us, highlights the feasibility of using cyclic peptides to target protein–protein interactions. The two proline residues in cy(WPHPY) provided substantial backbone rigidity, which was proven critical to the binding. This finding is consistent with previous reports that increased structural rigidity in cyclic peptides translates into higher binding affinities to disordered protein structures. In light of these results, we are currently implementing medicinal chemistry optimization strategies on cy(WPHPY), with an emphasis on preserving the structural rigidity and the orientation of side-chain functional groups. We believe that such efforts promise more potent and specific inhibitors against MMP2 activation and ultimately a clinically viable strategy for MMP2 inhibition.

2.5 References

1. Visse, R.; Nagase, H. Matrix Metalloproteinases and Tissue Inhibitors of Metalloproteinases: Structure, Function, and Biochemistry. *Circ Res* **2003**, 92, 827-839.
2. Page-McCaw, A.; Ewald, A. J.; Werb, Z. Matrix Metalloproteinases and the Regulation of Tissue Remodelling. *Nature Reviews Molecular Cell Biology* **2007**, 8, 221-233.
3. Li, Y. Y.; McTiernan, C. F.; Feldman, A. M. Interplay of Matrix Metalloproteinases, Tissue Inhibitors of Metalloproteinases and Their Regulators in Cardiac Matrix Remodeling. *Cardiovasc Res* **2000**, 46, 214-224.
4. Curran, S.; Murray, G. I. Matrix Metalloproteinases: Molecular Aspects of Their Roles in Tumour Invasion and Metastasis. *Eur J Cancer* **2000**, 36, 1621-1630.
5. Vartak, D. G.; Gemeinhart, R. A. Matrix Metalloproteases: Underutilized Targets for Drug Delivery. *J Drug Target* **2007**, 15, 1-20.
6. Henriët, P.; Emonard, H. Matrix Metalloproteinase-2: Not (Just) a “Hero” of the Past. *Biochimie* **2019**, 166, 223-232.
7. Hopkins, A. L. G., Colin R. The Druggable Genome. *Nature Reviews Drug Discovery* **2002**, 1, 727-730.
8. Pavlaki, M.; Zucker, S. Matrix Metalloproteinase Inhibitors (Mmpis): The Beginning of Phase I or the Termination of Phase Iii Clinical Trials. *Cancer Metastasis Rev* **2003**, 22, 177-203.
9. Vandenbroucke, R. E.; Libert, C. Is There New Hope for Therapeutic Matrix Metalloproteinase Inhibition? *Nature Reviews Drug Discovery* **2014**, 13, 904-927.
10. Dorman, G.; Cseh, S.; Hajdu, I.; Barna, L.; Konya, D.; Kupai, K.; Kovacs, L.; Ferdinandy, P. Matrix Metalloproteinase Inhibitors: A Critical Appraisal of Design Principles and Proposed Therapeutic Utility. *Drugs* **2010**, 70, 949-964.
11. Shi, Z. G.; Li, J. P.; Shi, L. L.; Li, X. An Updated Patent Therapeutic Agents Targeting Mmps. *Recent Pat Anticancer Drug Discov* **2012**, 7, 74-101.
12. Fingleton, B. Matrix Metalloproteinase Inhibitors for Cancer Therapy: The Current Situation and Future Prospects. *Expert Opin Ther Targets* **2003**, 7, 385-397.
13. Coussens, L. M.; Fingleton, B.; Matrisian, L. M. Matrix Metalloproteinase Inhibitors and Cancer: Trials and Tribulations. *Science* **2002**, 295, 2387-2392.

14. Overall, C. M.; Kleinfeld, O. Tumour Microenvironment - Opinion: Validating Matrix Metalloproteinases as Drug Targets and Anti-Targets for Cancer Therapy. *Nature Reviews Cancer* **2006**, *6*, 227-239.
15. Cathcart, J.; Pulkoski-Gross, A.; Cao, J. Targeting Matrix Metalloproteinases in Cancer: Bringing New Life to Old Ideas. *Genes and Diseases* **2015**, *2*, 26-34.
16. Fields, G. B. Mechanisms of Action of Novel Drugs Targeting Angiogenesis-Promoting Matrix Metalloproteinases. *Front Immunol* **2019**, *10*, 1278-1278
17. Cathcart, J.; Pulkoski-Gross, A.; Cao, J. Targeting Matrix Metalloproteinases in Cancer: Bringing New Life to Old Ideas. *Genes & Diseases* **2015**, *2*, 26-34.
18. Yosef, G.; Arkadash, V.; Papo, N. Targeting the Mmp-14/Mmp-2/Integrin $\text{Av}\beta 3$ Axis with Multispecific N-Timp2–Based Antagonists for Cancer Therapy. *J Biol Chem* **2018**, *293*, 13310-13326.
19. Devy, L.; Huang, L.; Naa, L.; Yanamandra, N.; Pieters, H.; Frans, N.; Chang, E.; Tao, Q.; Vanhove, M.; Lejeune, A.; van Gool, R.; Sexton, D. J.; Kuang, G.; Rank, D.; Hogan, S.; Pazmany, C.; Ma, Y. L.; Schoonbroodt, S.; Nixon, A. E.; Ladner, R. C.; Hoet, R.; Henderikx, P.; TenHoor, C.; Rabbani, S. A.; Valentino, M. L.; Wood, C. R.; Dransfield, D. T. Selective Inhibition of Matrix Metalloproteinase-14 Blocks Tumor Growth, Invasion, and Angiogenesis. *Cancer Res* **2009**, *69*, 1517.
20. Shiryayev, S. A.; Remacle, A. G.; Golubkov, V. S.; Ingvarsen, S.; Porse, A.; Behrendt, N.; Cieplak, P.; Strongin, A. Y. A Monoclonal Antibody Interferes with Timp-2 Binding and Incapacitates the Mmp-2-Activating Function of Multifunctional, Pro-Tumorigenic Mmp-14/Mt1–Mmp. *Oncogenesis* **2013**, *2*, e80.
21. Itoh, Y.; Takamura, A.; Ito, N.; Maru, Y.; Sato, H.; Suenaga, N.; Aoki, T.; Seiki, M. Homophilic Complex Formation of Mt1-Mmp Facilitates Prommp-2 Activation on the Cell Surface and Promotes Tumor Cell Invasion. *EMBO J* **2001**, *20*, 4782-4793.
22. Deryugina, E. I.; Quigley, J. P. Matrix Metalloproteinases and Tumor Metastasis. *Cancer Metastasis Rev* **2006**, *25*, 9-34.
23. Nagase, H.; Visse, R.; Murphy, G. Structure and Function of Matrix Metalloproteinases and Timps. *Cardiovasc Res* **2006**, *69*, 562-573.
24. Zucker, S.; Drews, M.; Conner, C.; Foda, H. D.; DeClerck, Y. A.; Langley, K. E.; Bahou, W. F.; Docherty, A. J. P.; Cao, J. Tissue Inhibitor of Metalloproteinase-2 (Timp-2) Binds to the Catalytic Domain of the Cell Surface Receptor, Membrane Type 1-Matrix Metalloproteinase 1 (Mt1-Mmp). *J Biol Chem* **1998**, *273*, 1216-1222.

25. Morgunova, E.; Tuuttila, A.; Bergmann, U.; Tryggvason, K. Structural Insight into the Complex Formation of Latent Matrix Metalloproteinase 2 with Tissue Inhibitor of Metalloproteinase 2. *Proceedings of the National Academy of Sciences* **2002**, *99*, 7414-7419.
26. Das, S.; Nag, A.; Liang, J.; Bunck, D. N.; Umeda, A.; Farrow, B.; Coppock, M. B.; Sarkes, D. A.; Finch, A. S.; Agnew, H. D.; Pitram, S.; Lai, B.; Yu, M. B.; Museth, A. K.; Deyle, K. M.; Lepe, B.; Rodriguez-Rivera, F. P.; McCarthy, A.; Alvarez-Villalonga, B.; Chen, A.; Heath, J.; Stratis-Cullum, D. N.; Heath, J. R. A General Synthetic Approach for Designing Epitope Targeted Macrocyclic Peptide Ligands. *Angew Chem Int Ed* **2015**, *54*, 13219-13224.
27. Dougherty, P. G.; Qian, Z.; Pei, D. Macrocycles as Protein–Protein Interaction Inhibitors. *Biochem J* **2017**, *474*, 1109-1125.
28. Heinis, C.; Winter, G. Encoded Libraries of Chemically Modified Peptides. *Curr Opin Chem Biol* **2015**, *26*, 89-98.
29. Moellering, R. E.; Cornejo, M.; Davis, T. N.; Del Bianco, C.; Aster, J. C.; Blacklow, S. C.; Kung, A. L.; Gilliland, D. G.; Verdine, G. L.; Bradner, J. E. Direct Inhibition of the Notch Transcription Factor Complex. *Nature* **2009**, *462*, 182-188.
30. Qian, Z.; Dougherty, P. G.; Pei, D. Targeting Intracellular Protein–Protein Interactions with Cell-Permeable Cyclic Peptides. *Curr Opin Chem Biol* **2017**, *38*, 80-86.
31. Tavassoli, A.; Lu, Q.; Gam, J.; Pan, H.; Benkovic, S. J.; Cohen, S. N. Inhibition of Hiv Budding by a Genetically Selected Cyclic Peptide Targeting the Gag–Tsg101 Interaction. *ACS Chem Biol* **2008**, *3*, 757-764.
32. Cardote, T. A. F.; Ciulli, A. Cyclic and Macrocyclic Peptides as Chemical Tools to Recognise Protein Surfaces and Probe Protein–Protein Interactions. *ChemMedChem* **2016**, *11*, 787-794.
33. Boehm, M.; Beaumont, K.; Jones, R.; Kalgutkar, A. S.; Zhang, L.; Atkinson, K.; Bai, G.; Brown, J. A.; Eng, H.; Goetz, G. H.; Holder, B. R.; Khunte, B.; Lazzaro, S.; Limberakis, C.; Ryu, S.; Shapiro, M. J.; Tylaska, L.; Yan, J.; Turner, R.; Leung, S. S. F.; Ramaseshan, M.; Price, D. A.; Liras, S.; Jacobson, M. P.; Earp, D. J.; Lokey, R. S.; Mathiowetz, A. M.; Menhaji-Klotz, E. Discovery of Potent and Orally Bioavailable Macrocyclic Peptide–Peptoid Hybrid Cxcr7 Modulators. *J Med Chem* **2017**, *60*, 9653-9663.
34. Naylor, M. R.; Bockus, A. T.; Blanco, M.-J.; Lokey, R. S. Cyclic Peptide Natural Products Chart the Frontier of Oral Bioavailability in the Pursuit of Undruggable Targets. *Curr Opin Chem Biol* **2017**, *38*, 141-147

35. Klemm, P. Manual Edman Degradation of Proteins and Peptides. *Methods Mol Biol* **1984**, 1, 243-254.
36. Lee, S. S.; Lim, J.; Cha, J.; Tan, S.; Heath, J. R. Rapid Microwave-Assisted Cnbr Cleavage of Bead-Bound Peptides. *J Comb Chem* **2008**, 10, 807-809.
37. Niedermeyer, T. H.; Strohm, M. Mmass as a Software Tool for the Annotation of Cyclic Peptide Tandem Mass Spectra. *PLoS One* **2012**, 7, e44913.
38. Maier, J. A.; Martinez, C.; Kasavajhala, K.; Wickstrom, L.; Hauser, K. E.; Simmerling, C. Ff14sb: Improving the Accuracy of Protein Side Chain and Backbone Parameters from Ff99sb. *J Chem Theory Comput* **2015**, 11, 3696-3713.
39. Hanwell, M. D.; Curtis, D. E.; Lonie, D. C.; Vandermeersch, T.; Zurek, E.; Hutchison, G. R. Avogadro: An Advanced Semantic Chemical Editor, Visualization, and Analysis Platform. *J Cheminform* **2012**, 4, 17.
40. Jakalian, A.; Jack, D. B.; Bayly, C. I. Fast, Efficient Generation of High-Quality Atomic Charges. Am1-Bcc Model: Ii. Parameterization and Validation. *J Comput Chem* **2002**, 23, 1623-1641.
41. Wang, J.; Wolf, R. M.; Caldwell, J. W.; Kollman, P. A.; Case, D. A. Development and Testing of a General Amber Force Field. *J Comput Chem* **2004**, 25, 1157-1174.
42. Case, D.; Babin, V.; Berryman, J.; Betz, R.; Cai, Q.; Cerutti, D.; Cheatham III, T.; Darden, T.; Duke, R.; Gohlke, H. The Ff14sb Force Field. *Amber* **2014**, 14, 29-31.
43. Chang, C. E.; Gilson, M. K. Tork: Conformational Analysis Method for Molecules and Complexes. *J Comput Chem* **2003**, 24, 1987-1998.
44. Jorgensen, W. L.; Chandrasekhar, J.; Madura, J. D.; Impey, R. W.; Klein, M. L. Comparison of Simple Potential Functions for Simulating Liquid Water. *The Journal of Chemical Physics* **1983**, 79, 926-935.
45. Case, D. A.; Cheatham, T. E., 3rd; Darden, T.; Gohlke, H.; Luo, R.; Merz, K. M., Jr.; Onufriev, A.; Simmerling, C.; Wang, B.; Woods, R. J. The Amber Biomolecular Simulation Programs. *J Comput Chem* **2005**, 26, 1668-1688.
46. Darden, T.; York, D.; Pedersen, L. Particle Mesh Ewald: An N· Log (N) Method for Ewald Sums in Large Systems. *The Journal of chemical physics* **1993**, 98, 10089-10092.
47. Troeberg, L.; Nagase, H. Monitoring Metalloproteinase Activity Using Synthetic Fluorogenic Substrates. *Curr Protoc Protein Sci* **2004**, 33, 21.16.21-21.16.29.

48. Toth, M.; Fridman, R. Assessment of Gelatinases (Mmp-2 and Mmp-9 by Gelatin Zymography. *Methods Mol Med* **2001**, *57*, 163-174.
49. Mahmood, T.; Yang, P. C. Western Blot: Technique, Theory, and Trouble Shooting. *N Am J Med Sci* **2012**, *4*, 429-434
50. Shao, S.; Li, Z.; Cheng, H.; Wang, S.; Perkins, N. G.; Sarkar, P.; Wei, W.; Xue, M. A Chemical Approach for Profiling Intracellular Akt Signaling Dynamics from Single Cells. *J Am Chem Soc* **2018**, *140*, 13586-13589.
51. Joo, S. H. Cyclic Peptides as Therapeutic Agents and Biochemical Tools. *Biomol Ther (Seoul)* **2012**, *20*, 19.
52. Chen, Y.; Barkley, M. D. Toward Understanding Tryptophan Fluorescence in Proteins. *Biochemistry* **1998**, *37*, 9976-9982.
53. Ciolczyk-Wierzbička, D.; Laidler, P. The Inhibition of Invasion of Human Melanoma Cells through N-Cadherin Knock-Down. *Med Oncol* **2018**, *35*, 42.
54. Olson, M. W.; Gervasi, D. C.; Mobashery, S.; Fridman, R. Kinetic Analysis of the Binding of Human Matrix Metalloproteinase-2 and -9 to Tissue Inhibitor of Metalloproteinase (Timp)-1 and Timp-2. *J Biol Chem* **1997**, *272*, 29975-29983.
55. Nguyen, Q.; Willenbrock, F.; Cockett, M. I.; O'Shea, M.; Docherty, A. J.; Murphy, G. Different Domain Interactions Are Involved in the Binding of Tissue Inhibitors of Metalloproteinases to Stromelysin-1 and Gelatinase A. *Biochemistry* **1994**, *33*, 2089-2095.
56. Stetler-Stevenson, W. G.; Kruttsch, H. C.; Liotta, L. A. Tissue Inhibitor of Metalloproteinase (Timp-2). A New Member of the Metalloproteinase Inhibitor Family. *J Biol Chem* **1989**, *264*, 17374-17378.
57. Lechapt-Zalcman, E.; Pruliere-Escabasse, V.; Advenier, D.; Galiacy, S.; Charriere-Bertrand, C.; Coste, A.; Harf, A.; d'Ortho, M. P.; Escudier, E. Transforming Growth Factor-Beta1 Increases Airway Wound Repair Via Mmp-2 Upregulation: A New Pathway for Epithelial Wound Repair?
58. Dufour, A.; Sampson, N. S.; Li, J.; Kuscu, C.; Rizzo, R. C.; DeLeon, J. L.; Zhi, J.; Jaber, N.; Liu, E.; Zucker, S.; Cao, J. Small-Molecule Anticancer Compounds Selectively Target the Hemopexin Domain of Matrix Metalloproteinase-9. *Cancer Res* **2011**, *71*, 4977.

59. Alford, V. M.; Kamath, A.; Ren, X.; Kumar, K.; Gan, Q.; Awwa, M.; Tong, M.; Seeliger, M. A.; Cao, J.; Ojima, I.; Sampson, N. S. Targeting the Hemopexin-Like Domain of Latent Matrix Metalloproteinase-9 (Prommp-9) with a Small Molecule Inhibitor Prevents the Formation of Focal Adhesion Junctions. *ACS Chem Biol* **2017**, 12, 2788-2803.
60. Cha, H.; Kopetzki, E.; Huber, R.; Lanzendörfer, M.; Brandstetter, H. Structural Basis of the Adaptive Molecular Recognition by Mmp9. *J Mol Biol* **2002**, 320, 1065-1079.
61. Agnew, H. D.; Coppock, M. B.; Idso, M. N.; Lai, B. T.; Liang, J.; McCarthy-Torrens, A. M.; Warren, C. M.; Heath, J. R. Protein-Catalyzed Capture Agents. *Chem Rev* **2019**, 119, 9950-9970.
62. Brew, K.; Nagase, H. The Tissue Inhibitors of Metalloproteinases (Timp)s: An Ancient Family with Structural and Functional Diversity. *Biochim Biophys Acta* **2010**, 1803, 55-71.
63. Nakada, M.; Nakamura, H.; Ikeda, E.; Fujimoto, N.; Yamashita, J.; Sato, H.; Seiki, M.; Okada, Y. Expression and Tissue Localization of Membrane-Type 1, 2, and 3 Matrix Metalloproteinases in Human Astrocytic Tumors. *The American Journal of Pathology* **1999**, 154, 417-428.
64. Morrison, C. J.; Butler, G. S.; Bigg, H. F.; Roberts, C. R.; Soloway, P. D.; Overall, C. M. Cellular Activation of Mmp-2 (Gelatinase a) by Mt2-Mmp Occurs Via a Timp-2-Independent Pathway. *J Biol Chem* **2001**, 276, 47402-47410

Chapter 3 : Towards MRI imaging probes for MMP2

3.1 Introduction

Atherosclerosis is one of the leading causes of death in the United States, coronary heart disease alone was responsible for every 1 in 7 deaths in the US in 2013.^{1,2} This high mortality rate makes it crucial to develop a better and easier diagnostic approach that can lead to improved treatment. The current diagnostic techniques involve blood tests, electrocardiogram, echocardiogram, computerized tomography scan, angiogram. Other than the angiogram and computerized tomography scan, the tests are not that indicative of plaque formation.³ An angiogram is an invasive test that uses an X-ray for the imaging of the blood vessels. A thin plastic tube or catheter is inserted through the femoral or radial artery that carries a dye, and with the help of fluoroscopy, the images are taken that shows the blood flow through the arteries. If a plaque is narrowing down the artery, the blood flow will have an impact on it which will be evident in the angiogram. It also gives an indication of how severe the block is. Computed tomography involves ionizing radiation, and in the case of substantial lesions, it can even overestimate the burden. In terms of image quality, Positron, Emission Tomography is not a good choice, and the dose that can offer a better image is not in an acceptable range.⁴

Due to the lack of better imaging systems, patients now go through angiography not only for therapeutic purposes but also for diagnostics which is inconvenient and uncomfortable. It also imposes certain risks, including injury to the artery that is used for catheterization, irregular heartbeats, even heart attack or stroke might get triggered.⁵ All these pushed the need for the development of a better diagnostic approach.

Developing an imaging procedure using Magnetic Resonance Imaging (MRI) to visualize the atherosclerotic plaques can lead to a user-friendly, non-invasive diagnostic procedure that will also be beneficial for early-stage detection plaques. MRI is also used in the detection of neurological cancers, gastrointestinal and liver lesions, staging, and diagnosis of prostate cancer. There are also some studies on coronary plaque imaging and carotid plaque cap rupture, which gave strong indications of the viability of this work.^{1,3}

Pathogenesis of atherosclerosis

Atherosclerosis is responsible for coronary heart disease (CHD), which alone is the primary cause of deaths worldwide, summing up to 15.9%.⁶ It is not only responsible for CHD but also for carotid, peripheral artery, and renal diseases. Atherosclerotic plaque formation starts with an injury to the endothelium. The injury is usually caused by inflammation due to an elevated level of cholesterol and hemodynamic imbalances.^{7,8} The injury to the endothelium leads to endothelial dysfunction, which induces the oxidation and accumulation of low-density lipoprotein or LDL. LDL increases the expression of chemokines which helps in the adhesion of monocytes, infiltration, and aggregation of platelets. This, in turn, leads to an inflammatory response. At first, the monocytes get directed towards the endothelium which then migrate from endothelium to sub-endothelium, where they turn into macrophages.⁹ These macrophages are then taken up into the oxidized LDL forming the foam cells.

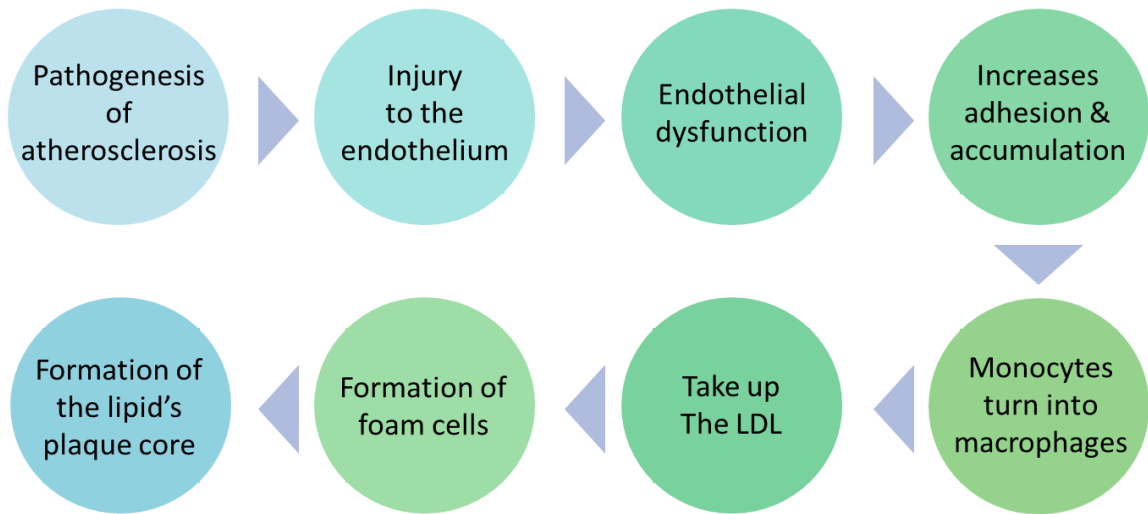


Figure 3.1: An illustration of atherosclerotic plaque formation process.

The foam cells later form the atherosclerotic plaque's lipid core. This chain of changes causes a phenotypic change in the vascular smooth muscle cells leading to the active synthetic stage (Figure 3.1). When it reaches the active synthetic stage, vascular smooth muscle cells migrate to the intima where they proliferate and cause excess production of extracellular matrix which converts the lesion into a fibrous state.¹⁰

Choice of biomarker

Developing a diagnostic imaging technique highly depends on the choice of the biomarker. For our purpose, targeting a biomarker that gets highly expressed during atherosclerosis can be advantageous to target. Several proteins like cytokines get overexpressed, but since atherosclerosis is an inflammatory process while selecting the biomarker, it is crucial to think about the changes associated with other inflammatory responses.¹¹ Besides, it would be easier to image something that does not circulate in a high amount in the blood and is highly localized on the plaque's surface.

Plaque formation is associated with the migration of the smooth muscle cells, monocytes, proliferation of the foam cells, and deposition of the extracellular matrix (ECM). Several studies showed the overexpression of MMP-2 and MMP-9 on the atherosclerotic plaques, specially MMP-2.^{12,13,14} One study showed, the MMP-2 knock out mice led to not only reduced intima formation but also decreased aneurysm, which demonstrated that it could promote ECM degradation or fibrosis.¹⁵ Multiple researches concluded that the distribution, as well as the content of MMP-2, is associated with the plaque's propensity of disrupting normal blood flow.^{16,17}

All these data inspired us to use MMP2 as our biomarker. From our previous study, we have already found a cyclic peptide, cy(WPHPY), that binds to proMMP2 at a nM binding affinity by inhibiting the protein-protein interaction between proMMP2 and TIMP2.¹⁸ We hypothesized that we could try to use this peptide since we already know that it binds to proMMP2 and modify it to make it suitable as an imaging agent.

3.2 Experimental

Materials

5(6)-carboxyfluorescein was purchased from ACROS (Pittsburg, PA) and Rhodamine B (Rhod), α -cyano-4-hydroxycinnamic acid (CHCA), cuprous iodide (CuI), from Sigma-Aldrich (St. Louis, MO). Rink amide resin with a loading capacity of 0.678 mmol/g was purchased from Aapptec (Louisville, KY) and peptide coupling reagent, 2-(1H-benzotriazole-1-yl)-1,1,3,3-tetramethyluronium hexafluorophosphate (HBTU, 99.6%) from Chem-Impex (Wood Dale, IL). All canonical Fmoc protected amino acids were obtained from Anaspec (Fremont, CA) and two unnatural amino acids Fmoc-L-

propargylglycine, Fmoc-L-azidolysine, from Combi-blocks (San Diego, CA). Triisopropylsilane (TIPS) was obtained from TCI (Portland, OR) and diisopropylethylamine (DIEA, 99.5%) from ACROS (Germany). Sodium chloride (NaCl), Tween 20, tris base, ascorbic acid, sodium phosphate monobasic monohydrate (NaH₂PO₄, 99.4%), sodium dodecyl sulfate (SDS), sodium phosphate dibasic anhydrous (Na₂HPO₄, 99.6%), bovine serum albumin (BSA), N,N'-dimethylformamide (DMF), acetonitrile (CH₃CN), diethyl ether (Et₂O), dichloromethane (DCM) ethyl acetate (EA), chloroform (CHCl₃) were purchased from Thermo Fisher Scientific (Waltham, MA). DOTA-NHS-ester was purchased from Macrocyclics.

Solid-Phase Peptide Synthesis

The peptides were synthesized manually following standard Fmoc SPPS coupling process or using the CSBio CS336S peptide synthesizer (Menlo Park, CA). If otherwise stated, the Rink Amide MBHA resin was used for the synthesis and usually, cyclization was carried overnight at rt with CuI (2.5 equivalent) and L-ascorbic acid (5 equivalent) in 20% piperidine/DMF solution. The unreacted excess copper was then removed with a 5% sodium diethyldithiocarbamate (w/v) and 5% DIEA (v/v) in DMF solution. If the peptides were fluorophore-labeled, then the dyes were coupled at the N terminal using the standard SPSS procedure overnight. Later the excess dye was washed away with DMF and DCM. The peptides were cleaved using cleavage solution that constitutes 95% TFA, 2.5% TIPS and 2.5% H₂O and after the cleavage, RP-HPLC (DIONEX Ultimate 3000) was used to purify the peptides with a semi preparative or preparative C18 reverse phase

column (Kinetex® 5 µm EVO, 250 × 10 mm; Kinetex® 5 µm EVO, 250 × 21.2 mm) using 0.1% TFA/H₂O and 0.1% TFA/CAN as mobile phase.

Competitive FRET Assay

For the competitive FRET assay, the concentration of rhodamine-conjugated cy(WPHPY) and fluorescein-labeled epitope were kept constant while changing the concentration of native Gd-DOTA-PEG5-cy(WPHPY). From the mixture, 65 µL solution was pipetted in a black Greiner 384 microwell plate and left for incubation at room temperature for about 30 minutes. After 30 minutes of incubation, the FRET signal was measured using Synergy H1 multimode microplate reader. Samples were set up in triplicates and prepared individually for each concentration. The average of these triplicates was calculated and analyzed. The same process was followed for Gd-DOTA-2° amine-cy(WPHPY). The representative results are shown here.

Competitive FP Assay

For the competitive fluorescence polarization assay, rhodamine-labeled cy(WPHPY), recombinant MMP2 protein, and Gd-DOTA-PEG5-cy(WPHPY) were used. The concentration of Rhod-cy(WPHPY) and recombinant MMP2 protein was kept constant while changing the concentrations of Gd-DOTA-PEG5-cy(WPHPY). 65 µL of this mixture was added to a black Greiner 384 microwell plate and incubated at room temperature for 30 minutes. After that, the polarization was measured using Synergy H1 microwell plate reader. For each concentration, samples were made in triplicates and prepared individually. The average was taken, and a representative result is presented here.

Cell Migration and Invasion Assay

Transwell plate with inserts was purchased from Corning. The inserts were 6.5 mm in diameter, had a pore size of 8.0 μm with a growth area of 0.33 cm^2 . At first, the insert was coated with ECM gel at a concentration of 2mg/ml and left in the incubator at 37 °C under 5% CO_2 for about 30 minutes. After 30 minutes, any excess gel solution was pipetted out, and inserts were washed gently twice with serum-free media. Then a suspension of 200k cells in 100 μL serum-free media was placed on top of the insert. 750 μL of complete medium containing 10% FBS was added in the lower chamber outside the insert. Later 100 μL of different concentrations of Gd-DOTA-PEG5-cy(WPHPY) in serum-free media was added to the insert. For the positive control, only serum free media in place of the peptide solution was used. The plate was kept in an incubator for 24 hours. After that, the insert was taken out, washed with PBS three times, and the cells were fixed with 4% paraformaldehyde in PBS solution. After 10 minutes, the paraformaldehyde solution was removed, and the inserts were washed with PBS three times. The inserts were then incubated in methanol at room temperature for 20 minutes. The insert was incubated with 0.2% crystal violet solution at room temperature for 15 minutes. After that, the crystal violet solution was removed, and the inserts were washed carefully with PBS three times. Noninvasive cells that stayed in the inside membrane of inserts were softly scraped off, and cells that passed through the membrane were imaged with an inverted microscope. For each condition, triplicates were prepared and analyzed.

3.3 Results & discussion

We tested two different spacers, PEG5 and 2° amine between cy(WPHPY) and Gd-DOTA to investigate how the bonding affinity changes. The spacers put a little distance between the cyclic peptide moiety and Gd-DOTA which might be advantageous in preserving the binding affinity with MMP2.

Binding affinity of Gd-DOTA-PEG5-cy(WPHPY) & Gd-DOTA-2amine-cy(WPHPY)

Once we synthesized the Gd conjugated peptides, we used competitive FRET assay to determine the binding affinity. For the competitive FRET, we kept the concentration of the fluorescein-labeled epitope and rhodamine-labeled cy(WPHPY) same with a gradual change in the concentration of Gd-DOTA-PEG5-cy(WPHPY). From the data, (Figure 3.2b) we could see that there is no apparent change in the signal, which indicated that either Gd conjugated peptide does not bind to MMP2 or has a lower binding affinity than cy(WPHPY) peptide and thus could not replace the competitor Rh-cy(WPHPY). The same situation happened for the Gd-DOTA-2°amine-cy(WPHPY) (Figure 3.2a).

Later we tested the binding affinity of both peptides on full length recombinant MMP2 protein. For the competitive FP, the concentration of the recombinant MMP2 protein and Rh-cy(WPHPY) kept constant while changing the concentration of the PEG5 and secondary amine conjugated Gd-peptide. In both cases, no noticeable change was observed. It is also possible that the Gd conjugated peptides are bulky and causing some disturbance in the local environment, and thus no apparent change could be seen (Figure 3.2c-d). But the 2° amine conjugated linker showed more problems with solubility

compared to the PEG5 one, which is why later we moved forward with Gd-DOTA-PEG5-cy(WPHPY) peptide.

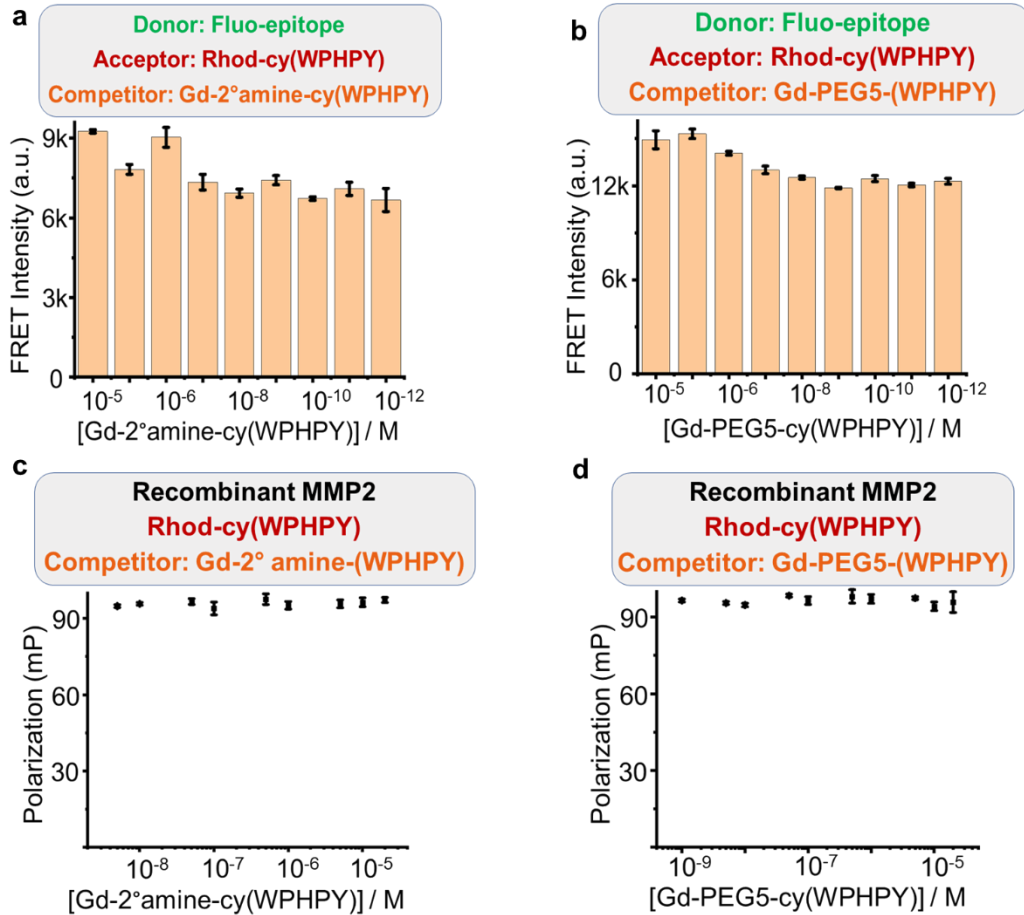


Figure 3.2. Binding affinity of Gd conjugated peptides. (a) (b) Different concentrations of Gd conjugated peptides were incubated with 200 nM rhodamine tagged peptide and 200 nM fluorescein-labeled epitope. For both linkers, there is no evident concentration-dependent FRET intensity change. (c) For the competitive FP, various concentrations of the Gd-2°amine-cy(WPHPY) were incubated with 100 nM of recombinant MMP2 protein and Rhod-cy(WPHPY), and no noticeable change is observed. (d) The same process is repeated for Gd-PEG5-cy(WPHPY), and no difference is observed.

Tryptophan fluorescence

In this situation, we wanted to find an assay where we could observe the binding affinity of the Gd-DOTA peptides with the recombinant protein without involving any tags. Since the cy(WPHPY) has tryptophan in the sequence, we could monitor the fluorescence intensity of tryptophan and whether it changes if we change the peptide concentration, keeping the recombinant protein concentration the same. Interestingly, we could see that when we incubate the peptide with the protein, the Trp fluorescence gets much higher than the fluorescence of the protein or the peptide by itself. This indicates that the peptide is interacting with the protein in a way to change the local environment and thus lead to a change in Trp fluorescence. The increase in signal difference is also concentration-dependent which we plotted using the hills equation, which led us to get an EC_{50} of about $0.8 \mu\text{M}$ (Figure 3.3a-b).

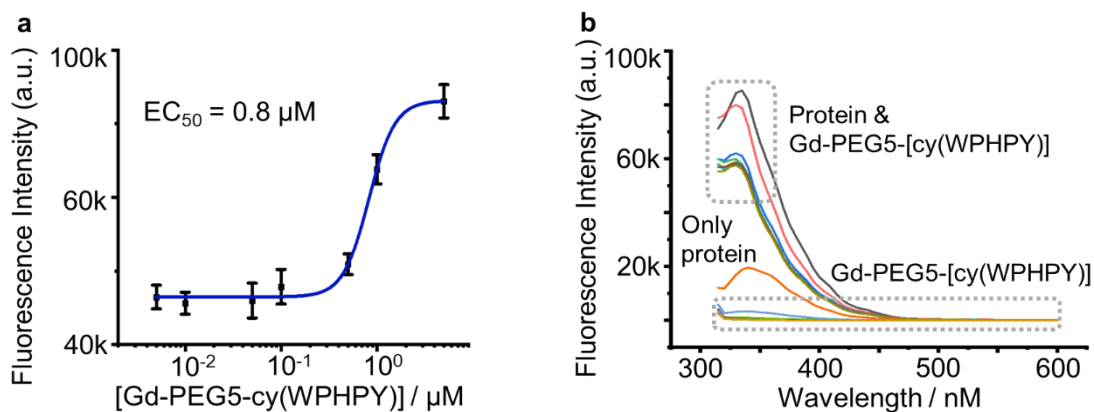


Figure 3.3. (a) The binding affinity of Gd-DOTA-PEG5-cy(WPHPY) against recombinant MMP2. With a change in the peptide concentration, there is a substantial concentration-dependent increase in the tryptophan fluorescence. (b) To clarify that the fluorescence intensity change is not because of an increase in the concentration of peptide, a spectral scan was done on the Gd conjugated peptide incubated with the recombinant protein and for the peptide and protein by itself. Figure b represents the

emission spectra of Trp fluorescence at different concentrations. The upper part shows an increase in fluorescence intensity when the peptide was incubated with recombinant MMP2. The lower part shows the fluorescence intensity only for the protein and the peptides by themselves.

Invasion property of Gd-DOTA-PEG5-cy(WPHPY)

Since we synthesized the Gd conjugated cy(WPHPY) for imaging purposes, it is important that we also check on the biological impact of this peptide. The precursor peptide cy(WPHPY) showed inhibitory activity towards cell migration and invasion, so we wanted to check when the peptide is conjugated to Gd, whether the inhibitory property stays.

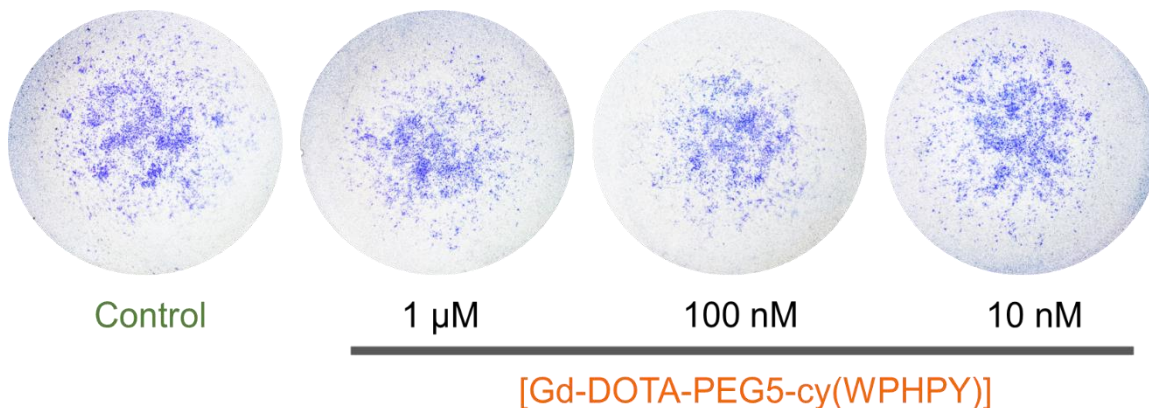


Figure 3.4. The invasion assay result for the Gd conjugated peptide. When cells were treated with different concentrations of the peptide, no apparent change in their invasion property was observed.

For this assay, we used the transwell plates. The surface of the inserts was covered with an extracellular matrix at first. If the Gd conjugated peptide shows any inhibitory activity, the MMP2 secreted from the cells won't be able to digest the extracellular matrix, and as a result, there would be fewer of the cells passing through the insert. After the inserts were treated with the matrix, WM115 cells were seeded and later incubated with Gd

conjugated peptide for about 24 hours. After 24 hours, the cells that passed through the insert were stained and checked under a microscope. There is almost no difference between the control and the ones treated with various concentrations of the Gd conjugated peptide, indicating that it does not impact the cell migration and invasion process.

3.4 Conclusion

We modified the cyclic peptide cy(WPHPY), which we found from our previous work, to make it suitable for MRI imaging. After conjugating the peptide with Gd, we found out that the modified peptide loses some of its binding affinity and does not impact the cell invasion property that the precursor peptide used to exhibit. In the future, we plan to use different linkers or unnatural amino acids to improve the binding affinity and make it better suited for imaging purposes.

3.5 References

1. Yuan, C.; Mitsumori, L. M.; Ferguson, M.S.; Polissar, N. L.; Echelard, D.; Ortiz, G.; Small, R.; Davies, JW.; Kerwin, WS.; Hatsukami, TS. In vivo accuracy of multispectral magnetic resonance imaging for identifying lipid-rich necrotic cores and intraplaque hemorrhage in advanced human carotid plaques. *Circulation* **2001**, 104, 2051–2056.
2. Libby, P.; Buring, J.E.; Badimon, L.; Hansson, G.K.; Deanfield, J.; Bittencourt, M.S.; Tokgozoglul, L.; Lewis, E.F. Atherosclerosis. *Nat Rev Dis Primers* **2019**, 5, 56.
3. Matsumoto, K.; Ehara, S.; Hasegawa, T.; Sakaguchi, M.; Otsuka, K.; Yoshikawa, J.; Shimada, K. Localization of coronary high-intensity signals on T1-weighted MR imaging: relation to plaque morphology and clinical severity of angina pectoris. *JACC Cardiovasc Imaging* **2015**, 8, 1143–1152.
4. Griffeth L. K. Use of PET/CT scanning in cancer patients: technical and practical considerations. *Proc (Bayl Univ Med Cent)* **2005**, 18, 321-330.
5. Tavakol, M.; Ashraf, S.; Brener, S. J. Risks and complications of coronary angiography: a comprehensive review. *Glob J Health Sci* **2012**, 4(1), 65–93.
6. Hafner, S. M.; Lehto, S.; Rönnemaa, T.; Pyörälä, K.; Laakso, M. Mortality from coronary heart disease in subjects with type 2 diabetes and in nondiabetic subjects with and without prior myocardial infarction. *N Engl J Med* **1998**, 339, 229–34.
7. Virmani, R.; Kolodgie FD, Burke AP, Farb A, Schwartz SM. Lessons from sudden coronary death: a comprehensive morphological classification scheme for atherosclerotic lesions. *Arterioscler Thromb Vasc Biol.* **2000**, 20, 1262–1275.
8. Simionescu, N.; Vasile, E.; Lupu, F.; Popescu, G.; Simionescu, M. Prelesional events in atherogenesis. Accumulation of extracellular cholesterol-rich liposomes in the arterial intima and cardiac valves of the hyperlipidemic rabbit. *Am J Pathol* **1986**, 123, 109–125.
9. Flavahan, N. A. Atherosclerosis or lipoprotein-induced endothelial dysfunction. Potential mechanisms underlying reduction in EDRF/nitric oxide activity. *Circulation* **1992**, 85, 1927–1938.
10. Singh, R. B.; Mengi, S. A.; Xu, Y. J.; Arneja, A. S.; Dhalla, N. S. Pathogenesis of atherosclerosis: A multifactorial process. *Exp Clin Cardiol* **2002**, 7, 40–53.
11. Soehnlein, O.; Libby, P. Targeting inflammation in atherosclerosis—from experimental insights to the clinic. *Nat Rev Drug Discov* **2021**, <https://doi.org/10.1038/s41573-021-00198-1>

12. Donnelly. R.; Collinson, D. J.; Manning, G. Hypertension, matrix metalloproteinases and target organ damage. *J Hypertens* **2003**, 21(9), 1627-30.
13. Huang, Y.; Mironova, M.; Lopes-Virella, M. F. Oxidized LDL stimulates matrix metalloproteinase-1 expression in human vascular endothelial cells. *Arterioscler Thromb Vasc Biol* **1999**, 19, 11, 2640-7.
14. Keeling, J.; Herrera, G. A. Human matrix metalloproteinases: characteristics and pathologic role in altering mesangial homeostasis. *Microsc Res Tech* **2008**, 71, 5, 371–9.
15. Galis, Z. S.; Sukhova, G.K.; Lark, M.W.; Libby, P. Increased expression of matrix metalloproteinases and matrix degrading activity in vulnerable regions of human atherosclerotic plaques. *J Clin Invest* **1994**, 94, 2493-2503.
16. Schafers, M.; Schober, O.; Hermann, S. Matrix-metalloproteinases as imaging targets for inflammatory activity in atherosclerotic plaques. *J Nucl Med* **2010**, 51, 5, 663-666.
17. Kuzuya M.; Nakamura, K; Sasaki, T; Cheng, X. W.; Itohara, S.; Iguchi, A. Effect of MMP-2 deficiency on atherosclerotic lesion formation in apoE-deficient mice. *Arterioscler Thromb Vasc Biol* **2006**, 26, 1120-1125.
18. Sarkar, P.; Li, Z.; Ren, W.; Wang, S.; Shao, S.; Sun, J.; Ren, X.; Perkins, N. G.; Guo, Z.; Chang, C. E. A.; Song, J.; Xue, M. Inhibiting matrix metalloproteinase-2 activation by perturbing protein-protein interactions using a cyclic peptide. *J Med Chem* **2020**, 63, 6979–6990.

Chapter 4: Cyclic peptide-based fluorescence reporters for ERK isoforms

4.1 Introduction

Mitogen-Activated Protein Kinase 3 (MAPK3/ERK1) and mitogen-activated protein kinase 1 (MAPK1/ERK2) are extracellular signal-regulated kinases. These enzymes act in a signaling cascade that regulates a broad spectrum of cellular processes, including differentiation, proliferation, cell cycle progression, and survival.^{1,2} The ERK pathway has been a point of interest for a very long time because of its association with different types of cancers. It becomes overactivated in various neoplastic cases, which prompted the development of many inhibitors targeting ERK and other members of the pathway, such as Ras, Raf, and MEK.³ Nevertheless, most patients had relapsed or experienced secondary effects after being treated with these inhibitors, either as a monotherapy or as part of a combination therapy regime.⁴ Interestingly, the resistant cells from Raf/MEK inhibition remained sensitive towards ERK, which highlighted the complex biological mechanisms behind the ERK signaling.^{5,6,7}

Studies to resolve the convoluted ERK signaling can be confounded by the sequence and function homology between ERK1 and ERK2 proteins.^{8,9,10} There are several prior works reporting differential outcomes by knocking down ERK1 versus ERK2 genes. Some studies observed that decreasing the expression of ERK1, but not ERK2, led to phenotypical changes.^{11,12} On the other hand, some studies stated that silencing ERK2 led to biological impacts, while silencing ERK1 had no such effects.¹³ These contradicting findings underscore the urgent need of developing reporters that could differentiate these isoforms.^{14,15}

In this chapter, we describe the development of specific reporters that can differentiate between ERK1 and ERK2. We used a high throughput screening strategy to identify cyclic peptide sequences that can bind to those proteins and use a fluorescence resonance energy transfer (FRET) mechanism to generate signal readouts.

4.2 Experimental

Materials

Rink amide MBHA resin with a loading capacity of 0.678 mmol/g was purchased from Aapptec (Louisville, KY), and all Fmoc-protected natural amino acids were purchased from Anaspec (Fremont, CA). Fmoc-L-propargylglycine and Fmoc-L-azidolysine were purchased from Combi-blocks (San Diego, CA). TentaGel S-NH₂ resin with a loading capacity of 0.28 mmol/g was obtained from Rapp Polymere GmbH (Tübingen, German). Tris base, Tween 20, sodium phosphate dibasic anhydrous (Na₂HPO₄, 99.6%), sodium chloride, sodium phosphate monobasic monohydrate (NaH₂PO₄, 99.4%), sodium dodecyl sulfate (SDS), bovine serum albumin (BSA), acetonitrile (CH₃CN), , ethyl acetate (EA), dichloromethane (DCM), N,N'-dimethylformamide (DMF), and ascorbic acid was purchased from Thermo Fisher Scientific (Waltham, MA). 2-(1H-benzotriazole-1-yl)-1,1,3,3-tetramethyluronium hexafluorophosphate (HBTU, 99.6%) was obtained from Chem-Impex (Wood Dale, IL) and Phenyl isothiocyanate (PhNCS), triisopropylsilane (TIPS) from TCI (Portland, OR). From Sigma-Aldrich (St. Louis, MO), α -cyano-4-hydroxycinnamic acid (CHCA) cuprous iodide (CuI), Rhodamine B, and cuprous iodide (CuI) were purchased. Piperidine was obtained from Alfa Aesar (Ward Hill, MA) and 5(6)-carboxyfluorescein, cyanogen bromide (CNBr) from ACROS (Pittsburg, PA).

Synthesis of the linear precursor peptide

The library was synthesized using the split and mix method on Tentagel S NH₂ resin. At first, the resins were swelled, and a mixture of ANP (5 equivalent), DIEA (10 equivalent), HATU (4.8 equivalent) in DMF was incubated with the beads at room temperature for about 2 hours. After 2 hours, the beads were washed with DMF (5 min × 3), and Fmoc protecting group was removed with 20% piperidine/DMF solution (10 min × 3) followed by washing with DMF (5 min × 3). Then for the subsequent coupling, a mixture of Fmoc-L-glutamic acid 5-allyl ester, DIEA, HATU in DMF is added to the beads and left on the rotator for about 2 hours at room temperature. The beads were then deprotected with 20% piperidine/DMF (10 min × 3) solution followed by washing with DMF (5 min × 3). The beads were then separated into 18 parts for the coupling of 18 different amino acids (L-stereoisomers of Ala, Arg, Asn, Asp, Gln, Glu, Gly, His, Ile, Leu, Lys, Phe, Pro, Ser, Thr, Trp, Tyr, and Val) dissolved in a solution of DIEA, HATU and DMF. The beads with the mixture were then left on a rotator for 2 hours at room temperature, followed by washing with DMF. This split and mix process was repeated for four more cycles. In the case of coupling one amino acid to all the beads like Fmoc-L-glutamic acid 5-allyl ester, Fmoc-propargylglycine, and Fmoc-azidolysine-OH, the beads were placed into one reaction vessel, and the same coupling method as ANP was applied.

Click reaction (CuAAC)

The beads were incubated with 20% piperidine/ DMF solution containing CuI (2.5 equiv) and ascorbic acid (5 equiv). The reaction was left at room temperature overnight. The

next day, the beads were washed with a solution of sodium diethyldithiocarbamate (5% w/v), DIEA (5% v/v) in DMF to get rid of the copper catalyst.

Ring-closing metathesis (RCM)

For the RCM reaction, the beads were vacuum dried first and placed in a 100 ml round bottom flask, mixed with 0.12 mmol of 2nd generation Grubbs catalyst (HG-II), and filled with argon. After that, anhydrous 1,2-dichloroethane was added in the flask and the temperature was set to 70 °C and left overnight with gentle stirring. The next day, another 0.12 mmol of Grubbs catalyst (HG-II) was added to the reaction and left for 16 hours. The beads were then washed with DCM followed by incubation with 0.2 M tris(hydroxymethyl)phosphine in isopropanol for about 12 hours at 80 °C. After 12 hours, the beads were washed with a mixture of DMF/H₂O (50:50) and later with DMF.

FRET Binding Assay

For the FRET binding assay, the peptides were labeled with rhodamine and the epitope with fluorescein. Different concentrations of rhodamine-labeled peptide were incubated with 100 nM fluorescein-labeled epitope. 65 µL of this mixture was pipetted in a Greiner black 384-well microplate and was left for incubation for about 30 minutes. After 30 minutes, the FRET signal was measured using Synergy H1 multi-mode microplate reader. All the samples were prepared individually, and for each concentration, the average FRET signal from triplicates was taken and analyzed. Representative results are presented here.

FP Binding Assay

For the FP assay, the concentration of rhodamine-conjugated peptides was kept constant while changing the concentration of the recombinant ERK proteins. The fixed concentration of the rhodamine-tagged peptide was kept at 100 nM in all samples. From the peptide-protein mixture, 65 μ L solution was pipetted in a Greiner 384 black microwell plate. Once the mixtures were added, the plate was incubated for about 30 minutes at room temperature. After 30 minutes, fluorescence polarization was measured using Synergy H1 multi-mode microplate reader. For each concentration, all the samples were prepared individually and in triplicates. An average polarization of the triplicates was taken and later analyzed.

Cell Culture

U87 cells were purchased from ATCC (the American Type Culture Collection). The cells were cultured in DMEM (Dulbecco's modified Eagle's medium), which was supplemented with 10% heat-inactivated FBS (Fetal Bovine Serum) and 100 U/mL penicillin/streptomycin. Cell cultures were maintained under 5% CO₂ in a 37°C incubator. When cells reached a confluency of 80-90%, it was passaged using a trypsin-EDTA solution.

Western Blot

U87 cells were treated with EGF (50ng/ml) and 10 nM trametinib. The cell lysates were collected every 5 minutes for 60 minutes. And later, western blot was carried out following standard protocols. The antibodies (#137F5, Cell Signaling Technology; #ab97051, Abcam) were used at 1:1000 and 1:10 000 dilutions, as recommended by the

manufacturers. The membrane was later treated with a chemiluminescent substrate, SuperSignal West Pico PLUS (Thermo Scientific), and the image was taken by the Odyssey® Fc Imaging System from LI-COR Biosciences, Lincoln, NE.

In vitro activity assay

Black 384 well plates were used for this assay. At first, the plate was blocked with 1% BSA PBST for about an hour and later washed with PBS 3 times. After that, inactive ERK1/2 with a final concentration of 200 nM was placed in the well, and later active MEK was added in different concentrations (100, 200, and 400 nM). The reaction was started by adding 10 µM ATP to the solution and was left at room temperature for about 45 minutes. After 45 minutes, the FRET pair, Cy5-B22 and Rhod-C14, was added to the solution, and the FRET intensity was measured. All the dilutions were done using HEPES buffer.

4.3 Results & discussion

Epitope targeted bicyclic peptide library screening

The similarity of ERK proteins makes it difficult to find something that can differentiate these two. Human ERK1 is slightly larger than ERK2 because of a 17-amino-acid extension at the N terminal and a 2-amino-acid addition at the C terminal.¹¹ To find reporters for these proteins, we focused on their sequence differences. We selected one epitope, shared by both ERK1, G₁₉₉-R₂₁₁, and ERK2, G₁₈₂-R₁₉₄ (G-F-L-T-E-Y-V-A-T-R-W-Y-R) and another one on ERK1, Y₃₂₇-E₃₄₁, (Y-L-E-Q-Y-Y-D-P-T-D-E-P-V-A-E) with 87% sequence homology with ERK2.

In addition to the sequence similarity, the structureless nature of these epitopes makes it more challenging to target them. We hypothesized that using a bicyclic peptide library could give us an advantage in finding the reporters for these homologous proteins. The inherent rigid backbone and three-dimensional spatial arrangement of the bicyclic peptide are more suitable for targeting complex epitopes. In our previous paper, we successfully found an inhibitor for a disordered oncoprotein, c-MYC.¹⁶ This recent development inspired us to target our coil-like ERK epitopes with the bicyclic peptide library.

The library was synthesized using a split and pool strategy where 18 natural amino acids were used as modular building blocks. The sequences started from an ANP linker, followed by an L-glutamic acid 5-allyl ester and two modular amino acids. Later, azidolysine was attached to the sequence, which served as the click handle followed by the conjugation of another two modular amino acids, a proline, an L-glutamic acid 5-allyl ester, another modular amino acid, and then an alkyne handle. Two cyclization processes, copper-catalyzed azide–alkyne cycloaddition (CuAAC) and Ru-catalyzed ring-closing metathesis (RCM) reactions were utilized to generate the bicyclic structures. The unique topology of this library gave us access to a three-dimensional chemical space, which we hypothesized would be advantageous in generating hits for these challenging epitopes.

The binding affinity of the hits

After the screening process, 17 hits were identified and sequenced (Figure 4.1a-c). Each of these hits was individually synthesized and screened against both epitopes. The hit sequences were conjugated with rhodamine B dye which would act as an acceptor, and the epitopes were conjugated with fluorescein, which would serve as a donor. Binding

between the rhodamine-conjugated peptide and the fluorescein-conjugated epitope would bring these two fluorophores closer and generate a FRET signal.

From the FRET data, the peptides that bind to any of these epitopes were identified, and the binding affinity was validated on full-length recombinant proteins using FP (Figure 4.1d). The FP data, along with the FRET data, confirmed a reporter pair for the ERK1 isoform. We found that peptide B22 binds to both ERK1 and ERK2, whereas peptide C14 binds to only ERK1 (Figure 4.2a-d).

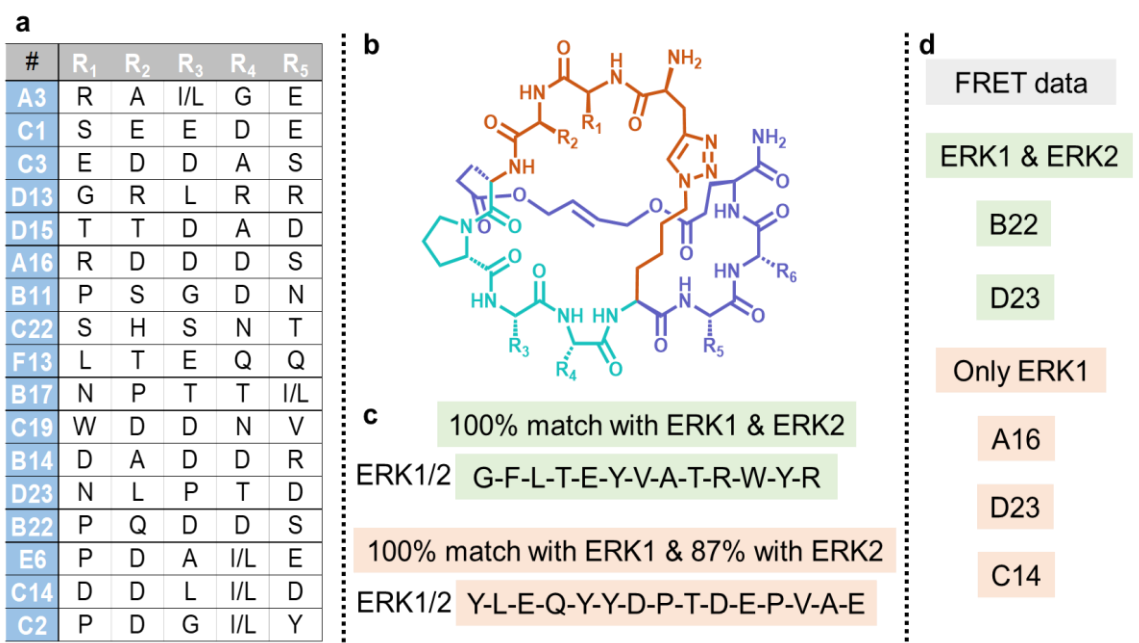


Figure 4.1. Finding preliminary leads from the hit sequences. (a) List of all 17 sequences. All these sequences were individually synthesized and tagged with rhodamine dye. (b) An illustration of a generic bicyclic peptide structure. (c) The epitope sequences, which were used in screening the library. The epitopes were synthesized and tagged with fluorescein. Later, each of the rhodamine-tagged peptides was tested against the fluorescein-tagged epitopes, and the binding was evaluated using FRET signal intensity. (c) List of identified hits obtained from the FRET data.

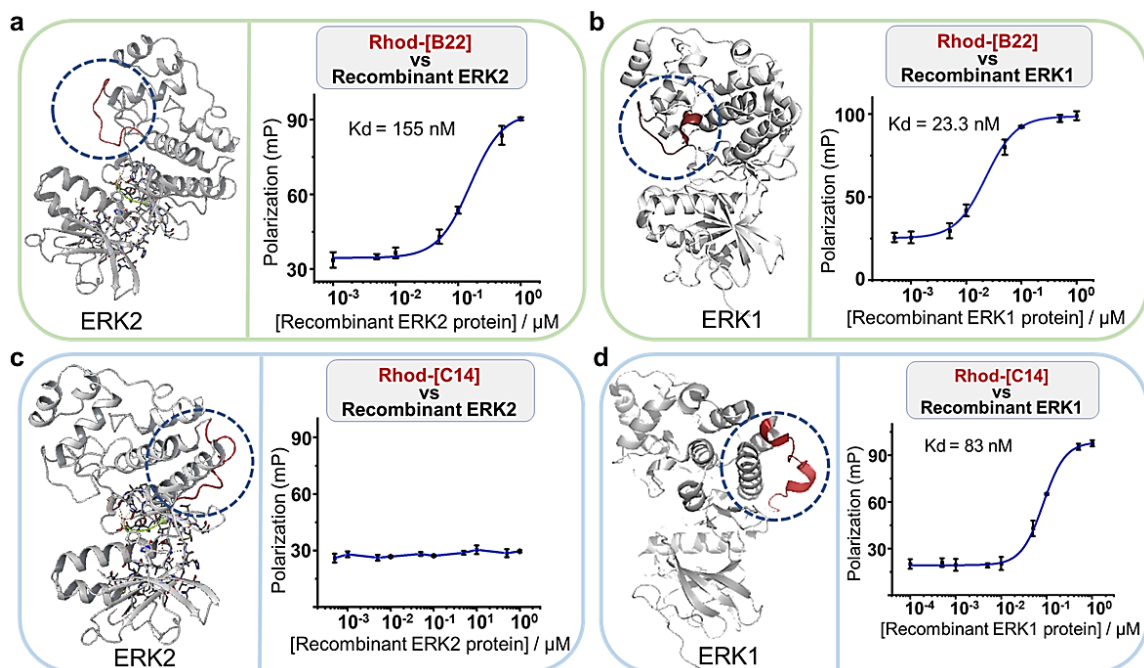


Figure 4.2. Validation of the hit sequences. (a) Crystal structure of ERK2, adapted from PDB, 3W55 file where the ERK2 epitope, G₁₈₂-R₁₉₄ is featured in red and appears to be a random coil. The right part of the panel shows FP data where 100 nM Rhod-B22 was treated with different concentrations of recombinant ERK2 protein. (b) Crystal structure of ERK1, adapted from 2ZOQ, PDB where epitope, G₁₉₉-R₂₁₁, is featured in red and appears to be structureless. The right side shows the FP result for Rhod-B22 (100 nM) when it is incubated with different concentrations of recombinant ERK1. (c) Crystal structure of ERK2 as in 3.2a (3W55, PDB), but it features a different epitope, Y₃₁₂-E₃₂₆, highlighted in red, which also appears to be a random coil, and the right panel shows FP data for Rhod-C14 (d) Crystal structure of ERK1 as in 3.2b (2ZOQ, PDB). The epitope, Y₃₂₇-E₃₄₁, is highlighted in red which appears to be a combination of alpha-helix and random coil, and the right panel shows the FP result for Rhod-C14.

FRET-based reporting process to probe lysates

We further confirmed the reporter pair's activity by incubating them with cell lysates collected from different conditions. For this experiment, B22 was conjugated to Cy5, and C14 to Rhodamine B. When Cy5-B22 and Rhod-C14 was incubated with lysates from EGF-stimulated cells, it showed a decreased FRET intensity compared to the control, whereas lysates from trametinib-treated cells showed increased FRET signal. These results were consistent with our design, where the FRET pair reported the amount of the unphosphorylated (inactivated) ERK1 (Figure 4.3a-d, 4.4a, 4.4b).

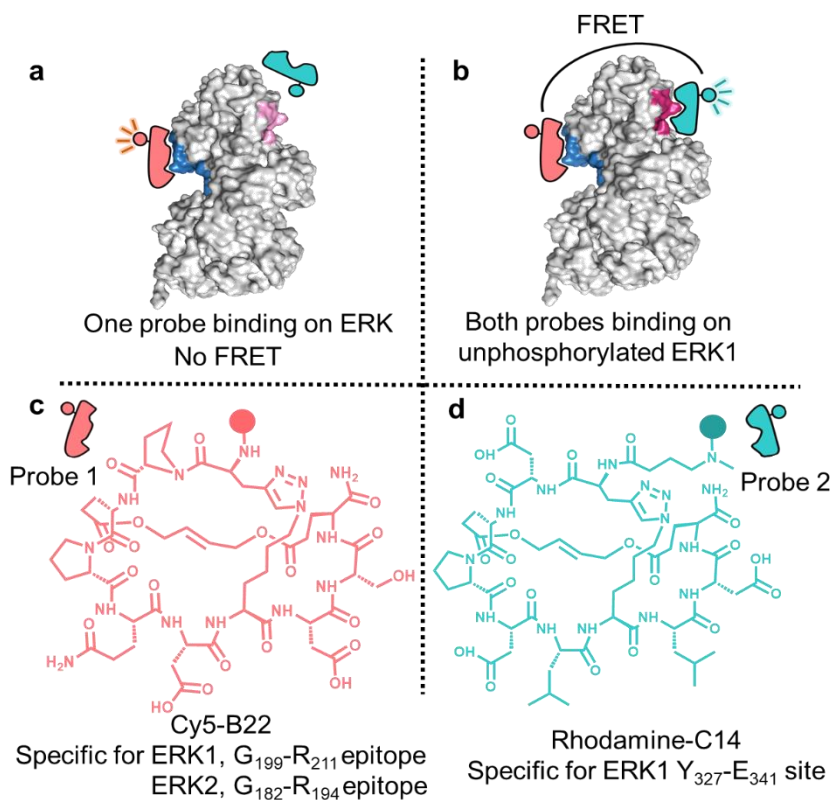


Figure 4.3. (a) FRET based unphosphorylated ERK1 detection method. For the FRET signal to generate, both the peptides need to be binding on the same ERK1 protein. (b) Structures of Cy5-B22 (probe 1) and Rhod-C14 (probe 2).

In vitro kinase assay

To further ensure that the reporter pair targeted the inactivated ERK1, we designed an *in vitro* activity assay using the full-length inactive recombinant ERK1 protein, the immediate upstream protein (MEK), and ATP. MEK is a dual-specificity kinase that phosphorylates both Tyr and Thr sites on ERK with the help of ATP. We incubated the inactive ERK1 protein with ATP and the active MEK protein. Here, we kept the concentrations of ERK1 and ATP constant and gradually increased the MEK concentration, which was expected to generate more copies of active ERK1. Since our probe recognized the unphosphorylated ERK1, we should see a decrease in the FRET signal. Indeed, the data showed reduced FRET signals with increased MEK concentrations (Figure 4.4c).

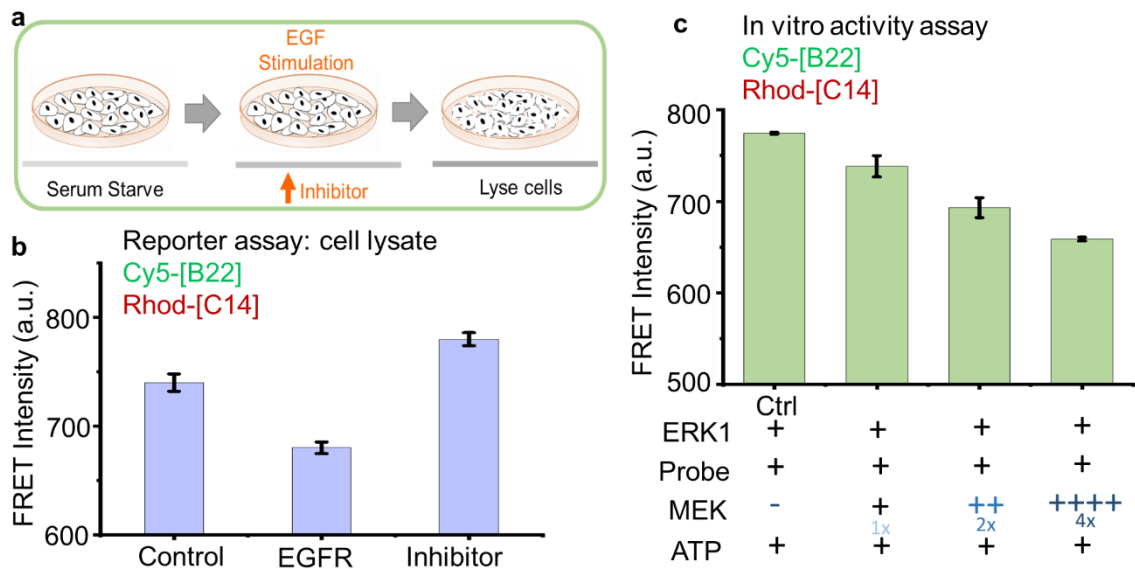


Figure 4.4. (a) Illustration of different treatment conditions. Serum starved U87 cells were stimulated with 50 ng/ml EGF which should increase the presence of more active ERK proteins, followed by treatment with 10 nM MEK inhibitor, trametinib. (b) Changes in FRET signal in the lysates that were collected right after treatment with EGF and

inhibitor. (c) The results of in vitro kinase activity where with an increase in active MEK, we could see a decrease in the FRET signal.

4.4 Conclusion

We have developed a pair of bicyclic peptide sensors for ERK1 isoform through epitope-targeted library screening processes. These ERK sensors can specifically translate the level of unphosphorylated ERK1 protein to fluorescence signal readouts. In the future, we plan to use this pair for studying ERK signaling dynamics under different perturbations in single cells.

4.5 References

1. Meloche, S.; J. Pouyssegur. The ERK1/2 mitogen-activated protein kinase pathway as a master regulator of the G1- to S-phase transition. *Oncogene* 2007, 26, 3227-3239.
2. Cargnello, M.; Roux, PP. Activation and function of the MAPKs and their substrates, the MAPK-activated protein kinases. *Microbiol Mol Biol Rev* **2012**, 76, 496.
3. Buscà, R.; Pouyssegur, J.; Lenormand, P. ERK1 and ERK2 Map Kinases: Specific Roles or Functional Redundancy? *Front Cell Dev Biol* **2016**, 4, 53.
4. Rusconi, P.; Caiola, E.; Brogginì M. RAS/RAF/MEK inhibitors in oncology. *Curr Med Chem* **2012**, 19, 1164-76.
5. Welsh S. J.; Corrie P. G. Management of BRAF and MEK inhibitor toxicities in patients with metastatic melanoma. *Therapeut Adv. Med Oncol* 7, **2015**, 122–136.
6. Morris E. J.; Jha, S.; Restaino, C. R.; Dayananth, P.; Zhu, H.; Cooper, A.; Carr, D.; Deng, Y.; Jin, W.; Black, S.; et al. Discovery of a novel ERK inhibitor with activity in models of acquired resistance to BRAF and MEK inhibitors. *Cancer Discov* **2013**, 3, 742–750.
7. Jabbour, E. Chronic myeloid leukemia: first-line drug of choice. *Am J Hematol* **2016**, 91, 59–66.
8. Crews, CM.; Alessandrini, A.; Erikson, RL. The primary structure of MEK, a protein kinase that phosphorylates the ERK gene product. *Science* **1992**, 258, 478-80.

9. Seger R.; Seger, D.; Lozeman, FJ.; Ahn, NG.; Graves, LM.; Campbell, JS.; Ericsson, L.; Harrylock, M.; Jensen, AM.; Krebs, EG. Human T-cell mitogen-activated protein kinase kinases are related to yeast signal transduction kinases. *J Biol Chem* **1992**, *25*, 267, 25628-31.
10. Zheng, C.F.; Guan, K.L. Properties of MEKs, the kinases that phosphorylate and activate the extracellular signal-regulated kinases. *J Biol Chem* **1993**, *268*, 23933-9.
11. Li, C.; Scott, D. A.; Hatch, E.; Tian, X.; Mansour, S. L. Dusp6 (Mkp3) is a negative feedback regulator of FGF-stimulated ERK signaling during mouse development. *Development* **2007**, *134*, 167–176.
12. Maillet, M.; Purcell, N. H.; Sargent, M. A.; York, A. J.; Bueno, O. F.; Molkenin, J. D. DUSP6 (MKP3) null mice show enhanced ERK1/2 phosphorylation at baseline and increased myocyte proliferation in the heart affecting disease susceptibility. *J Biol Chem* **2007**, *7*, 31246–31255.
13. Frémin, C.; Bessard, A.; Ezan, F.; Gailhouste, L.; Régeard, M.; Le, S. J.; Gilot, D.; Pagès, G.; Pouysségur, J.; Langouët, S.; Baffet, G. Multiple division cycles and long-term survival of hepatocytes are distinctly regulated by extracellular signal-regulated kinases ERK1 and ERK2. *Hepatology* **2009**, *49*, 930-939.
14. Qin, J.; Xin, H.; Nickoloff, B. J. Specifically targeting ERK1 or ERK2 kills melanoma cells. *J Transl Med* **2012**, *10*, 15.
15. Jung, S. M.; Park, S. S.; Kim, W. J.; Moon, S. K. Ras/ERK1 pathway regulation of p27KIP1-mediated G1-phase cell-cycle arrest in cordycepin-induced inhibition of the proliferation of vascular smooth muscle cells. *Euro J Pharmacol* **2012**, *681*, 15–22. d
16. Li, Z.; Shao, S.; Ren, X.; Sun, J.; Guo, Z.; Wang, S.; Song, M. M.; Chang, C. A.; Xue, M. Construction of a sequenceable protein mimetic peptide library with a true 3D diversifiable chemical space. *J Am Chem Soc* **2018**, *140*, 14552– 14556.

Concluding remarks

The critical association of PPIs with different diseases, pathological conditions, and their vast unexplored network make them valuable molecular targets. Modulating PPIs with small molecules can be challenging because of larger protein interaction surfaces and shallow to no binding pockets, where suitably modified peptides could offer a solution.

In chapter 2, we described our way towards finding a cyclic peptide inhibitor for modulating a protein-protein interaction responsible for the MMP2 activation. MMP2 is involved in diverse biological functions from tissue repair, remodeling, angiogenesis to inflammation, tumor metastasis, and much more. While designing the strategy to find an inhibitor, we avoided the highly sought-after catalytic process inhibition. The substantial homology of MMP2 with other MMPs often led to off-target effects, consequently resulting in numerous side effects. Instead, we focused on the PPI between TIMP2 and proMMP2, which is unique in the activation process. The interface of this PPI also presents an epitope (D₅₇₀-A₅₈₃) on proMMP2 that has little structural homology with other MMPs, but the segment is a structureless coil with no binding pockets. Inspired by recent work on cyclic peptides in PPI modulation, we used a cyclic peptide library against the epitope. This led us to find a cyclic peptide that can specifically inhibit the MMP2 activation by modulating the PPI between proMMP2 and TIMP2.

Our previous work on MMP2 inhibition, and multiple studies demonstrating the overexpression of MMP2 on the atherosclerotic plaque, encouraged us to modify the cyclic peptide inhibitor from our last work to an imaging agent. Lack of noninvasive, patient-friendly imaging procedures is one of the main obstacles to the treatment of

atherosclerosis. We conjugated Gd-DOTA and different spacers on cy(WPHPY), which resulted in a decrease in binding affinity to the μM level. In the future, we plan to add other modifications to the peptide to make it suitable as an MRI imaging agent.

In chapter 3, we used a bicyclic peptide library to find reporters for differentiating ERK isoforms. The relation of ERK proteins with different cancers, the sensitivity of the Ras/MEK inhibitor-treated resistant cells to ERK, and the contrasting results from various studies on ERK1/2 emphasize the need for reporters that can differentiate these isoforms. We strategized utilizing the inherent rigid structure and three-dimensionally diversified side chains of the bicyclic peptides for finding binders that can recognize one of the isoforms specifically. After screening, validating the hits on recombinant ERK proteins, and in vitro activity assay, we established a FRET-based reporting system to identify unphosphorylated ERK1.

Overall, cyclic peptides are now emerging as a unique class of compounds that offers multifaced uses. Their use in modulating PPI has increased significantly over the past few years. Conformational rigidity, better binding affinity, and resistance to hydrolysis-these advantageous features of cyclic peptides make them an excellent choice for targeting complex epitopes for therapeutic, probing, and imaging purposes.